A Tribological Investigation
of Windscreen Wiper Performance

By

Oana Dobre

Thesis Submitted to Imperial College London for

the Degree of Doctor of Philosophy and

Diploma of Imperial College (DIC)

October 2016

Tribology Section

Department of Mechanical Engineering

Imperial College London

Acknowledgments

Declaration of originality

This thesis contains the author's work and all quotations from other sources are acknowledged and clearly stated.

Declaration of copyright

Journal papers

1.5 Tom Reddyhoff, **Oana Dobre,** Julian Le Rouzic, Nicolaas-Alexander Gotzen, Hilde Parton, Daniele Dini, ''Friction-induced vibration in windscreen wiper contacts*''. Journal of Vibration and Acoustics*, vol: 137, no. 4, p. 41009, 2015.

Abstract

This project focused on understanding windscreen-wiper/glass interactions with an aim to reduce friction and wear, improve wiping quality and prevent friction induced vibration, (also known as squeak). To achieve this, the contact between windscreen and wiper was simulated under laboratory conditions using a UMT2 Tribometer, which loaded a stationary rubber profile against a rotating glass disc. Then, a range of measurement and analytical techniques were used to characterize the effect of conditions on different aspects of wiper performance.

Different surface conditions were reproduced by applying a range of common treatments to the glass, including hydrophobic and hydrophilic coatings. In addition to this, a new method of partially forming self-assembled monolayers was devised in order to produce test specimens with a controlled range of surface energies. It was shown that friction reduces with increasing surface energy, which is attributed to a smaller volume of water being entrained into the contact. Following this, a range of non-steady state friction behaviours were studied. These included combined friction and wear tests, where under severe conditions it was shown how friction performance is dominated by the formation and removal of burs, which prevents water from being entrained into the contact. In addition, drying tests were conducted to understand "tacky" behaviour (*i.e.,* the peak in friction peak under partially lubricated conditions). This was shown to be controlled by decreasing the surface tension of the water, through the addition of detergent, and provided evidence to support the theory that water menisci are responsible for increasing surface area. Static friction behaviour was also investigated, and the effects of start-up velocity and stationary duration on friction were quantified and explained. The practical implications of these results are discussed in terms wiper design and material selection.

To study friction induced vibration, (FIV), friction, sound and high speed video measurements were combined with finite element modelling of a rubber wiper/glass contact. In agreement with previous research, FIV only occurs when the friction versus speed curve has a negative gradient; a factor, which, in combination with the low stiffness of the materials, can lead to vibrational instabilities in the mixed regime. Results also showed that friction induced vibration is strongly affected by surface condition, and only occurs for a certain range of surface energies. This is explained by the fact that both high and low surface energies alter the gradient of the Stribeck curve thereby preventing FIV

(*i.e.,* low surface energies prevent sufficient liquid entering the contact and high surface energies attract water molecules to the surface of the glass producing a film that reduces friction). In order to study the source of squeak, simultaneous measurements were realised by a high speed camera, microphone, and laser Doppler vibrometer (LDV). This showed that although both the wiper and glass vibrate with the same frequency, it is the latter that transmits sound to the air. Results from the high-speed camera and microphone have shown that the frequency of the rubber vibration equals to the frequency of the emitted sound and the water vibration. This frequency is the same as the eigen frequencies determined from a finite element model of the wiper, which was developed. These observations led to the conclusion that friction induced noise occurs only when bending modes of the wiper are excited and this has important implications for the control of FIV since it shows that emitted sound can be eliminated by modifying the blade geometry during the design stage. Another important observation is that the frequency of squeak decreases with increasing volume of water present on the glass. This is attributed to the water effectively adding mass onto the vibrating system and hence reducing its natural frequency. Additionally, capillary waves have been for the first observed in the water surrounding the wiper contact. Based on the understanding gained, a number of recommendations are made regarding means of reducing windscreen wiper noise.

Finally, in order to monitor the wiping performance of the rubber wiper, a fluorescence microscopy technique was developed to view the sliding contact. This has enabled the fluid film thickness within the blade/glass contact to be assessed and also manufacturing defects, such as notches and inclusions, to be identified as the cause of wipe quality issues, such as hazing and hairlines.

Table of Contents

List of figures

List of tables

List of equations

$$E^* = E' + i \times E''$$
(1)

$$\frac{E''}{E'} = tan\delta$$
(2)

$$\log(a_T) = \frac{-C_1(T - T_{ref})}{C_2 + (T - T_{ref})}$$
(3)

$$F = F_{adhesion} + F_{deformation} + F_{Tearing}$$
(4)

$$\frac{1}{\mu} = c*P_N + b$$
(5)

$$\mu = \pi S(9R/16E)^{2/3} W^{-1/3}$$
(6)

$$F_T = F_A + F_{HB} + F_C$$
(7)

$$M\frac{d^2X}{dt^2} + c\left(\frac{dX}{dt} - v\right) + k(X - vt) = -F$$
(8)

$$M\frac{d^2x}{dt^2} + c\frac{dx}{dt} + kx = -F$$
(9)

$$F = F_v - \lambda\left(\frac{dX}{dt} - v\right)$$
(10)

$$M\frac{d^2x}{dt^2} + c\frac{dx}{dt} + kx = -\left(F_v - \lambda\frac{dx}{dt}\right)$$
(11)

$$M\frac{d^2x}{dt^2} + (c - \lambda)\frac{dx}{dt} + kx = -F_v$$
(12)

$$\zeta = \frac{c - \lambda}{2(Mk)^{\frac{1}{2}}}$$
(13)

$$x = Ae^{-\zeta\omega_n}sin\left[\omega_n(1 - \zeta^2)^{\frac{1}{2}}t + \varepsilon\right]$$
(14)

$$x = A_1 e^{\left[-\zeta\omega_n + \omega_n(\zeta^2-1)^{\frac{1}{2}}\right]t} + A_2 e^{\left[-\zeta\omega_n - \omega_n(\zeta^2-1)^{\frac{1}{2}}\right]t}$$
(15)

$$x = (A_1 + A_2 t)e^{-\zeta\omega_n t}$$
(16)

$$\gamma_{SG} = \gamma_{SL} + \gamma_{LG}cos\theta$$
(17)

$$\gamma_L(1 + cos\theta) = 2\sqrt{\gamma_S^d \gamma_L^d} + 2\sqrt{\gamma_S^p \gamma_L^p}$$
(18)

$$v = \lambda_{air} * f_{Doppler}/2$$
(19)

$$f_{Doppler} = -(f_{beat} - f_{rest})$$
(20)

$$U = C_{10}(\bar{I}_1 - 3) + \frac{1}{D_1}(J^{el} - 1)^2$$
(21)

$$\bar{I}_1 = \bar{\lambda_1}^2 + \bar{\lambda_2}^2 + \bar{\lambda_3}^2$$
(22)

$$\mu_0 = 2C_{10}$$
(23)

$$K_0 = \frac{2}{D_1}$$
(24)

$$I_{AN} = \frac{I_{BN} - I_{BG}}{max(max(I_N - I_{BG}))} \tag{25}$$

$$h = \frac{a p_{max}}{E^*}\left[-\left(2 - \frac{r^2}{a^2}\right)cos^{-1}\frac{a}{r} + \sqrt{\left(\frac{r^2}{a^2} - 1\right)}\right] \tag{26}$$

Nomenclature

A = constant determined by the initial state of the system

a = contact radius (m)

A_1 = constant determined by the initial state of the system

A_2 = constant determined by the initial state of the system

b = y axis intercept

c = damping coefficient

c_1 = constant

C_1 = empirical constat

C_2 = emirical constant

δ = angle delta (°)

E^* = contact modulus (Pa)

E' = storage modulus (Pa)

E'' = loss modulus (Pa)

E = elastic modulus (Pa)

f_{beat} = beat frequency (Hz)

$f_{Doppler}$ = Doppler shit (Hz)

f_{rest} = rest frequency (Hz)

F_A = adhesion friction (N)

F_{HB} = hysteresis friction (N)

F_C = cohesion friction (N)

F_x = friction force (N)

F_z = nornal load (N)

hv_{EM} = emitted photon energy

hv_{EX} = excited photon energy

I_{AN} = intensity after normalisation

I_{BG} = intensity background noise

I_{BN} = intensity before normalisation

I_N = intensity of the flat field correction

k = spring constant

L = sample length (m)

M = mass (kg)

P = load (N)

P_N = normal pressure (Pa)

p_{max} = maximum pressure (Pa)

r = distance from the centre of the contact (m)

R = reduced radius (m)

R_a = absolute value of roughness (nm)

R_q = root mean square value of roughness (nm)

S = interfacial shear stress (Pa)

S_1' = excited electronic singlet state

S_1 = relaxed singlet exicted state

T = temperature (°C)

$tan\delta$ = los tangent

T_{ref} = reference temperature (°C)

v = velcoity (m/s)

W = load (N)

X = displacement of mass (m)

α = thermal expansion

γ_{LG} = liquid interface free energy (mJ/m²)

γ^d = apolar forces

γ^p = polar forces

γ_{SG} = solid surface free energy (mJ/m²)

γ_{SL} = solid/liquid interfacial free energy (mJ/m²)

η = viscosity (Pa s)

μ = coefficient of friction

θ = contact angle (°)

λ = gradient of friction versus speed

λ_{air} = wavelength of air (nm)

v = Possion ratio

ζ = damping ratio

ω = undamped natural frequency (rad/s)

Chapter 1

Introduction

1 Introduction

Wiper blades have been and will continue to be in used in all automobiles for many years. Current trends are towards manufacturing of wiper blades that are more durable and efficient in terms of wiping quality. However, this requires a deeper understanding of wiper friction, wear and lubrication. In addition, customers' demands for quieter vehicles has led to the requirement for research aimed at reducing noise from components such as windscreen wiper blades.

Despite these challenges, there have been few studies into the tribological performance of windscreen wiper blades, and even fewer have tackled non-steady state issues such as friction induced vibration, the effect of wear on friction, and wiping defects. The research described in this thesis is aimed at addressing this deficit.

1.1 Windscreen wiper system

The windscreen wiper system is an important part of vehicle safety due to its function of efficiently removing water and debris from the windscreen. A typical windscreen wiper system consists of six main components, all interconnected with each other, such as windscreen wiper motor, worm and wheel gear, wiper linkage, wiper arms and wiper blades (see Figure 1) [1].
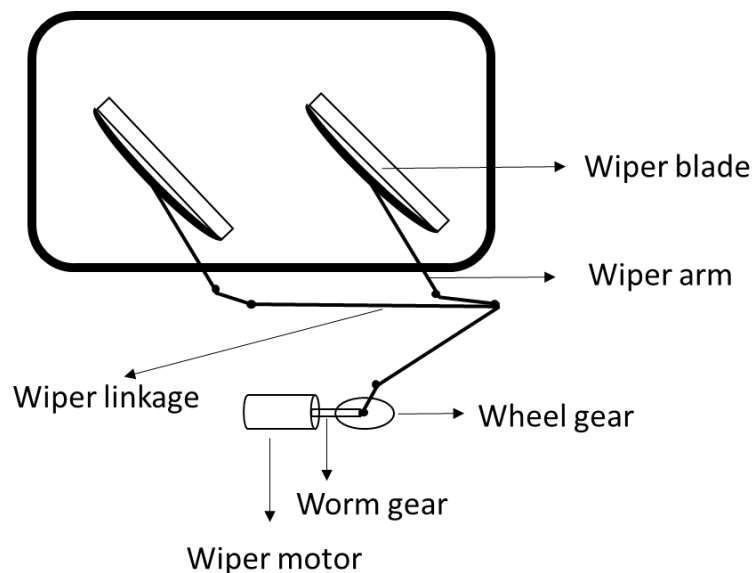
Figure 1. Windscreen wiper blade system at the macroscopic level [1][2].

Wiper blades are attached to a metallic wiper arm and pressed on the windscreen by a spring. The spring is integrated into the wiper blade arm to ensure an even distribution of pressure and adaptation to the curve of the windscreen. The load necessary for the wiper blade to bend on the windscreen and ensure a good wiper quality is typically 17 N/m [3]. There are various designs for the wiper arm or holder, depending on the type of blade to be accommodated; these including standard wiper blades, spoiler wiper blades, flat wiper blades and flat wiper blade upgrades. The reason for the availability of many types of wiper blades is due to different windscreen curvatures. Some cars have a double windscreen curvature and hence require the wiper to be long and capable of flexing on the contour of the glass [4][5].

The wiper arm is connected to the driving motor via a worm and wheel gear through a wiper linkage to move the wiper blades back and forward, as shown in Figure 1. The worm gear reduction reduces the speed and increases the torque of the motor. The motor must be high-powered, sufficiently quiet, and operate on a current from 2 to 4 A to remove a large volume of water or snow from the windscreen [6]. However, if more space is available, a twin-motor driven wiping system can be used.

There are different types of windscreen wiper systems. For example, tandem, opposed, single arm system controlled or uncontrolled [1] can be used. The most common windscreen wiper system is the tandem due to the repeated wiping of the area in front of the driver.

Depending on the required geometry, wiper blades are manufactured by one of the two fabrication processes: extrusion process for simple and low-cost geometries and injection-moulding for more complicated shapes.

To predict and verify the blade lifetime, a variety of tests can be performed. For example by a durability tests, in which the wiper blade is run on the windscreen for up to 1,500,000 cycles, ozone tests, in which wiper blades are placed under ozone for up to 15 hours [7]. Depending on the type of wiper blade material, the automotive industry recommends the replacement of the blade after 6 or 12 months [1]. If the recommended time of use is exceeded, the deficient quality of the blade can lead to marks on the windscreen. Another effect of aging is poor wipe quality. The wiper blades cost is low in comparison with various parts of the car (packages varies from £5 to £40 depending on the design and rubber type of the blade [8]), but they play an important role for the driver's safety.

1.2   Research goals

The main aim of this project is to examine the mechanisms governing the tribological interaction between rubber wiper blades and vehicles' windscreens. The first objective is to characterize friction under different conditions and also the effect of wear on friction, to aid energy saving and cost reduction measures. The second objective is to explain the mechanisms responsible for friction induced vibration for further elimination of noise, which can be disturbing for the drivers. The final objective is to measure film thickness to understand how to remove water efficiently from windscreen for ensuring the security and comfort of drivers.

This thesis contains eight chapters, and, as shown by the flow chart in Figure 2, has the following structure:

Chapter 1 – Introduction – describes the objectives and aims of the project. The main objectives are to reduce friction and wear, avoid noise and improve wiping quality.

Chapter 2 – Literature review – details relevant theoretical background and then provides a review of techniques already used to investigate and characterize dynamic instabilities and lubrication of existing compliant contacts. This chapter presents the most important work done in the past, as well as discusses the gaps existing in the field.

Chapter 3 – Materials and methods – presents the experimental techniques used to characterize the wiper system components in terms of friction, film thickness, roughness, surface energy and chemical composition, which help to understand the effect of surface and fluid properties on wiper blade performance.

Chapter 4 – Sample preparation – illustrates different methods used to prepare the samples. These include the application of surface monolayers to modify surface energy, the roughening of the rubber specimens using sandpaper and the roughening of the glass specimens using an etchant.

Chapter 5 – Friction measurements – characterizes the frictional response of wiper blades and studies the influence of contact parameters on friction. The parameters studied, include the geometry, surface coatings, surface energy, counter specimen roughness, wear, of the wiper blade coated or uncoated.

Chapter 6 – Friction induced vibration – focuses on the elucidation of the mechanism by which friction induced vibration occurs. This involves simultaneous noise measurements using laser Doppler vibrometer, high speed camera and microphone setup, which enable the measured frequencies of vibration of components to be compared and location of noise source.

A Finite Element Model using ABAQUS was created to mimic the wiper blade vibration. This is important as the experimental results show that friction induced vibration occurs when the vibrational mode of the wiper becomes excited. This model can help to prevent friction induced vibration by manufacturing wipers with the Eigen frequencies away from the critical audible frequency range.

Chapter 7 – Film thickness measurements – documents work aimed at visualizing sealing performance at the micro-scale for analyzing problematic macro-scale phenomena such as hazing and hair lines. To do this, film thickness in the contact and outside the contact was measured using fluorescence and a sealing limit was determined.

Chapter 8 – Conclusions – presents the conclusions and suggests future work to be carried out.

The most novel aspects of this work include understanding and elucidating the mechanism by which friction induced vibration occurs and developing a method to determine the sealing limit (maximum acceptable film thickness left on the glass after wiping process). These aspects will help automotive manufacturers to avoid the squeak and improve the wiping quality of windscreen wipers, which will result in better development of products and improved customer satisfaction.
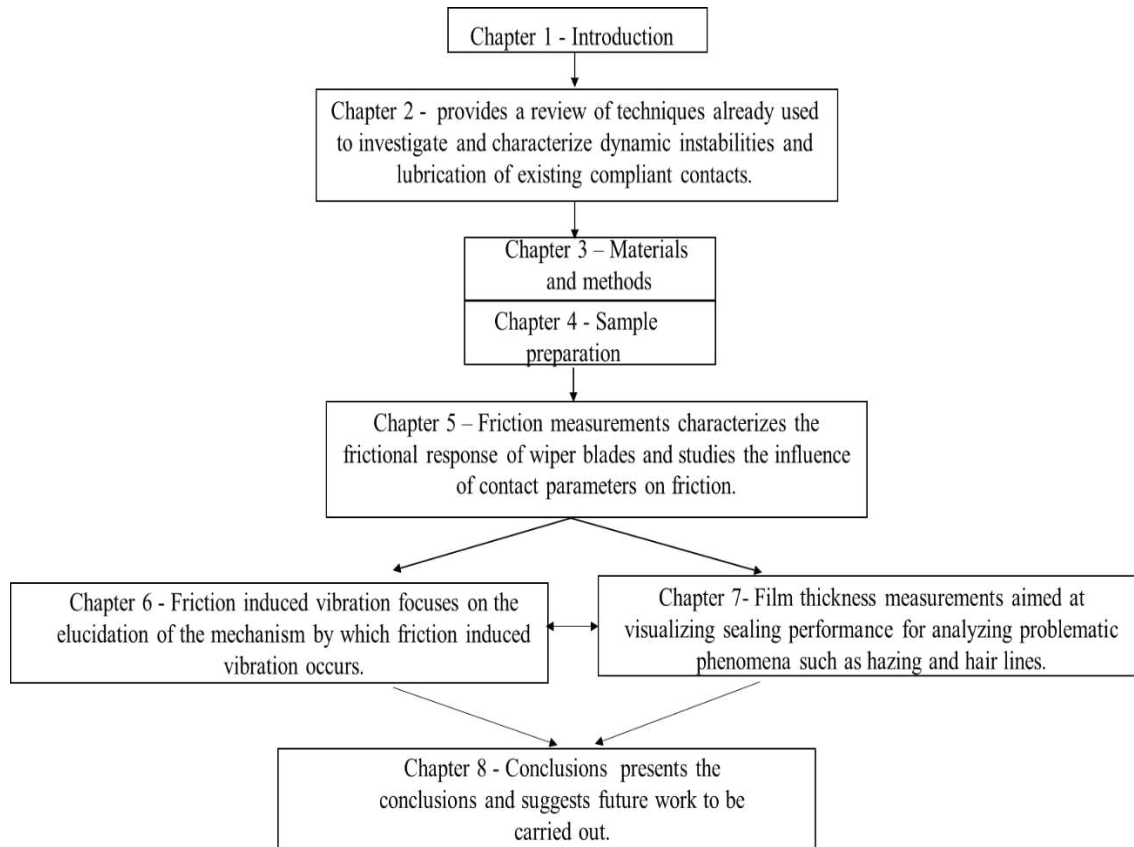
Figure 2. Flow chart showing the organisation of the thesis chapters.

Chapter 2

Literature Review

2 Literature Review

This review outlines the current understanding, obtained from theoretical and experimental methods, in areas that are related to windscreen wiper operation. First, a brief history of windscreen wipers is given, followed by basic theory on viscoelastic materials and the current state of literature on compliant contacts. Particular attention is then paid to research into the behaviour of rubber materials in terms of their friction and wear mechanisms. Next, the behaviour of rubber under both submerged and drying conditions is reviewed. Finally, a summary of research specifically on wiper blade behaviour is given along with an outline of the understanding of friction induced vibration.

2.1 History of wiper blades

2.1.1 Development of wiper blades

1903.   Wiper blades were supposedly invented by Mary Anderson during her trip from Alabama to New York [9]. She then registered a patent (US 743,801) for a windscreen wiper blade in the USA on the 10th of November 1903 [10]. This patent was called a "window cleaning device for electric cars and other vehicles." The exact design was never produced commercially; however, the invention closely resembled windscreen wiper devices commonly found on many early car models [11].

1903.   At the same time, an Irish inventor, James Henry Apjohn, invented a method of moving two brushes up and down on a vertical plate glass windscreen, which was patented in the UK in 1903 [12][13].

1911.   The first company which registered a patent for windscreen wiper blades was Sloan & Lloyd Barnes in April 1911, Liverpool, England [12].

1917.   John R. Oishei founded the Tri-Continental Corporation in 1917, and introduced the first windscreen wiper for two parts of a windscreen [14].

1926.   Bosch developed the first electric windscreen wiper system in 1926 [3].

1960.   Major progress in the development of wiper blades has been made since 1960, as shown in Figure 3 [15].

1971.   First intermittent windscreen wiper was invented by Bosch [15].

1981.   Trico developed the first electric rear wiper system [16].

1994.   Bosch starts using synthetic rubbers due to the various mixture possibilities and superior mechanical properties.

2000.   Bosch introduces flat blade technology [15].

2013.   Bosch has the world's biggest windscreen wiper factory, in Tienen, Belgium, which produces 350,000 wipers per day [15].

2014.   Trico developed a premium hybrid dual-shield technology blade, which has a high-strength polymer shell to protect the blade components from wind damage, road debris and rusting [16].
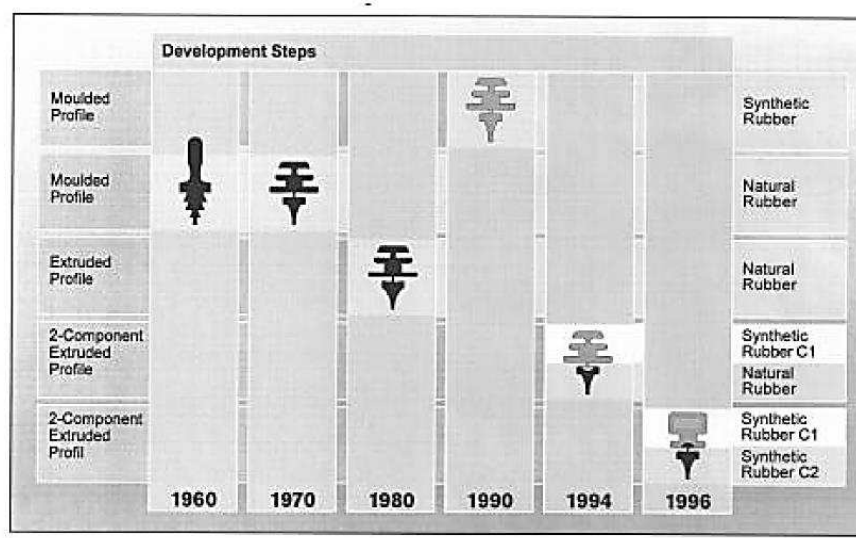
Figure 3. Evolution of the wiper blade from1960 to 1996 [15].

2.2 Viscoelastic material behaviour

Before the friction behaviour of soft contacts can be studied, it is necessary to understand the basic principles of viscoelastic behaviour. Therefore, this brief section outlines some basic theory on the viscoelastic properties of materials.

When a cyclic stress is applied to a polymer material (*e.g.*, rubber), the response shows a combination of both viscous and elastic behaviour. The viscous response arises because the stress causes an irreversible process of long polymer chains sliding over each other which dissipates energy in the same way as when viscous liquids are deformed. The elastic response arises because the stress causes the chains to contort and change shape. This process is reversible, and energy is stored rather than lost (the chains will return this energy once the force is removed).

As shown in Figure 4, the elastic response occurs in phase with the loading, while the viscous response lags behind by 90 degrees. When the stress and strain are out of phase by an angle delta (δ), with a value in between 0 and 90, these materials exhibiting such behaviour are classified as viscoelastic.
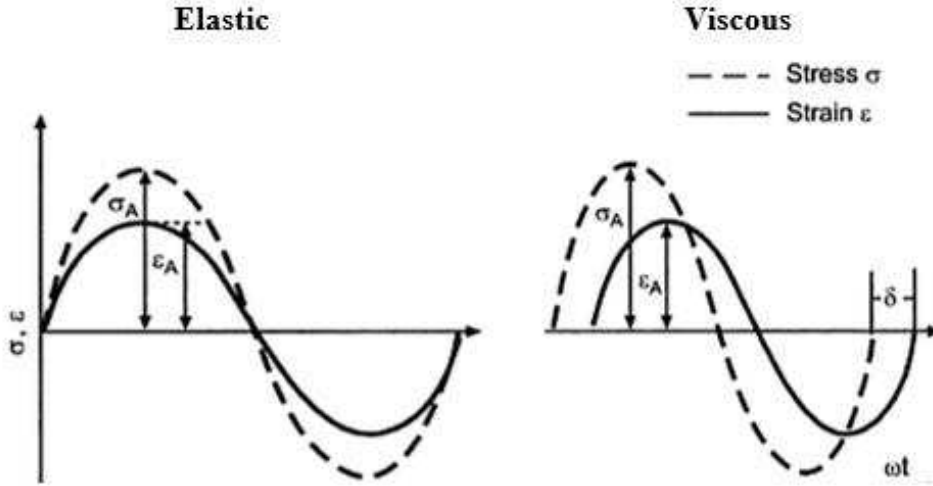
Figure 4. Schematic representation of sinusoidal oscillating stress and resulting strain for a linear elastic material [17].

The modulus of a material is the ratio of stress to strain and, in the case of a viscoelastic material, this must contain both the viscous and the elastic part, which are 90 degrees out of phase with each other. This is most conveniently represented in complex number form:

$$E^* = E' + i \times E''$$
(1)

where E' is the storage modulus (*i.e.,* the elastic part) and E'' is the loss modulus (*i.e.,* the viscous part). Another important quantity is the ratio of the loss modulus to the storage modulus:

$$\frac{E''}{E'} = tan\delta$$
(2)

This is known as the loss tangent (*tan δ*) and used as a measure of the energy loss in relation to energy stored [17]. Materials with a high loss tangent have high internal friction. The complex modulus and loss tangent of a viscoelastic material varies strongly as a function of deformation frequency, as shown in Figure 5. This behaviour can be explained as follows: at the low frequency, the behaviour is viscous as the long polymer chains have enough time to slide over each other. However, at high frequencies, the chains

have less time to respond and instead they twist and contort, showing elastic behaviour. Between these two behaviours there is a smooth transition.
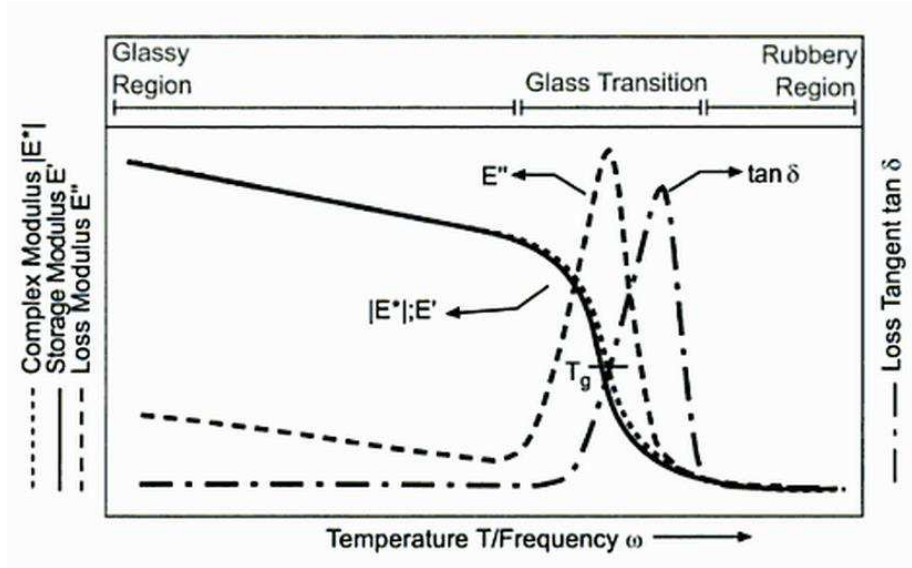
Figure 5. Complex modulus storage modulus E', loss modulus E", and loss tangent tan δ for an amorphous thermoplastic as a function of temperature or frequency [17].

The effect of temperature on viscoelastic properties is exactly the opposite to that of frequency. For instance, high temperatures increase the flexibility of chain molecules, so they behave as they would at reduced frequency. Conversely, low temperatures cause stiffening that affects viscoelastic properties as if the frequency were increased. An empirical equation was suggested by Williams Landel and Ferry (WLF) [18], which predicts the equivalent shift in frequency, a_T, associated with a particular change in temperature (equation 3).

$$log(a_T) = \frac{-C_1(T-T_{ref})}{C_2+(T-T_{ref})}$$

(3)

where T is the temperature relative to a reference temperature T_{ref} and C_1 and C_2 are empirical constants to be found experimentally.

2.3   Compliant contacts

Compliant contacts, also known (incorrectly) as soft contacts, are found in various applications in nature and engineering (*e.g.*, rubber seals, windscreen wipers, synovial joint lubrication, and human skin contacts). These contacts involve one or both contacting bodies with very low Young's modulus and are characterised by large contact areas and low pressures. The study of compliant contacts is challenging due to the complications that arises from highly deformable, dissipative, and non-reflective components.

2.3.1   Introduction to dry sliding compliant contacts

This section is concerned with the friction arising from a dry contact formed by loading a compliant and a hard specimen against each other. For brevity, this compliant/hard type of contact will be denoted C/H.

When hard materials, such as metals, slide against each other, friction typically arises due to the energy dissipated in plastically shearing of the contacting interface. This typically occurs at welded asperity contacts (*i.e.*, the interfaces formed by raised high spots on component surfaces), when local shear stresses exceed the yield strength of the material. When compliant materials, such as rubber, are involved, the situation is different due to lower elastic moduli and higher internal losses (occurring over a wide range of frequencies) [19]. Here, energy dissipation and friction also result from the viscoelastic behaviour of the compliant material.

When dealing with compliant contacts, it is necessary to distinguish between two dissipation mechanisms, both of which may contribute to the overall friction experienced by the contact: adhesion resulting from the molecular interaction between the two surfaces, and hysteresis, deformation losses due to repeated loading and unloading of the compliant component.

There are a number of ways in which the repeated loading and unloading, necessary for deformation losses, can occur. Firstly, it can occur if the location of the contact moves relative to the compliant component so that fresh material is continually being compressed and released. As shown in Figure 6a, this is prevalent in components such as tyres, but only occurs in windscreen wiper operation during reversal.

The second mechanism that can give rise to hysteresis (deformation) friction occurs due to the surface topography of the hard component [20]. Here, if the surface is sufficiently rough, the asperities that pass through the contact will themselves cause the compliant component repeatedly to deform and dissipate energy.

This mechanism, which is effectively a micro-scale example of the case shown in Figure 6b, can probably be ignored in windscreen wipers where the surfaces are assumed to be sufficiently smooth (roughness of the glass is around 1 nm).
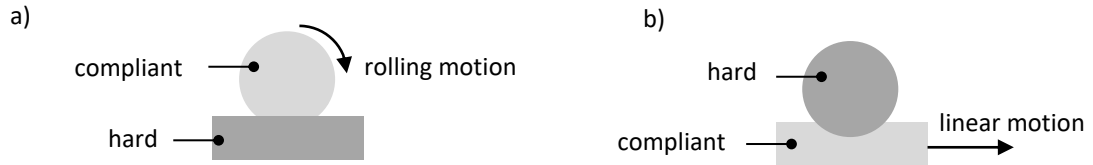
Figure 6. Examples of motion that give rise to deformation friction (in both cases, the contact moves relative to the compliant body).

In summary, for compliant materials, rubber friction mechanisms can be divided into three categories: adhesion, hysteresis (deformation) and tearing (equation 4) [21][22][23].

$$\mathbf{F} = \mathbf{F_{adhesion}} + \mathbf{F_{hysteresis\,(deformation)}} + \mathbf{F_{tearing}} \qquad (4)$$

Of these three components, the adhesion is the most relevant to the operation of windscreen wipers. The adhesion occurs due to the Van der Waal's forces between the surfaces and contributes to the friction force necessary to separate the surface as shown in Figure 7a.
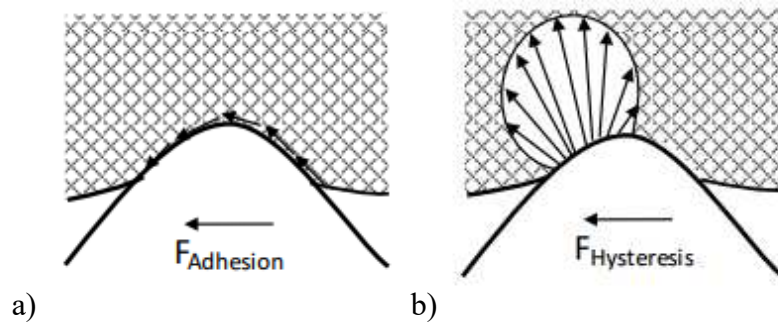
Figure 7. Rubber friction mechanisms: a) Adhesion and b) hysteresis. Adapted from [24].

The hysteresis (deformation) component (see Figure 7b), as stated above, arises when the relative motion of the two components causes repeated loading and unloading of the rubber material. If the material exhibits viscoelastic behaviour (*i.e.,* in addition to elastic behaviour, it dissipates energy when deformed, in a fashion similar to a viscous liquid) repeating loading and unloading also gives rise to friction. The tearing or cohesion friction component represents the wear at the interface. The cohesion friction loss as a fraction of the total wiper blade coefficient of friction is negligible in comparison with the adhesion and hysteresis.

2.3.1.1   Adhesion as a rubber friction mechanism

This section presents the origin of the adhesion mechanism. Thirion [25] was the first to identify the adhesion mechanism. He reported his findings of friction testing obtained by sliding gum rubber of multiple sizes on smooth glass. As shown in Figure 8a, the coefficient of friction reduces with an increase in pressure. He used the following equation 5 to describe his results:

$$\frac{1}{\mu} = c_1 * P_N + b \tag{5}$$

where μ is coefficient of friction, P_N is the applied normal pressure, c_1 is constant, and b is a y-axis intercept. Thirion assumed that a linear relationship existed between $1/\mu$ and P_N at lower values of P_N. The left-hand side of equation represents the inverse of the coefficient of friction (μ) at zero pressure, whereas right-hand side represents the rubber friction adhesion force on a smooth surface, when the pressure rises to infinity.

The coefficient of friction versus load was recalculated from Thirion [25] as shown in Figure 8b. Thirion's experiments indicates that the coefficient of friction of the samples with different sizes is different for the same applied load. This implies that the apparent friction is dependent on the contact area. When the rubber is sliding on a smooth surface, the adhesion will be greater because the real contact area increases.
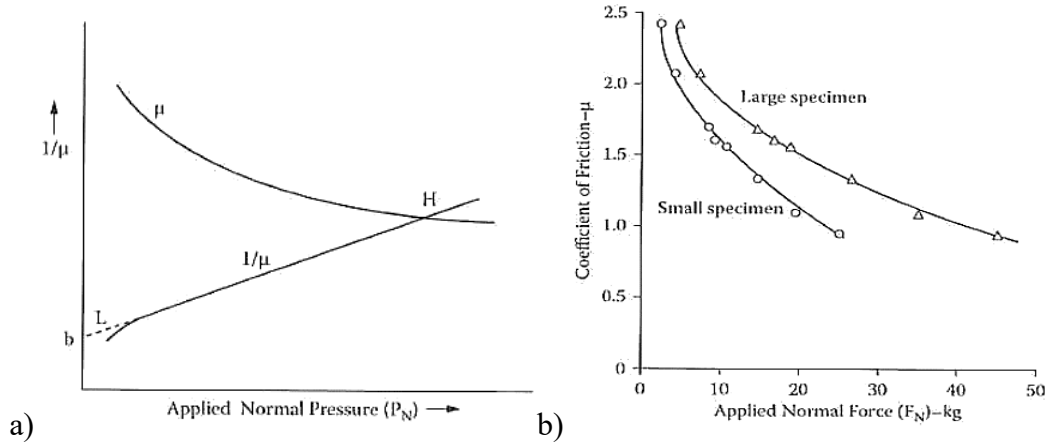
Figure 8. a) Thirion's inverse coefficient of friction for rubber versus glass and b) coefficient of friction (μ) versus applied load (F_N) recalculated from Thirion [25].

Another concern is the dependence of adhesion on properties such as sliding speed, temperature and load in C/H contacts. Grosch [26] was one of the first to establish a link between adhesive friction and viscoelastic material properties. He measured friction in a C/H contact at a range of speeds. When the results were plotted, they showed that friction increases up to a certain speed then plateaus and decreases (see Figure 9a). It was noticed that this dependence of friction on speed follows a similar relationship to the dependence of the loss modulus (see Figure 5). This suggested that adhesion was caused by the viscoelastic properties of the material. Grosch [26] went on to show that the WLF equation (see equation 3) could be applied to shift each friction curve (measured at a different temperature) onto a single master curve as shown by Figure 9b.
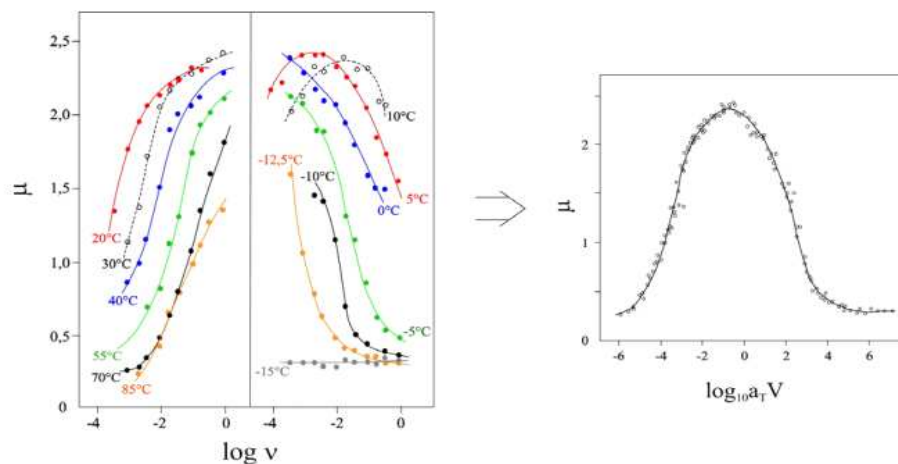
Figure 9. a) Adhesive friction plotted against sliding speed, different curves represent different temperatures; b) the same data fitted onto a master curve using the WLF equation [14].

36

Similar work was recently published by Putignano et al. [27], who showed that the viscoelastic friction is strongly influenced by temperature. Experiments were carried out by measuring the viscoelastic friction at different temperatures between a Polytetrafluoroethylene (PTFE) ball and a rubber sheet at a constant load for a wide range of speeds. These experimental results were compared with those obtained using a numerical model, which separates viscoelastic losses from Coulomb contributions as published by Carbone and Putignano [28].

An important concept in understanding adhesion in C/H contacts, which explains Grosch's results, is the model developed by Schallamach [29] and others. This model, as depicted in Figure 10, shows how the adhesion behaviour results from the motion of the long elastomer molecules, which repeatedly attached to the hard surface, are then stretched, before detaching and relaxing. It follows from this understanding that friction will respond to changes in temperature and material composition in a similar way to how the molecular structure changes. For instance, if an increase in temperature causes the structure of the material to absorb more energy, then this will result in a decrease in friction. This is an important result, which enables adhesion to be predicted and by changes in bulk properties, which are available in the literature or can be measured easily using Dynamic Mechanical Analysis (DMA) techniques.
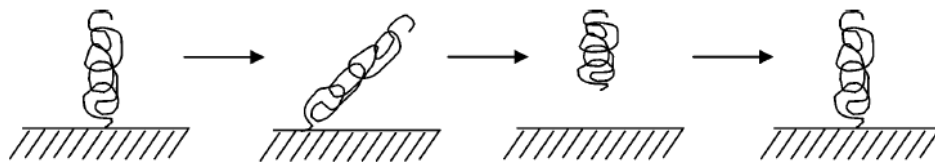
Figure 10. The classic depiction of a polymer chain in contact with a laterally moving counterface. The chain a) stretches, b) detaches, c) relaxes and d) reattaches to the surface to repeat the cycle [30].

An important finding by Vorvolakos and Chaudhury [30] is that dry friction between a compliant and a hard component reduces with molecular weight of the polymer. This can be explained by the model shown in Figure 10, since the number of chains supporting the load decrease as the length of the molecules increases.

2.3.1.2 Bulk deformation hysteresis mechanism

Tabor [31] introduced his findings on rubber friction mechanisms, after studying rolling steel cylinders or spheres of different diameters on smooth rubber blocks. He derived a theoretical expression for these conditions and examined if hysteresis losses of rubber would continue to be constant, when different spheres diameters were tested. The spheres were rolled on dry, clean and preformed rubber grooves with different radii and no interfacial slip was allowed. When the tests were repeated in lubricated grooves, no decrease in rolling friction was noticed. Bulk deformation hysteresis was identified, when the rolling cylinders or spheres compressed or stretched the rubber elastically. Rubber was shown to exhibit elastic release in dry and wet conditions as spheres were moved out of contact. Such extension and compression lead to energy losses providing hysteresis (deformation) friction. This deformation can take place without significant wear. Greenwood and Tabor [32] also conducted experiments to measure the sliding and rolling friction between a hard body and a rubber surface under lubricated conditions and then compared their findings with results presented by Sabey [33]. Based on the comparison, they concluded that the friction in rubber is mainly due to high hysteresis losses, when adhesion is small.

Additionally, extensive work on viscoelastic rolling and sliding friction incorporating thermal and roughness effects was explored by Putignano and co-workers [34][35][36]. Results show the importance of accounting for viscoelastic effects in order to obtain an accurate simulation of sliding rough contacts. It was also shown that viscoelasticity is not only involved in dissipative effects, but also gives rise to the anisotropy of the deformed surface at contact.

2.3.1.3 Friction decreasing with increasing load

Roth *et al.* [37] studied soft rubber compounds (rubber used to make tyre treads) sliding friction on various surfaces. Figure 11a shows their rubber friction results obtained for various applied loads on specimens moulded on roughened glass. The coefficient of friction of rubber was calculated as a ratio of the measured force to the mass of the specimen. The rubber friction decreases with the applied pressure. In Figure 11b, the rubber friction decreases with the increase in load. In these experiments, the coefficient of friction appears to be dependent on the contact area.
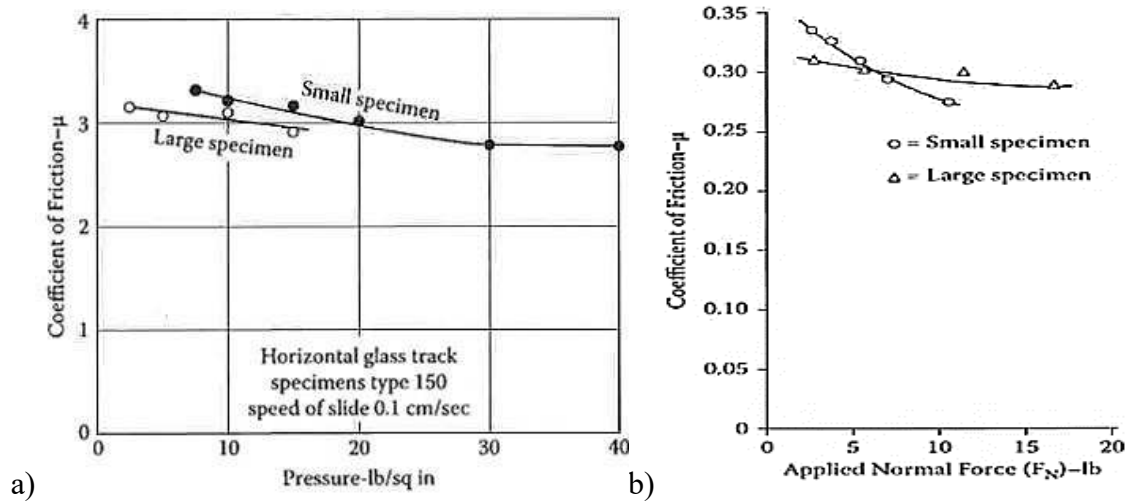
Figure 11. a) Coefficient of friction versus applied pressure b) coefficient of friction versus applied load for rubber specimens with different sizes on glass track [37].

In 1952, Schallamach presented two theories related to the load dependence and the velocity and temperature dependence of rubber friction. In the first theory [38], friction is proportional to the real contact area, when each asperity is assumed hemispherical. According to the second theory, frictional sliding of rubber is a rate process [29]. Roberts later established a coupling optical observation method to measure the friction in lubricated conditions [39][40].

2.3.1.4 Correlation of friction to the real area of contact and roughness

In 1952, Schallamach [38] conducted friction experiments produced by sliding moulded rubber drag sleds on a smooth glass. To approximate the real contact area of rubber with glass, Schallamach applied the Hertz equation at the suggestion of Bowden [41]. This is believed to be the first time that the Hertz equation was applied to examine rubber friction. Also, Schallamach assumed that the asperities were hemispherical, and the glass track is perfectly flat.

To determine the deformation of the asperities, three moulded rubber samples with different stiffnesses (soft, medium and hard) and with a hemispherical shape, were compressed onto the glass surface. It was found that the radii of the apparent contact areas of the three rubbers in contact with the glass were proportional to $F_N^{1/3}$. Schallamach [38] results are presented in Figure 12a and b which show that the rubber friction decreases with increasing load and pressure applied. There is little uncertainty that magnitude of the adhesive friction force depends on the real area of contact.

39
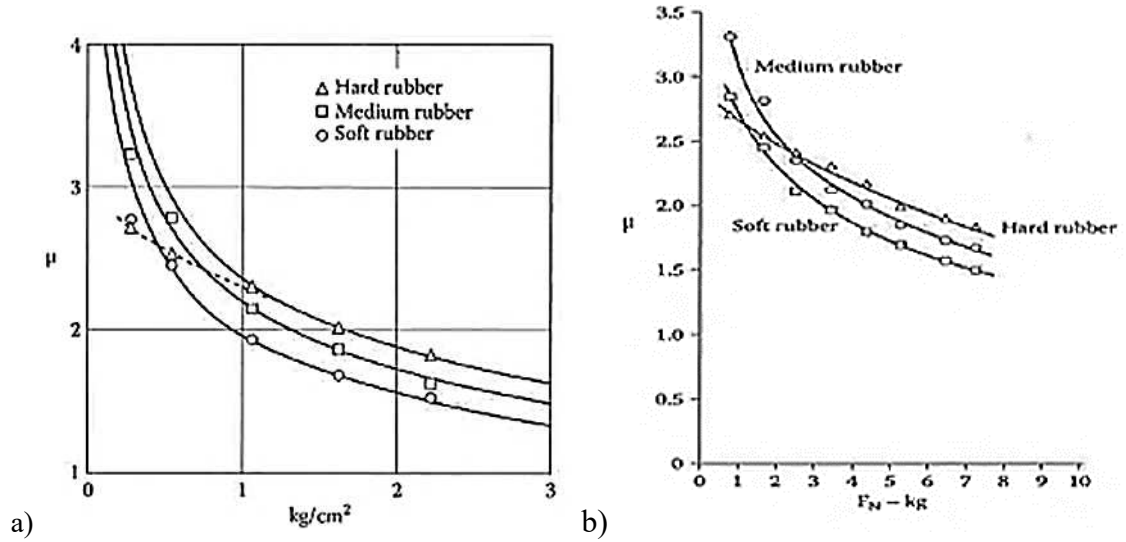
Figure 12. a) Coefficient of rubber friction (μ) versus applied pressure and b) coefficient of friction (μ) versus applied force (FN) recalculated from Schallmach [38].

More specifically, the effect of load on friction as predicted by Schallamach [29] and Barquins [42], using Hertz theory, is given by:

$$\mu = \pi S(9R/16E)^{2/3}W^{-1/3} \tag{6}$$

where R is the reduced radius, E is the elastic modulus, S is the interfacial shear stress and W is the load.

Persson [43] presented a new theory of rubber friction for rough surfaces. According to his theory, hysteresis is linked with the long-wavelength surface roughness, while adhesion is linked with the short-wavelength surface roughness. For rough surfaces, a large fraction of friction is attributed to the energy "dissipation" caused by internal frictions of the rubber (previously known as hysteresis). The adhesion component plays a vital role when surfaces are clean which leads to extra viscoelastic deformation at low sliding velocities. The results of this theory have been compared with other experimental results [18][22] and its rationality has been confirmed by numerous studies related to rubber friction [44][45]. Persson's theory is based on the assumption that the contact pressure probability distribution is due to a diffusive process in terms of the magnification at which the interface is observed [36][46]. This allows solutions to be exact in full-contact conditions and may fail in partial contact conditions [21].

2.3.1.5 Wear of compliant materials and rubber

Rubber wear has an influence on the performance of the wiper blades both in terms of friction force and sealing capabilities. There are different causes of wear of rubber wiper blades. The most common causes are the use of the wiper blade for more than six months (recommended time for the wiper to be changed by automotive manufacturers) and the degradation of the wiper blades due to the exposure to the sunlight and snow over a period of time. Friction coefficient is one of the important properties of the rubber contact to determine the type of wear. Figure 13 shows the schematic diagram of the friction and wear mechanisms of elastomers.
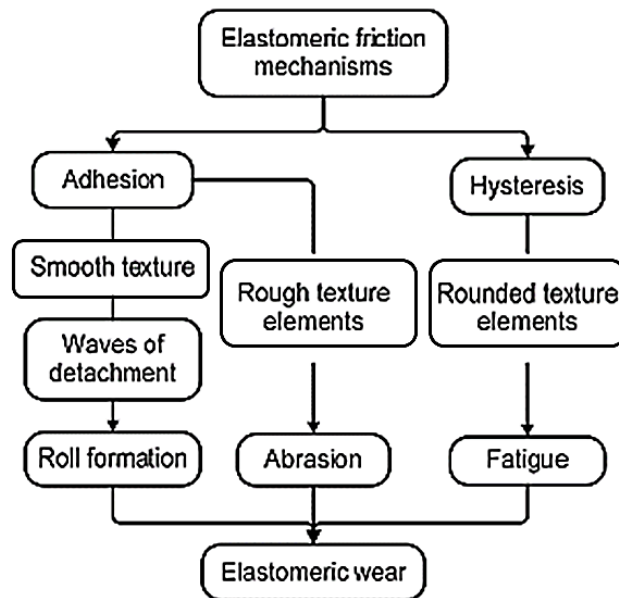
Figure 13. Schematic diagram of the friction and wear mechanism in rubber-like materials [49].

When rubber is sliding against a rough surface, distinct types of wear can be identified, such as abrasion and fatigue wear. Abrasion wear occurs because of tearing of the sliding surface of the elastomer, whereas fatigue wear happens on the surface of an elastomer slides repeatedly against hard substrates with rounded asperities [47]. Figure 14 shows the mechanism of the unidirectional abrasion of the rubber [48]. It consists of parallel ridges lying perpendicular to the sliding direction and regions where wear is concentrated at the base. The wear pattern is related to the rate of wear, increasing with the frictional load and with the compliance of the rubber [49].
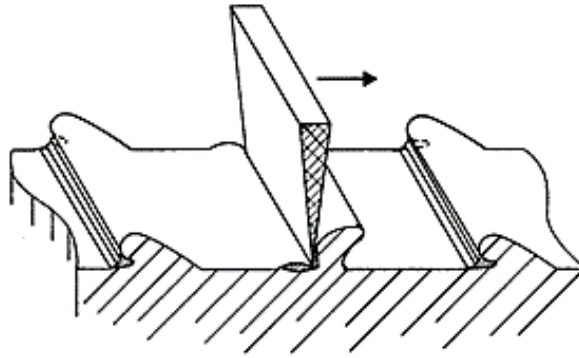
Figure 14. Sketch of surface wear pattern (cross section), showing parallel ridges lying perpendicular to the sliding direction and regions where wear is concentrated at the base [48].

Also, Roberts [49] mentions that when the abrasion wear occurs, large pieces of debris are produced because the crests detach from time to time. On the other hand, when rubber is sliding on a smooth surface, the adhesion forces are responsible for the friction and give rise to adhesive/smearing wear as discovered by Schallamach [50].

2.1.3.6   Rubber friction in other applications

Rubber friction is also important in the context of rubber sealing applications and in the design of shoes and tyres. The rubber is designed to enhance friction and grip in shoes as inappropriate grip can cause slipping and falling leading to death and injury in the workplace. Hence, are an important consideration for many companies [51].

The coefficient of friction in shoe soles and floors has been adopted to ascertain the slipperiness level [52] and a slip is more likely to occur at a low coefficient of friction. In the UK, there are two shoe-surface tests to evaluate the risk of the slipping during a heel strike, such as the pendulum test device (BS 7976-2:2002 characterizes flooring slip-risk) and a second test (BS EN ISO 13287:2007 characterizes footwear slip-risk) to assess the slip resistance of occupational footwear [53]. The outsoles of the shoes are mostly in contact with the hard surfaces with a specific roughness as shown in Figure 15a. Therefore, the friction between the shoe and hard surface (road) arises from the rubber outsoles being deformed on the asperities of the road (see Figure 15b).

Chang *et al.* (2001a) mentioned that during a slip, the friction of a shoe-floor interface (rubber-hard substrate), is dependent on the material properties, contact area, pressure, velocity, contact and time.
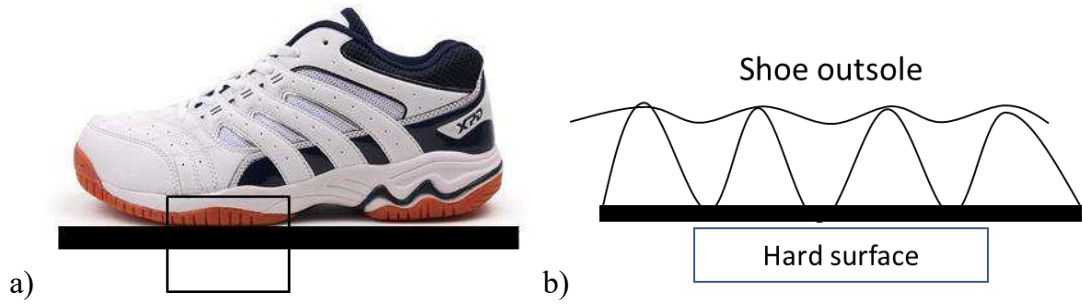
Figure 15. a) Interaction between rubber and hard surface and b) Friction mechanism interaction between the rubber and hard surface. Adapted from [22].

Rubber friction has also been studied in automobile tyres system. The friction between automobile tyres and the road is important as it determines the maximum acceleration, and minimum stopping distance [54]. In 1966, a unified theory for tyres' friction was proposed by Kummer [55]. This theory was expressed by equation 7, shown below:

$$F_{T=}F_A + F_{HB} + F_C \qquad (7)$$

where F_T is overall friction developed between sliding tyre and the pavement, F_A, friction contribution from the adhesion between the rubber and the pavement, F_{HB}, friction contribution from bulk deformation hysteresis in the rubber and F_C, cohesion loss from the rubber wear and tear.
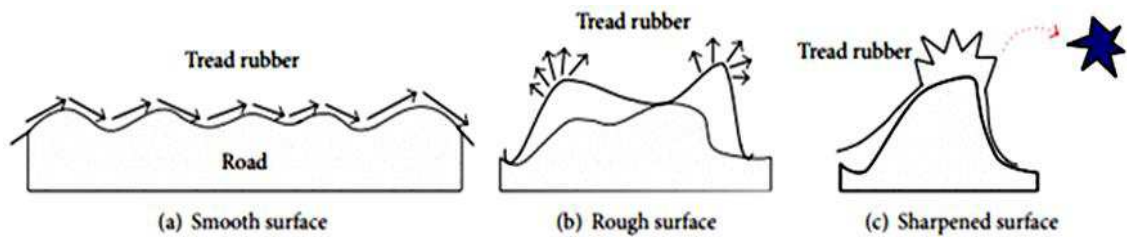
Figure 16. Friction mechanism on texture of road surface [56].

The adhesion represents the molecular interaction between the rubber and the components of the road. The adhesion is higher on a dry and smooth road and the hysteresis friction loss is lower (see Figure 16a). On wet and rough roads, the adhesion is less, and hysteresis friction loss is higher (see Figure 16b). The cohesion friction is high when the road surface is very rough (see Figure 16c). The cohesion friction loss compared to the total tyre coefficient of friction is negligible in comparison to the adhesion and hysteresis losses. The grip, especially on the icy or snowy road surfaces, depends on the friction mechanism [57].

2.3.2 Wet sliding compliant contacts

2.3.2.1 Lubrication regimes and the Stribeck curve

The concept of the lubrication regimes was introduced by Richard Stribeck [58] to explain the effect of speed, viscosity, and load on friction of a liquid lubricated contact. There are three different lubrication regimes:

- **Boundary lubrication** occurs at low speed where there is insufficient entrainment of lubricant to separate surfaces. Friction results from the shearing of the contacting interface and is therefore strongly influenced by the presence thin surface films.

- **Mixed lubrication** occurs at intermediate speeds where fluid entrainment of fluid is sufficient partially to separate the sliding surfaces. Here, the applied load is supported by a combination the fluid film and regions of asperity contact. Friction decreases with speed due to the separation of surfaces.

- **Hydrodynamic lubrication** occurs when fluid entrainment has completely separated the surfaces. Here, the friction coefficient increases with velocity due to the viscous losses in the fluid.

Figure 17 shows a typical Stribeck curve representing the variation of friction coefficient with Stribeck parameters (velocity v, viscosity η and load P).
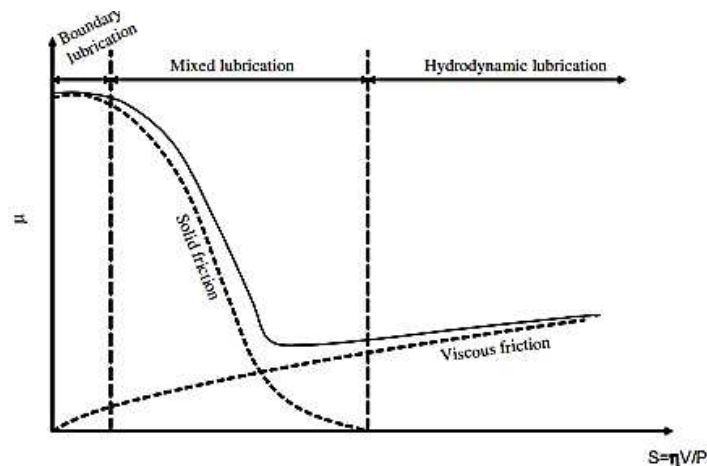
Figure 17. Stribeck curve shows the friction coefficient (μ) against Stribeck parameter (S = velocity v × viscosity η / load P) [59].

When a sliding contact between a wiper blade and a glass surface submerged in liquid is considered, it can be understood that there are four possible sources of friction. These are: a) adhesion between the rubber and the glass, b) the hysteresis (deformation) friction, c) mixed friction from shearing of surface layers, and d) fluid friction from shearing the fluid film. These contributions are shown pictorially in Figure 18. This complex, interconnected system explains why windscreen wiper friction is an intricate and challenging area of research.
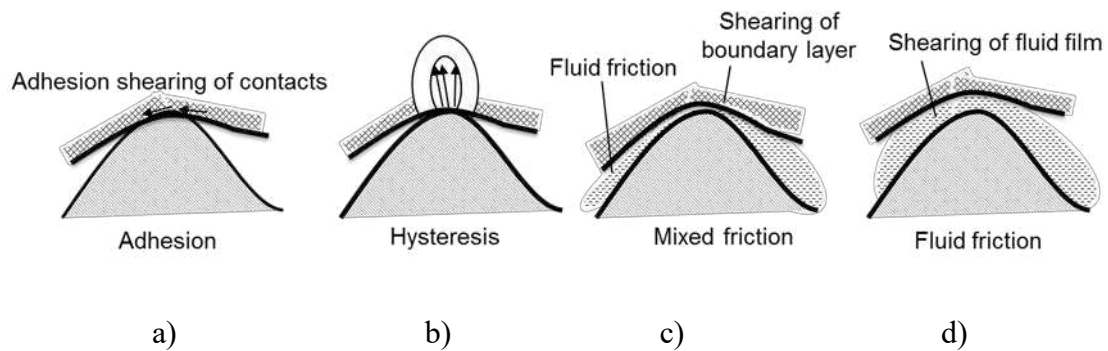
Figure 18. Representation of typical friction sources: a) adhesion, b) hysteresis, c) mixed lubrication, and d) fluid friction adapted from [60].

2.3.2.1.1   Boundary regime

A considerable amount of research has been carried out on boundary lubrication of metals; however, this is less relevant to the current project since metals have a highly polar surface and therefore interact differently to rubber in the presence of boundary lubricating chemicals. Considerably less work has focussed on boundary lubrication of rubber, except that by Richards and Roberts [61]. They measured the thickness of boundary films in lubricated rubber contacts using a new apparatus which uses a laser. The behaviour of surfactant solution boundary films in rubber/glass contact and films in rubber/rubber contact have been explored.

2.3.2.1.2   Mixed regime

The mixed regime is of considerable importance when considering windscreen wiper behavior. Firstly, rubber wipers operate mainly in the mixed regime. Furthermore, the negative slope of the friction vs. speed curve, which is characteristic of the mixed regime, is responsible for squeak vibration, described in the final section of this review.

The action of fluid that is trapped between the polymer and the surface at low entrainment speeds will result in a decrease of polymer's deformation, which smoothens the hard surface [19]. The hydrodynamic behaviour will reduce friction by separating the sliding surfaces due to the emergence of a liquid film at higher speed.

Persson and Scaraggi [62] predicted the transition from boundary lubrication to hydrodynamic lubrication using Hertz theory for soft contact with random roughness. They simulated the Hertzian contact and coefficient of friction as a function of [(viscosity x sample length)/ load] ($\eta L/F$) and v velocity for wiper blades and compared it with experimental results (see Figure 19).

a)   b)

c)   d)
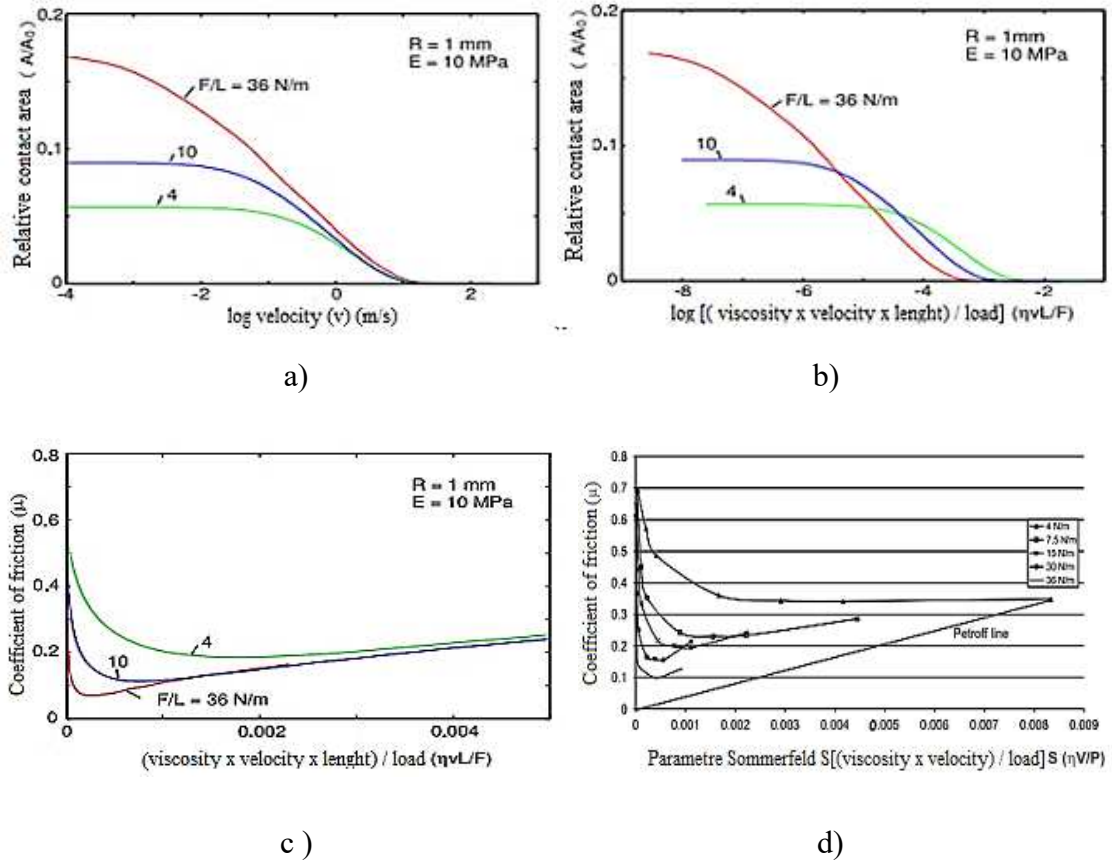
Figure 19. a) Relative contact area vs. log(v), b) Relative contact area against log($\eta vL/F$), c) Coefficient of friction against $\eta vL/F$ simulation and d) experimental result [62].

Figure 19a and b describe the relative (projected) contact area as a function of the logarithm of (viscosity x sample length) / load ($\eta L/F$) and as a function of velocity (v), respectively. It should be noted that the relative contact area for low sliding velocities is

based nonlinearly on the load, but this is due to the rise of the nominal contact area A_0 with increasing load ($A_0 \sim F^{1/2}$ for the cylinder contact), and A is proportional to the load in the current case. In Figure 19c shows the same but on a linear scale. The results presented in Figure 19d are related to the results obtained by Koenen *et al.* [59], although in this application it is likely that the surfaces are smoother and the rubber elastic modulus is higher than the rubber elastic modulus used in the model calculation. In addition, the radius of curvature of the rubber edge in contact with the glass surface is likely to be smaller than R = 1 mm used above.

Persson and Scaraggi also modelled a full Stribeck curve that includes all three lubrication regimes by developing (approximate) analytical expressions for fluid flow factor and frictional shear stress factor [63]. Numerical results for a rubber cylinder with different surface roughness sliding on a lubricated flat disc, under different pressure conditions, were studied. In addition to this, the role of the elastic deformation of the surfaces due to presence of lubricant was also discussed.

2.3.2.1.3   Hydrodynamic regime

A contact is operating in the Hydrodynamic regime when there is sufficient fluid entrainment to completely separate the sliding surfaces. Under these conditions, it is relatively straightforward to predict contact behaviour, since micro- and nano-scale surface effects play a less critical role. The hydrodynamic behaviour will reduce friction by separating the sliding surfaces due to the emergence of a liquid film at higher speeds.

For contacts with rigid surfaces lubricants iso-viscous (hydrodynamic conditions), film thickness and friction can be simply predicted using Reynolds' Equation, which is based on the liquid pressure that is developed between sliding [64].

If the pressure in the contact is sufficiently high, then the effect of pressure on viscosity must be considered. For windscreen wipers, however, pressure is low (around 1 MPa) and changes in viscosity are negligible. If the sliding components are compliant, then Reynolds' Equation must be solved along with deformation equations in order to predict film thickness as demonstrated by de Vicente *et al.* [65][66].

Bongaerts *et al.* [67] studied the influence of surface roughness and hydrophobicity on friction in soft lubrication. He used the same method as Vicente to obtained full Stribeck

curves. It was found that the surface roughness and hydrophobicity level have a significant influence on friction in boundary and mixed lubrication regimes. However, as expected, frictional properties did not seem to be affect by the surface properties in the hydrodynamic regime.

2.3.3 Drying conditions

For a contact between rubber and glass, there is a third environment than can occur in addition to the dry and wet conditions outlined above. This is namely the "tacky" (or in this research as "drying") regime and exhibits unusually high friction and squeaking noises. This behaviour has generally been attributed to meniscus effects, as shown in Figure 20 [19].
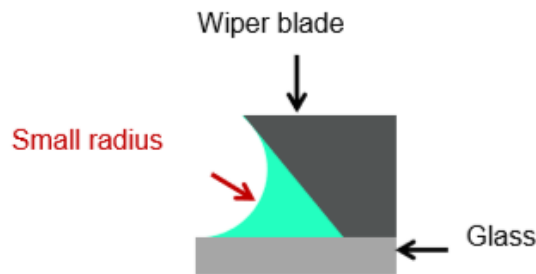
Figure 20. Simple schematic diagram showing capillary mechanism increasing friction under tacky conditions.

Experiments [68] have shown that the presence of a water capillary bridge between rubber and glass pulls the rubber into contact with the substrate and the real contact surface is higher than the one in perfectly dry contact. In order to explain the significant increase in friction given the pressure applied in the nominal contact area is already significant in wiper blade applications, it was estimated that the additional contribution of capillary bridges must be very high (typically resulting in friction being increased by about a factor of two), in the order of MPa [20].

The increase in friction can be based on two counts: the negative capillary pressure acts to increase the attractive force between the rubber and glass, leading to an increase in the real contact area (area of dry contact) [69]. This increase results in a greater level of work to shear these junctions and hence friction increases. In addition, the menisci are often entrapped within the contact region [69], resulting in shear of the fluid against the substrate as the contact moves [68][70]. This can prevent the wiper from functioning

correctly. To alleviate this problem, capillary adhesion can be reduced by surface treatment of the rubber with halogenation [59].
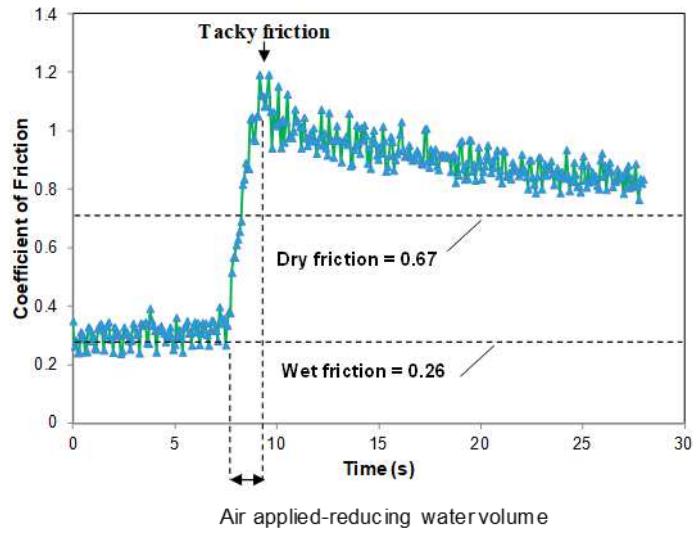
Figure 21. Friction against time for wiper specimen sliding at against untreated glass under drying/tacky conditions (steady-state friction values for dry and submerged friction are also given for reference). The normal load is 17 N/m, and the sliding speed is 0.25 m/s [71].

Figure 21 shows the variation in friction with time, for a contact under "drying" conditions. Initially, the contact is submerged in water and friction is low. From this point onward, water is removed from the specimens by evaporation as a stream of air is aimed at the glass disc. After ~8 seconds, the contact itself begins to dry, and friction increases to reach a maximum when the tacky condition is reached. The maximum value of the coefficient of friction is much higher than for the same contact under dry conditions. As the remaining water is removed from the contact, (*i.e.*, from ~10 seconds onwards), friction approaches that for the steady-state dry condition.

A major factor that is linked to tacky friction and also helps to describe the wiping quality is related to contact angle value of the surface. When a droplet is deposited on a surface, the liquid interacts with the solid and forms a sphere-like shape. The tangent (angle) of the sphere in contact with a flat surface is known as the contact angle. By measuring the value of the contact angle of a surface, the surface can be classed as a hydrophobic or hydrophilic surface. If the contact angle is lower than 90°, the surface is classed as hydrophilic, while if it is larger than 90°, it is classed as hydrophobic (Figure 22) [72]. Windscreen coatings are, in most cases, hydrophobic with a contact angle around 100-

110°. Lower polarity (low surface energy) of the surface is preferred by car manufacturer because it does not form a water film [72]. More specifically, since water is a polar liquid it is attracted to and spreads readily on surfaces which are similarly polar; therefore non polar surfaces result in beading and non-continuous water films, which are more easily removed.
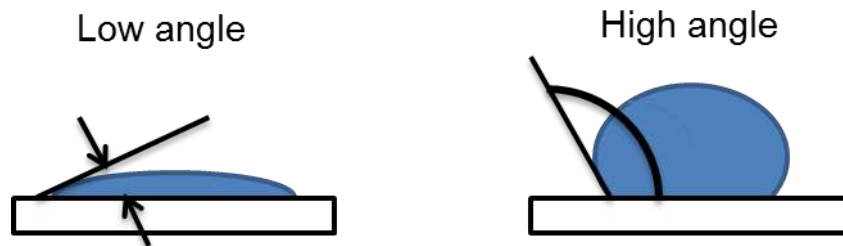
Figure 22. Water contact angle measurement of windscreen adapted from [72].

2.3.4 Experimental techniques for compliant contacts

In recent years, research on wiper blades has attracted increasing attention from car manufacturers. The important aspects for them are: wipe quality, friction reduction, and avoidance of noise. One of the aims of this thesis is to study the wiping quality and detect the sealing limit. To achieve these aims, the water film thickness between the wiper blades and the glass inside and outside contact should be measured. However, there are still relatively few publications in this area. In this section, these papers are discussed briefly. Fagervall and Nyman [72] found an improvement in wiping quality could be achieved by applying different coatings on a windscreen, such as titanium oxide and fluorine-silicone. However, the thickness of such coatings was limited to less than 1 μm due to legal requirements. Koenen [59] carried out experimental research, simulating a water lubricated wiper/glass contact. Results showed that friction varied with speed according to typical Stribeck curve behaviour, as outlined in section 2.3.2.1. Deleau *et al.* [68] found two factors which contribute to the friction in a dry contact, namely the adhesion force and energy dissipation force resulting from the deformation of the wiper materials.

A rig was adapted to measure the thin film between wiper blades and glass by Deleau *et al.* [68] (Figure 23). This equipment was used to study the quality of wiping and estimate the film thickness of the fluid in contact by Interferometry. Roberts [73] found this method unsatisfactory for a glass plate and hemispherical smooth rubber surface.
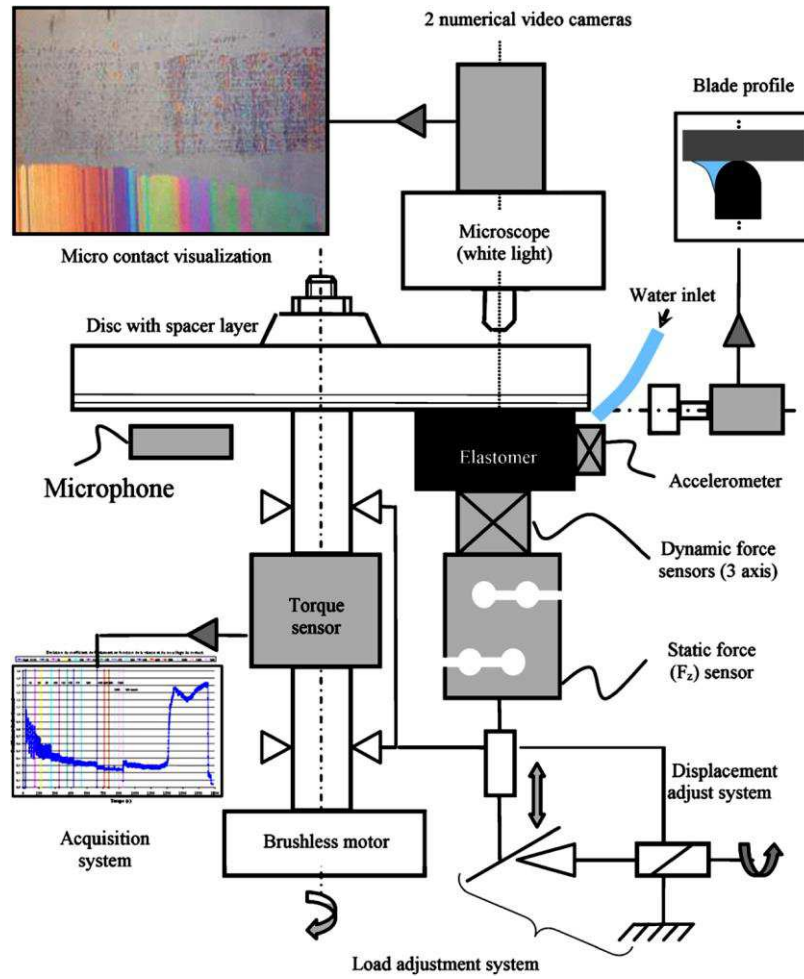
Figure 23. Description of the IRIS Tribometer [68].

Another technique used to measure the film thickness is Laser Induced Fluorescence (LIF). Poll *et al*. [74] presented such experimental results on the fluid film thickness in a rotating rubber lip, and explained that the LIF technique is significantly flawed. Thereafter, film thickness of a compliant contact was successfully measured by Myant *et al*. [75]. In this study, the contact was between an elastomer hemisphere and an uncoated glass disc, lubricated by fluorescent dye-containing oil. They detected a minimum value of film thickness of 300 nm, when only one fluorescent dye is used. To measure a film less than 300 nm, a new technique was developed, called two-dye LIF radiometric by Hidrovo [76].

An ultrasonic reflection technique was used to measure the film thickness in the isoviscous elastic lubrication regime [77]. Here, an ultrasonic transducer is excited by a voltage signal from pulser-receiver so that it sends an ultrasonic wave towards a lubricant film and also measure the reflection. The film thickness of the lubricant can then be determined from the proportion of the wave that is reflected back, the frequency of the

ultrasonic wave, the density, and the speed of sound. However, the lateral resolution of this technique limits its application to contacts with very small contacts area.

2.4   Influence of noise and friction on the wiping mechanism

The focus of this section is on reducing noise between the windscreen and wiper blade, which can cause an unwanted distraction to car drivers. There are a few papers that describe the research on the initiation of this noise – a phenomenon, which is believed to result from friction-induced vibration between the wiper blade and the glass.

There are four different types of noise that occur in wiper blades:

(1) "Reversal noise" occurs due to the impact of rubber against glass as the wiper changes direction [78].

(2) "Flutter," "chatter," or "beep noise" [79] is a vibration of the whole wiper arm and typically has a frequency around a few hundred hertz.

(3) Wiper noise has also been reported by various researchers, with a frequency between 500 and 1000 Hz occurring close to reversal [80]. This noise can be reproduced in a lab using a contact between glass rubber wiper (*i.e.*, without the full wiper arm assembly) [68] [80]

(4) Although largely unresearched, another type of noise is known to drivers and the wiper industry. As with type (3) above, this noise occurs close to reversal, however its frequency is typically between 2500 and 3500 Hz and is particularly problematic since this falls within the most sensitive frequency range of the human ear [81].

The current concern is with the third and fourth types of noise, which are typically heard before and after reversal. This observation led Goto and co-workers to suggest negative damping, due to the slope of the friction versus speed curve, as the cause of this instability [80], a well-known mechanism that occurs in contacts under mixed lubrication [82][83].

This was subsequently confirmed by Le Rouzic and co-workers, who compared vibration analysis and friction measurement [84]. This type of friction-induced vibration is believed to be caused by the negative gradient of the friction versus speed (*i.e.*, Stribeck curve) and is related to classic "stick–slip" behaviour, which is thought to arise in dry contacts due to the rapid instantaneous transition between static and kinetic friction [85].

The studies by Goto *et al.* [80] and Le Rouzic *et al.* [84] have advanced our understanding of why friction-induced instabilities arise in windscreen wipers; however, a number of unanswered questions remain regarding the generation of audible noise and the role of different parameters. For example, does the frequency of vibration depend on conditions within the contact or on the structure and material properties of the rubber wiper? An additional complication arises due to the meniscus of water that builds up at the rubber wiper lip as it passes over the glass surface. The water meniscus is likely to affect the emitted noise; however, no studies have been carried out to elucidate its role. A further area of uncertainty is how the condition of the contacting surfaces affects friction induced vibration.

A number of researchers have used a simple spring-mass-damper system to analyse quasi-harmonic friction induced vibration [82] [86] [87]. Although these models often only describe very simple systems (for instance the sliding of single flat rigid blocks) undergoing relatively low frequency vibration, they provide some basic insights into squeak behaviour and its possible prevention. The differential equations of motion for these systems contain a damping term, which is the product of a damping coefficient and the sliding velocity. For a system undergoing non-oscillatory motion, the damping term is positive and results in a force that opposes motion and dissipates energy. If a component exhibits Stribeck behaviour, however, where friction decreases with speed, then the damping term can become negative so that energy is added to the system rather than dissipate. This unstable behaviour results in squeak.

A simple mathematical model, which explains this type of instability, was initially proposed by Eaton [88] (Figure 24). This model is summarised in the following section since it provides a clear explanation as to why squeak occurs and how it can be controlled.
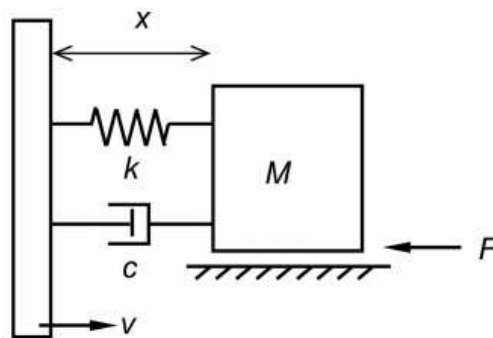
Figure 24. Damped linear system subject to disturbances.

The equation of motion for mass M is given by

$$M\frac{d^2X}{dt^2} + c\left(\frac{dX}{dt} - v\right) + k(X - vt) = -F \tag{8}$$

where X is the displacement of the mass M at time t

v is the drive velocity

c is the damping coefficient of the dashpot

k is the spring contact

F is the frictional resistance.

If v is constant, equation 6 can be written in terms of the spring extension, x:

$$M\frac{d^2x}{dt^2} + c\frac{dx}{dt} + kx = -F \tag{9}$$

For small variations about the velocity v, the friction force may be expressed as:

$$F = F_v - \lambda\left(\frac{dX}{dt} - v\right) \tag{10}$$

where λ is the gradient of the friction versus speed curve (*i.e.*, Stribeck curve), as shown in Figure 25. Combining equations 9 and 10 gives:

$$M\frac{d^2x}{dt^2} + c\frac{dx}{dt} + kx = -\left(F_v - \lambda\frac{dx}{dt}\right) \tag{11}$$

which can simply be rearranged to give:

$$M\frac{d^2x}{dt^2} + (c - \lambda)\frac{dx}{dt} + kx = -F_v \tag{12}$$

The solution to this differential equation has several forms and depends on a quantity known as the damping ratio:

$$\zeta = \frac{c - \lambda}{2(Mk)^{\frac{1}{2}}} \tag{13}$$

For $|\zeta| < 1$:

$$x = Ae^{-\zeta\omega_n}\sin\left[\omega_n(1 - \zeta^2)^{\frac{1}{2}}t + \varepsilon\right] \tag{14}$$

for $|\zeta| > 1$:

$$x = A_1 e^{\left[-\zeta\omega_n + \omega_n(\zeta^2-1)^{\frac{1}{2}}\right]t} + A_2 e^{\left[-\zeta\omega_n - \omega_n(\zeta^2-1)^{\frac{1}{2}}\right]t} \tag{15}$$

and for $|\zeta| = 1$:

$$x = (A_1 + A_2 t)e^{-\zeta\omega_n t} \tag{16}$$

where ω is the undamped natural frequency, $\omega=(k/m)^{1/2}$, and A, A_1 and A_2 are constants determined by the initial state of the system.

The responses of the system, described by equations 14 – 16, are shown in Figure 26 where the strong effect of the damping ratio, ζ, on the subsequent motion can be seen. Most notable is the fact that unstable oscillatory motion occurs when the damping ratio is negative. Examining equation 13, shows that such negative damping will occur, if the drive damping, c, is low and friction-velocity gradient, λ, is high.

Therefore, when a system with these atributes is subject to a disturbance, the response will be oscilliatory with increasing amplitude (*i.e.*, unstable, shown by Figure 26d). This simple model shows why oscillations occur in windscreen wiper systems, in which the negative slope of the Stribeck curve (due to the reduction in friction due to the increased entrainment of water) outweighs the drive damping (due to the damping properties of the rubber blade material).
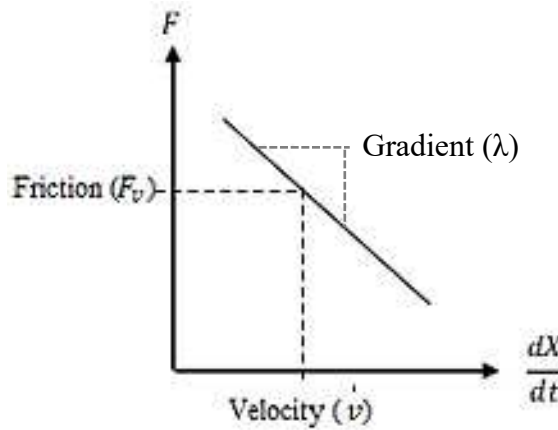
Figure 25. Representation of friction versus speed behaviour.

55
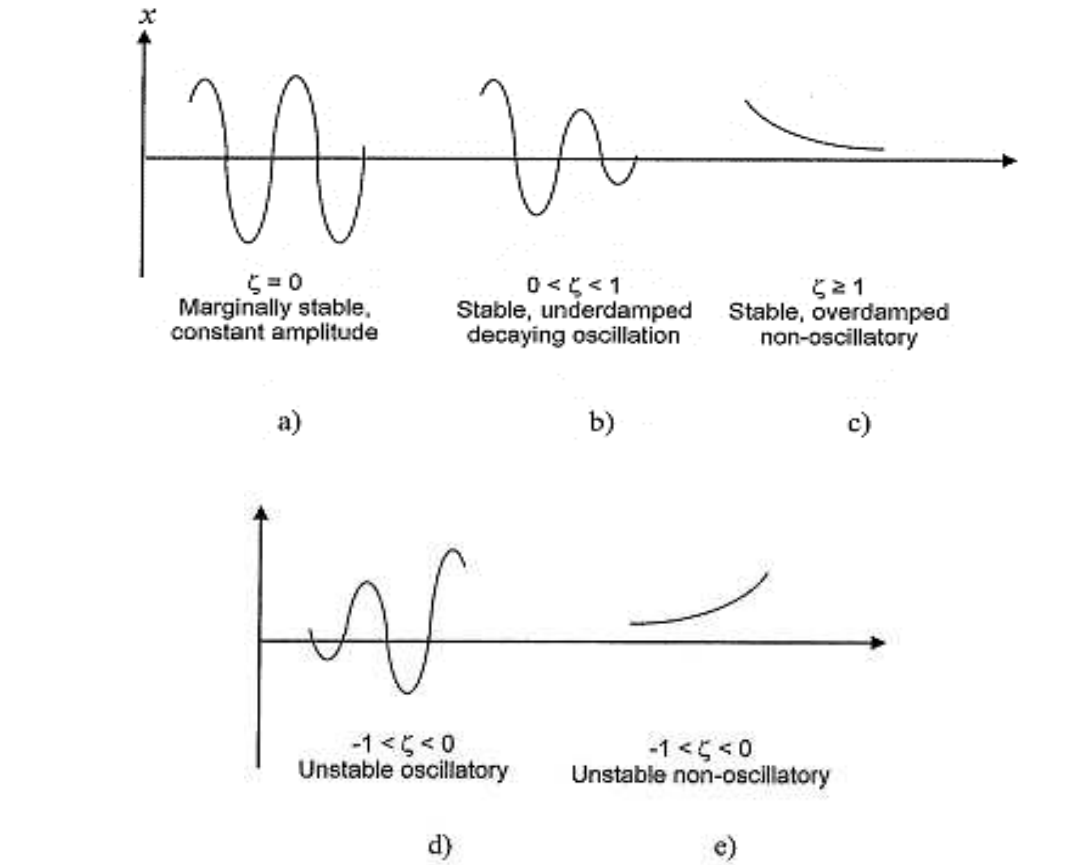
Figure 26. System responses, depending on damping ratio, ζ [40].
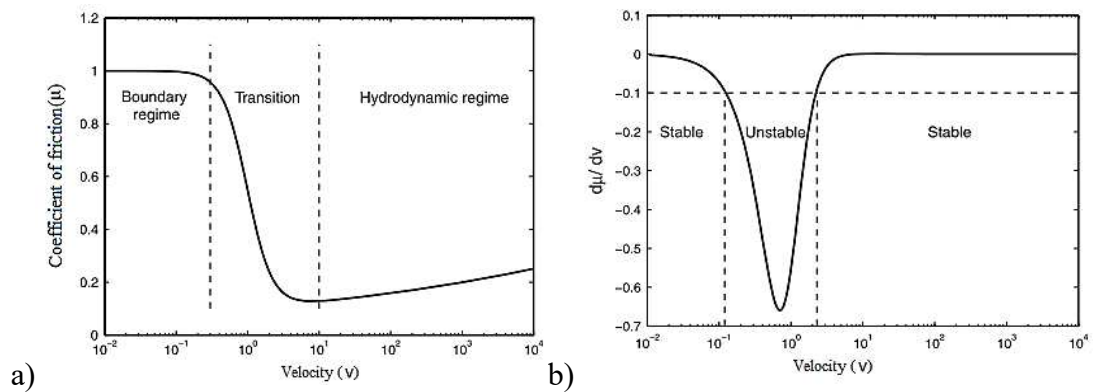
Figure 27. Correlation between a) Stribeck master curve and b) instability of mathematical model system for wiper blades [37].

A similar analysis was carried out by Le Rouzic *et al.* [37], who importantly combined theoretical predictions of instability with measured recordings of squeak. The agreement between the two proved that squeak occurs due to negative damping characteristics caused arising from the shape of the Stribeck curve in the mixed regime (Figure 27a and b).

2.5 Summary

This review has covered the following interlinked areas. It started by describing the function of windscreen wipers and then detailed the theory regarding the friction of compliant materials under both dry and water submerged conditions. The review has shown that it is important to investigate more closely a number of different dynamic phenomena that effect wiper performance but remain poorly understood. These include *i*) friction-induced vibration, *ii*) rubber friction (static and kinetic) and *iii*) wear. Each of these factors are interconnected with the following corresponding aspects of wiper performance and design: *i*) noiseless operation, *ii*) motor selection, *iii*) durability and component life. While friction studies of lubricated compliant contacts have been explored in general in the last decade, film thickness behaviour has received considerably less attention. The liquid film thickness separating sliding surfaces is a critical parameter connecting each of the dynamic phenomena mentioned above. The only film thickness measurement technique to have been tried here is interferometry and this was applied mainly outside the wiper contact. A disadvantage of this technique is that it requires the two surfaces in contact to be reflective. Unfortunately, however, rubber wipers are not reflective, which limit the use of this method. Therefore, the most promising technique to measure the wiper film thickness appears to be laser-induced fluorescence.

Finally, many studies have been proposed to model friction induced vibration of compliant contacts; however, this issue has not yet been resolved. For instance, the source of the squeak noise and the role of different parameters involved in this situation are still not fully elucidated.

Chapter 3

Materials and Methods

3 Materials and Methods

In this chapter, material properties of rubber and glass specimens are first presented. Following this, the methods used to characterize a rubber/glass contact, in terms of friction, squeak frequency and film thickness are described.

3.1 Materials

3.1.1 Rubber specimens

Wipers are made of natural or synthetic rubbers (elastomers), which are polymers with long chains that make up a randomly coiled structure. In their amorphous state, these molecules show a low degree of crosslinking, which gives a high degree of mobility to material that causes a permanent intermolecular movement. It is therefore necessary to vulcanize or polymerize the rubber to bind the polymer chains together and increase the number of crosslinking nodes (Figure 28) [89]. This leads to better mechanical proprieties such as higher elasticity and reasonable stiffness at high temperatures.
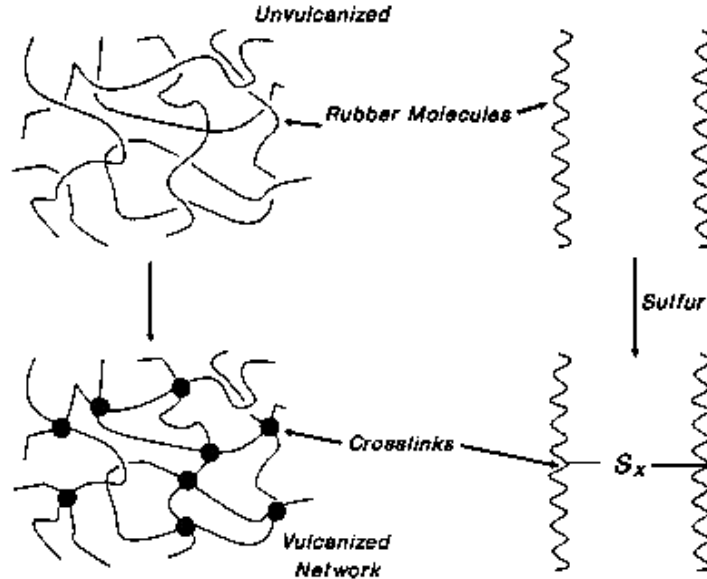
Figure 28. Rubber vulcanisation process [89].

The rubber used for wipers is also chlorinated to increase its resistance to abrasive wear and lower its friction in wet and drying conditions. In addition to this, the wipers are often coated with hydrophobic coatings which have similar effects as chlorination.

Examples of some of the widely used rubbers, used in this study, include ethylene-propylenediene monomer (EPDM), ethylene-propylene monomer (EPM), chloroprene rubber (CR) and natural rubber (NR).

The elastic proprieties of the wipers were provided by Bosch. Their Young's Modulus or elastic modulus varied from 1 MPa to 6 MPa and their Poisson's ratios (v) were around 0.5. As discussed in Chapter 4, wipers with various coatings and roughnesses were used to investigate their effects on tribological performance. Various materials and geometries of wiper blades with different profile geometry and surface coatings were used in this work (Table 1).

Table 1 Specimen characteristics

Material	Profile	Coating
YL	P68612	PPC
PQ	P37612	PPC
HG	P32611	Graphite
FX	P37614	Graphite
L	P32611	PPC

The name of the wiper defines profile geometry and material. For example, the first letter refers to head material and second letter refers to lip material. There are different types of materials that have been combined in the manufacture of the wiper blades profiles used in this study: the first combination type involves the lip of the wiper blade being made of a material (Y, F, P, H, L) and the remainder being made by another material (L, Q, G, X), and the second combination involves the lower section of the lip (the division line of the materials is under the hinge) being made from one material and the remainder of the wiper being made from another (see Figure 29).
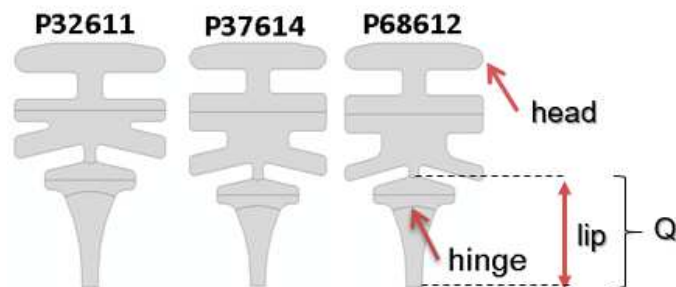
Figure 29. Wiper blade cross section for different profiles.

The first two numbers from the profile name represent the identification number of geometry, the third number is the width of the profile in mm and the last two numbers height of beam gap in mm. Figure 30 shows the dimensions of the P32611 wiper blade profile.
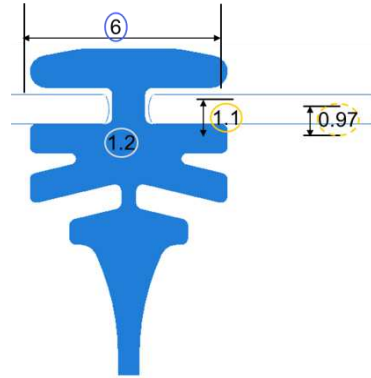
Figure 30. Schematic drawing of P32611.

The YL wiper blades with and without a plastic powder coating-PPC are the specimens that were most studied and analysed in this project.

3.1.2   Glass specimens

For the friction experiments, glass microscope slides were used as specimens to simulate the windscreen surface in the rubbing experiments. These are made of soda-lime glass (Corning Inc., USA) and are naturally hydrophilic. The dimension of the glass is 75×25 mm^2 and its thickness ranges from 0.90 to 1.10 mm. The reason for choosing microscope slides as specimens is that they are uniform and possess similar roughness to that of the windscreen of the cars. Also, their low cost meant that a new slide could be used for each test, thus reducing problems of contamination and therefore uncertainties in terms of repeatability.

For the film thickness experiments, another type of specimen was used. These were circular glass discs (75 mm in diameter and 1 mm in thickness). This larger size was required to enable the contact to be viewed from beneath using a microscope (as described in Section 3.6). The glass discs had no coating, were naturally hydrophilic and had a Young's modulus, Poisson's ratio and refractive index of 70 GPa, 0.24 and 1.517 respectively.

3.2 Methods for characterising the wiping components

This section describes how the surface of the components was characterised in terms of roughness, surface energy and chemical composition. This was necessary in order to understand how these properties affect friction and wear behaviour.

3.2.1 Contact angle measurements

The contact angle is the angle formed between a solid and a liquid. In this work, it was measured by the Static Sessile Drop Method (Figure 31a). The contact angle is important because it can be used to characterise surface energies of solids. The contact angle measurements are related to surface tensions or energies via Young's Equation:

$$\gamma_{SG} = \gamma_{SL} + \gamma_{LG}cos\theta \tag{17}$$

where γ_{SG} is the solid surface free energy, γ_{SL} is the solid/liquid interfacial free energy, γ_{LG} is the liquid surface free energy and $\theta\,°$ is the contact angle.

To measure the contact angle, a droplet was placed at a random location on the specimen surface and a photograph was taken. The contact angle was then evaluated using the drop analysis plugin of the Image J software. This software fits the drop to a predetermined profile to determine the contact angle (an example is shown in Figure 31b).
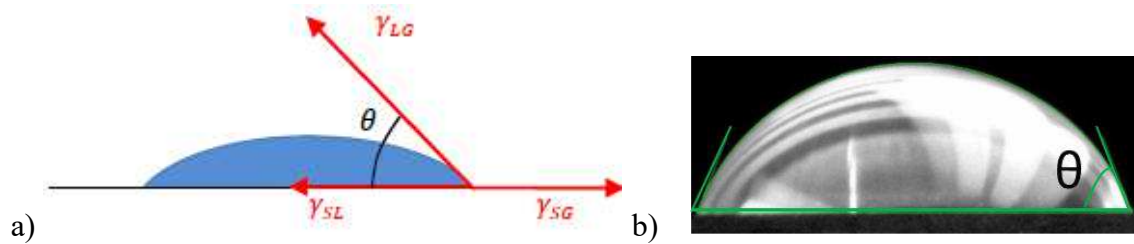
Figure 31. a) Method of Static sessile Drop and b) contact angle measurement using Image J software [69].

The surface energy was calculated by combining the OWRK Equation (Owens, Wendt, Rabel and Kaeble) and Young Equation (Equation 18) [90][91]:

$$\gamma_L(1 + cos\theta) = 2\sqrt{\gamma_S^d \gamma_L^d} + 2\sqrt{\gamma_S^p \gamma_L^p} \tag{18}$$

where γ^d are the apolar forces and γ^p are the polar forces. The OWRK Equation is used when the effect of polar or disperse interactions on wettability and adhesion is studied. To calculate the surface energy, the values of the components of superficial tension for the two solvents are necessary (Table 2). The contact angle results (average of three measurements) for the different coatings are shown in Table 3 and have been validated against similar measurements made by the company.

Table 2 Values of the components of superficial tension for the two solvents [4].

Solvent	γ(mJ/m^2)	γ_L^{LW}(mJ/m^2)	γ_L^{AB}(mJ/m^2)	γ_L^+(mJ/m^2)	γ_L^-(mJ/m^2)
Water	72.80	21.80	51.00	25.50	25.50
Ethylene Glycol	48.00	29.00	48.92	1.92	47.00

Table 3 Contact Angle and Surface Energy measurements of three different coatings and bare glass.

Rectangular Glass	Contact Angle (°)		Surface Energy (mJ/m^2)
	Water	Ethylene Glycol	
Bare Glass	18	15	82.21
Ceroxide	25	20	77.09
HGT	54	40	47.36
OTS	82	72	23.09

3.2.2 Roughness Measurements

Two techniques were used to measure the roughness of the wiper blades and glass coatings: Atomic Force Microscopic (AFM) and Wyko Scanning White Light Interferometry (SWLI). The former was used to measure the roughness of the glass coatings while the latter was used for the roughness of the wiper blades.

3.2.2.1   Atomic Force Microscopy (AFM)

The AFM consists of a tip that is located at the free end of a cantilever and is positioned close to the sample surface. When the tip and the sample surface are in contact the cantilever bends. The AFM images are realised from the movement of the tip, which maintains the repulsive force constant between tip and surface during the scanning process.

With this technique it is possible to characterise different materials (conductive, semi-conductive, biological materials) in different environments (air, liquid, vacuum) [92]. The limitations of this technique are that the scanning area is restricted, and that the maximum height is 10-20 µm.

AFM measurements were carried out on a Multimode Atomic Force Microscope Nanoscope IIIa (Digital Instruments, USA) in tapping mode at room temperature. The scanned area for imaging the samples was $2 \times 2\mu m^2$. 2D and 3D AFM images of octadecyltrichlorosilane (OTS) coated glass microscope slides are shown in Figure 32a and b.

a)   b)
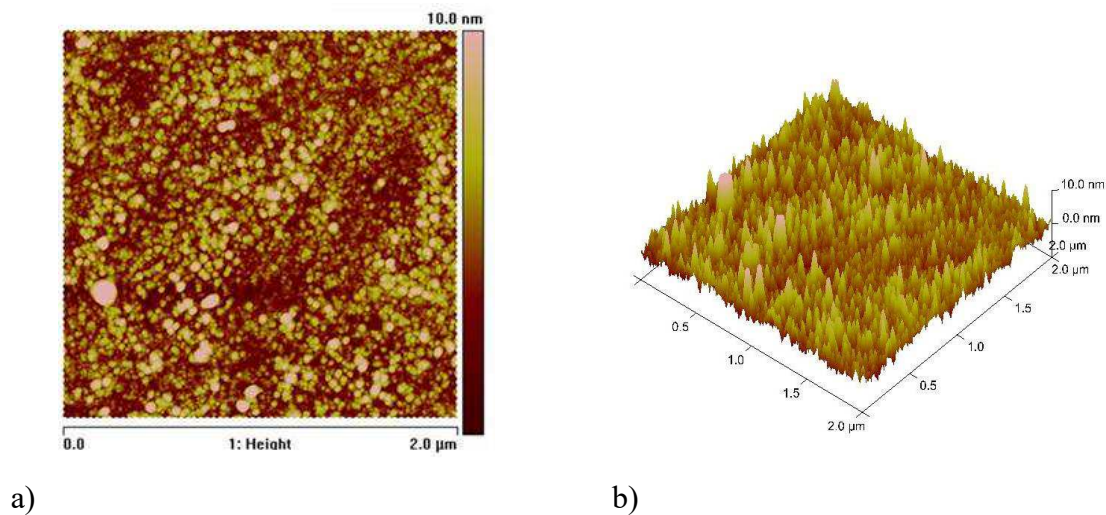
Figure 32. a) 2D AFM image and b) 3D AFM image of OTS coating on glass slide.

The AFM tips are silica nitride Veeco NP-S type (force constant 0.06 N/m). The colorized height scale on the left-hand side of the image runs from 0 nm (dark brown) to 10 nm (pink). The absolute value of roughness, R_a, of the coating was 1.49 nm and the root mean square roughness, R_q, of the coating was 2.02 nm. The clusters of raised surfaces are polymerized OTS that remain on the film surface after the coating procedure.

3.2.2.2   Wyko Scanning White Light Interferometry (SWLI)

Wyko Scanning White Light Interferometry was used to characterise the topography of the surfaces. The technique is based on the principle of the Michelson interferometer. A light source with a coherent wavelength in the micron range is collimated and split into two beams: an objective and a reference beam.

The object beam is reflecting from the object measured and the reference beam is reflected from the reference mirror. These beams are captured and combined at the beam splitter and the overlapping beams are recorded with a CCD camera.

Using this technique, 3D images are obtained, which represent the height distribution of the surface sample. The advantage of this technique was that the surfaces are not required to be in contact, so the sample surface is not damaged.

A Wyko NT9100 Optical Profiler was used to capture topographical images of the wiper blades and measure the roughness of the surfaces. To make the wiper blade surface reflective, gold was sputtered on the blade before measurements. An example of a Wyko image of a wiper specimen is shown in Figure 33 .
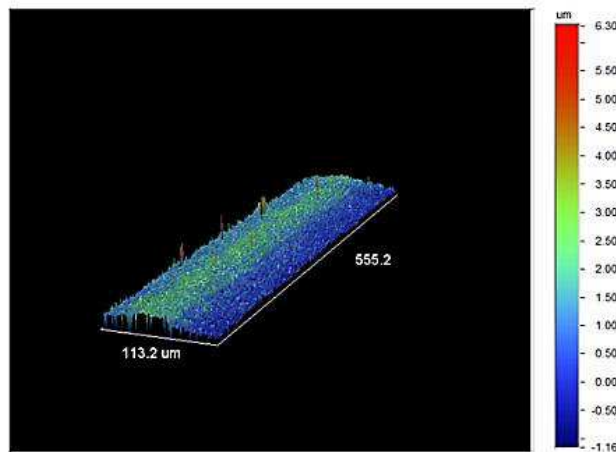
Figure 33. 3D image of the YL naked coated with gold.

Here, the R_a was 0.545 μm and the R_q was 0.653 μm. As described in the Chapter 4, the Wyko was used to measure the roughness of the etched and smooth glass slides before friction measurements were carried out.

3.3   Friction measurements method

Frictions measurements were performed with a UMT2 (Universal Materials Tester), manufactured by CETR, Campbell, USA (Figure 34a). In order to realistically replicate the wiper windscreen system, all the friction measurements were operated in pin-on-disc mode with rotating glass specimen and a stationary wiper blade (Figure 34b). Reciprocating mode was not used because of the complex changes in loading, which occur during reversal.

Friction force (Fx) and normal load (Fz) were measured using strain gauges, attached to the housing above the stationary wiper blade specimens. Sensitive, low-load sensors were chosen for this purpose, incorporated in a 2D force sensor platform with a range 0.05 to 5 N and resolution 0.25 mN. Using this equipment, sliding speeds were varied from 0 to 1.8 m/s.

a)

b)

c)
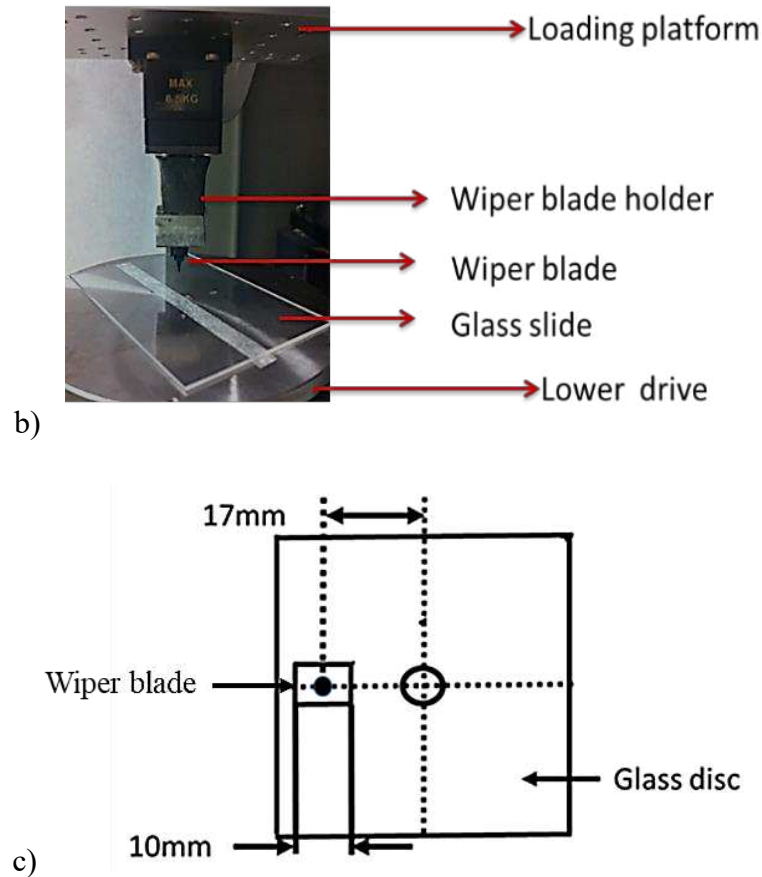
Figure 34. a) UMT Tribometer; b) Set-up and specimens; and c) Plan view of the specimens.

Figure 34c shows a plan view of the wiper blade and the glass disc. This shows that the length of the wiper blade is 10 mm and the radius of the wear track is 17 mm. The wipers were cut from their full length into these 10 mm sections in order fit within the friction test rig. Given the length of the wiper specimens, the range of applied loads (0.07 to 0.45 N) corresponds to distributed loads, ranging from 7 to 45 N/m (such loads are typical in automotive wiping applications).

3.4   Sound measurements methods

Vibrations induced by friction were measured with three different pieces of apparatus as follows: high speed camera, Laser Doppler Vibrometer (LDV) and microphone.

3.4.1 High speed camera

A FASTCAM-SA3 High Speed Camera manufactured by Photron, USA was used to record videos and analyse the behaviour of the soft contact (Figure 35).

Figure 35. Photograph of SA3 Fastcam.

This camera can record at up to 120,000 fps. It has a CMOS sensor with a maximum resolution of 1024 x 1024 (17μ) pixels at up to 2,000 fps. To study the movement of every part of the wiper blade in detail a Navitar macro-zoom lens was used. All the videos recorded by using this camera were processed in Matlab to detect the frequency of the wiper blade and water.

3.4.2 Laser Doppler Vibrometer (LDV)

A Laser Doppler Vibrometer was used to study the vibration of the wiper blade. LDVs operate by detecting the Doppler frequency shift of coherent light that is scattered from a moving target [93]. The measured frequency shift can then be used to calculate a time-resolved measurement of the target velocity v, from

$$\mathbf{v} = \lambda_{air} * f_{Doppler}/2 \tag{19}$$

$$f_{Doppler} = -(f_{beat} - f_{rest}) \tag{20}$$

where $f_{Doppler}$ is the Doppler shift, f_{beat} is the difference in frequency between signal and reference beam (*i.e.,* the beat frequency), f_{rest} is the rest frequency, and λ_{air} is the wavelength in air [94].
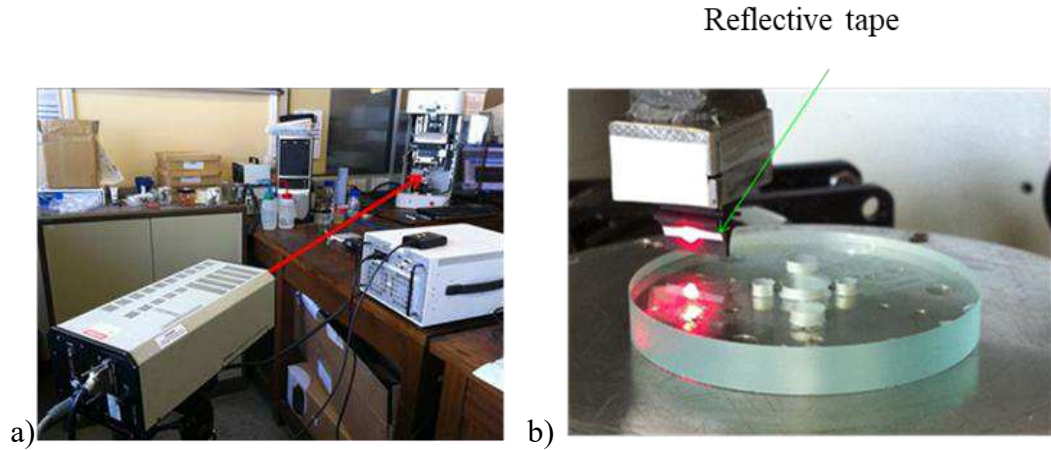
Figure 36. Photographs of LDV set-up: a) laser and sliding rig, b) glass disc/wiper blade arrangement.

A photograph of the laser set-up is shown in Figure 36a, and a photograph of the specimen, reflective tape and laser spot is given in Figure 36b.

3.4.3 Microphone

In order to measure the sound of the squeak, a 70-16 KHz condenser microphone was used. This was connected directly to a laptop and sound was recorded and converted into wav files using Audacity, a freeware package. Acquisition rates up to 96 KHz can be achieved using this set-up. As shown in Figure 37, the microphone was positioned close to, and directed towards the sliding contact.
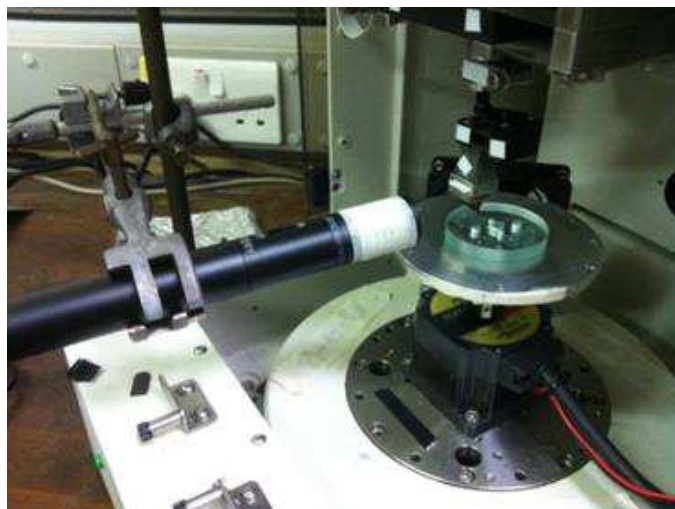
Figure 37. Photograph of Microphone set-up.
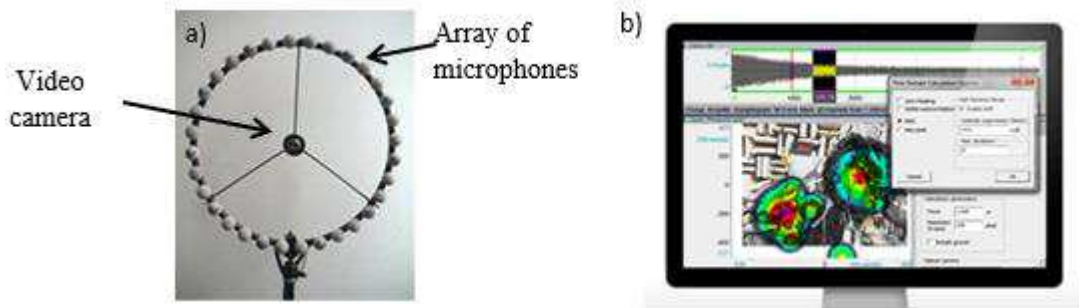
Figure 38. Acoustic camera system: a) Photograph of ring array of microphones, b) NoiseImage software.

Measurements were also carried out with an acoustic camera, in order to identify the location of the emitted friction induced noise. This piece of equipment was borrowed from the EPSRC Equipment Pool and consists of a ring array of microphones centred around a video camera (Figure 38a).

Recordings are made by simultaneously acquiring the output from the 32 microphones and video camera. After each recording, the signal from the microphones is processed by a triangulation calculation (using NoiseImage Software Figure 38b), which uses the phase difference between each measurement to locate the source of the recorded sounds. The geometrical distribution of recorded sounds is then superimposed onto each frame recorded with the video camera.

A further refinement is that the process can be applied to individual frequency ranges, which makes it ideal for analysing the friction induced vibration noise from wiper contacts (since it means that the frequency range in question 2-5 kHz can be isolated from low frequency background noise).

3.5   Finite Element modelling method

A finite element (FE) model was developed to detect the resonance frequencies of the wiper blade and compare them to the vibration response obtained experimentally. Specifically, the software package ABAQUS was used to predict Eigen-frequencies of the system. The most important part of the model is the material definition.

The elastic properties of the elastomers makes it very difficult to simulate their behaviour using a Finite Element Modelling method. In general, rubber is modelled as an incompressible hyperelastic material, as well as elastoplastic material under plastic dominant deformations and the assumption of isochoric plastic flow [95].

The proprieties of the materials were obtained from Dynamic Mechanical Analysis (DMA) data performed by the industrial partner (Bosch, Tienen, Belgium). These data were used to obtain the material input files, while density, expansion, hyperelasticity, and viscoelasticity parameters were obtained from experimental characterization made by Bosch. Isotropic expansion was defined by the coefficient of thermal expansion, α obtained from fitting data at different temperatures. Hyperelasticity was introduced by modelling the material using a neo-Hookean formulation; enabling us to capture the time-independent response of the material and predict the nonlinear, stress–strain characteristics at large deformations.

The form of the neo-Hookean strain energy potential is:

$$U = C_{10}(\bar{I}_1 - 3) + \frac{1}{D_1}(J^{el} - 1)^2 \tag{21}$$

where U is the strain energy per unit reference volume, C_{10} and D_1 are temperature-dependent material parameters (shown in Table 4), $\bar{I}_1$ is the first deviatoric strain invariant defined as:

$$\bar{I}_1 = \overline{\lambda_1}^2 + \overline{\lambda_2}^2 + \overline{\lambda_3}^2 \tag{22}$$

where the deviatoric stretches $\overline{\lambda_i} = J^{-\frac{1}{3}}\lambda_i$; J is the total volume ratio; J^{el} is the elastic volume ratio as defined below in "thermal expansion"; and λ_i are the principal stretches. The initial shear modulus and bulk modulus are given by:

$$\mu_0 = 2C_{10} \tag{23}$$

$$K_0 = \frac{2}{D_1} \tag{24}$$

Table 4 Temperature dependent materials parameters of PQ$_1$step material.

Material	C_{10}	D_1
P	1.1120595	0.001
Q$_1$step	1.156692	0.001

In addition to this, a Prony series approximation was used to define the viscoelastic (time-dependent) behaviour of the rubber. This has 3 parameters: g_i Prony- shear relaxation or shear traction relaxation modulus ratio, k_i Prony- bulk relaxation or normal traction relaxation modulus ratio, tau_i Prony- relaxation time, which are shown in Table 5.

The unknown Prony coefficients were derived using standard shear and bulk stress-relaxation tests by minimizing the difference between the series description and the experimental measurements; shear and bulk relaxation moduli, long term moduli, and relaxation times were then used as inputs for the viscoelastic description implemented in ABAQUS. A representation of ABAQUS model is shown in Figure 39, showing boundary conditions, distributed mass of water and displacement applied to end of a wiper.

Table 5 Prony series approximation parameters of PQ$_1$step material.

Material P	g_i Prony	k_i Prony	tau_i Prony	Material Q$_1$step	g_i Prony	k_i Prony	tau_i Prony
1	0.81933	0	2.0564e-07	1	0.99984	0	1.2427e-10
2	0.042136	0	6.7301e-06	2	1.9071e-05	0	5.9211e-06
3	0.021235	0	3.5298e-05	3	1.9071e-05	0	5.9211e-06
4	0.00099077	0	6.7145e-05	4	1.3667e-05	0	2.6392e-05
5	0.01269	0	0.00017337	5	1.1673e-05	0	6.9819e-05
6	0.0092962	0	0.00072864	6	1.1949e-05	0	0.00035235
7	0.0067601	0	0.0027057	7	1.007e-05	0	0.0022015
8	0.0064386	0	0.0060589	8	1.0319e-05	0	0.015325
9	0.0052895	0	0.013039	9	1.0941e-05	0	0.17015
10	0.0040864	0	0.03804	10		0	
11	0.0046687	0	0.048341	11		0	
12	0.0052758	0	0.21099	12		0	
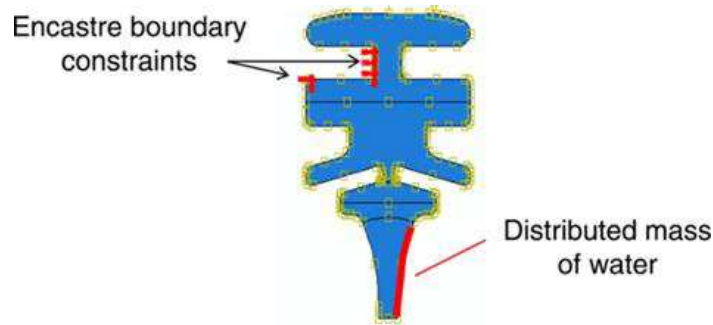
Figure 39. Representation of ABAQUS model, showing boundary conditions, distributed mass of water and displacement applied to end of wiper.

Stiffness, mass, damping matrices and friction induced damping effects are considered in the solution of the eigenvalue problem. The nonlinear material was linearized before the qualitative estimation of the eigenvalues of the system for the specific blade/holder was calculated. The boundary conditions were determined from high magnification video images of the wiper/holder set-up in the real experiment and after implemented in the ABAQUS model.

3.6 Film thickness measurements using Laser Induced Fluorescence

The film thickness left on the glass after wiping was measured using a Laser Induced Fluorescence (LIF) technique. Although other techniques, such as interferometry, exist to measure film thickness, the limitation of the interferometry method is that both surfaces in contact are required to be reflective. The advantage of interferometry is its resolution, 2 ± 1 nm [96], and minimum measurable film thickness of around 0.5 nm, whereas fluorescence has the limitation of having a minimum measurable film thickness of around 300 nm [75].

The laser induced fluorescence technique is based on photo-excitation of a fluorescent dye. This technique consists of three stages (Figure 40) that take place in specific molecules known as fluorescent dyes or fluorophores.

The initial stage is excitation, where a laser or an incandescent lamp provides a photon with $h\nu_{EX}$ energy, which is absorbed by the fluorophore and generates an excited electronic singlet state (S_1'). This intermediate excited-state has a finite lifetime, generally from 1 to 10 ns. The conformational modifications of the fluorophore during the lifetime state, is dependent on various possible interactions with the fluorophore's molecular

73

environment. The first essential consequence of this process is that the energy resulting from the S_1' state is partially scattered to a relaxed singlet excited state (S_1),
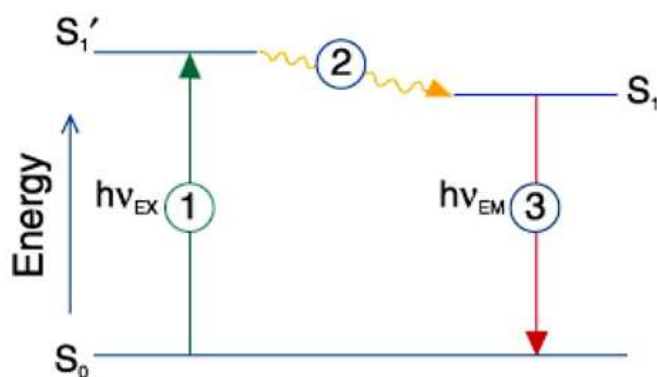
Figure 40. Laser induced fluorescence principle [76].

The ratio of the number of the fluorescence photons emitted to the number of the photons absorbed (fluorescence quantum yield), determines the relative extent of the excited state life time.

The third stage is the fluorescence emission representing the returning of the fluorophore to its S_0 state, when a photon with hv_{EM} energy is emitted. This emitted photon has a lower energy and different wavelength than the photon excited with hv_{EX} energy due to the energy dissipation during the excited state life time stage. The difference in absorption wavelength and emission wavelength of the fluorophore is called Stokes shift (Figure 41) [97].
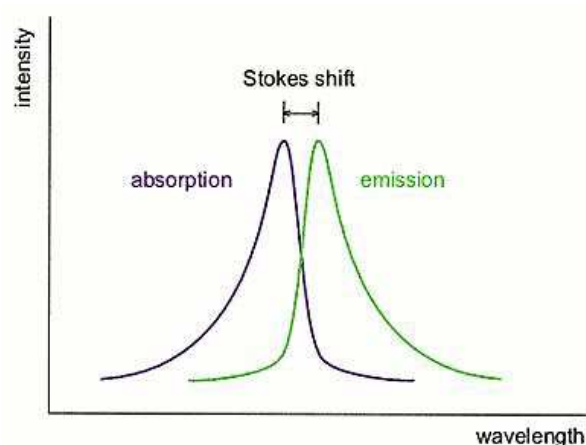
Figure 41. Stokes shift of a dye [97].

3.6.1 Dye selection

A selection of dyes was made on the basis of their cost, availability, solubility in water, quantum yield, absorption and emission wavelength. In this study, the dye Sulforhodamine G (Sigma –Aldrich) was chosen because it is soluble in aqueous solutions and its absorption wavelength value is 529 nm. Figure 42 shows the absorption and emission of dye, dichroic mirror, filter and lens characteristics. The concentration of the dye was set at 0.05 % wt.
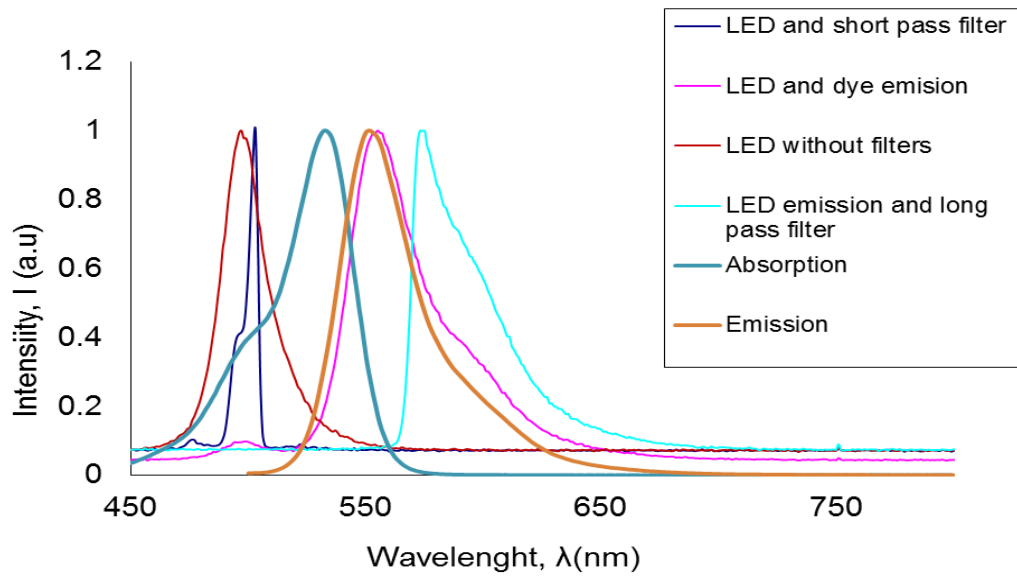
Figure 42. Absorption and emission of the Sulforhodamine G dye, LED spectrum and filter characteristics are also shown.

3.6.2 Apparatus to measure film thickness

Two different rigs, an EHD ultra-thin film thickness and CETR tribometer with an inverted fluorescent microscope were used to measure the water film thickness in contact and the film thickness left on the windscreen.

An EHD rig (PCS-Instruments, UK) and special optical setup were utilised to measure the water film thickness in contact and film thickness left on the glass. This rig was modified so that low loads and rapid stop-start motion could be applied and a high power pancake motor (Printed Motor Works, UK) was used to driven the glass disc. During the tests, the wiper is loaded against the transparent, plain BK7 glass disc (PCS instruments, UK) and the glass disc is rotating. This experimental set-up is shown in Figure 43.
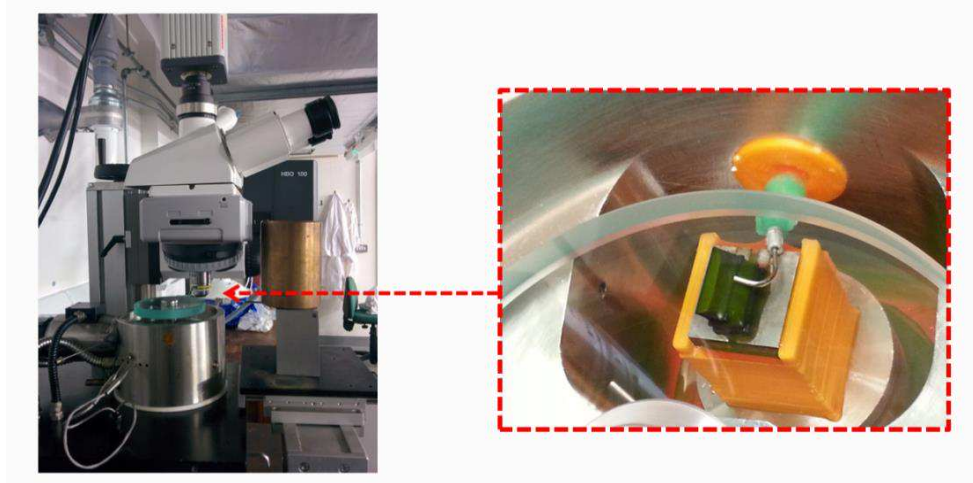
Figure 43. The EHD experimental set-up for measuring film thickness.

A solid-state, diode-pumped pulsed laser (Laser2000 Ltd, Northants, UK), which produced green light, with peak intensity at 532 nm wavelength was used to excite the fluorescent dye. The laser has a maximum power output of 40 mW at 3 kHz. The wavelength emitted from the contact is higher than the excitation wavelength of the laser (due to Stokes shift, described above). This enables the separation of the wavelengths by using a 532nm, dichroic mirror (Chroma, USA) positioned between objective and camera. A barrier filter (Chroma, USA) located above the dichroic mirror is used to filter any light which is not produced by the excited fluorescent dye. The fluorescent dye sulforhodamine G that emits light in the range of 580–640 nm was selected, so that it emissions were observable by the camera [98].

A microscope (Axiotech Vario, Zeiss) was mounted on a XYZ stage to capture images of the wiper/glass contact using Image intensified B/W camera. To visualise the film left on the glass-wiper contact, a 2X objective with a wide field of view was used. A monochromatic camera (Rolera MGi, QImaging, UK) was used to capture the images. The size of an image is 512×512 -pixels. Acquired images were converted to grey scale intensity maps using a Matlab program written for this purpose. Figure 44 illustrates the Laser Induced Fluorescence EHL rig optical set-up.
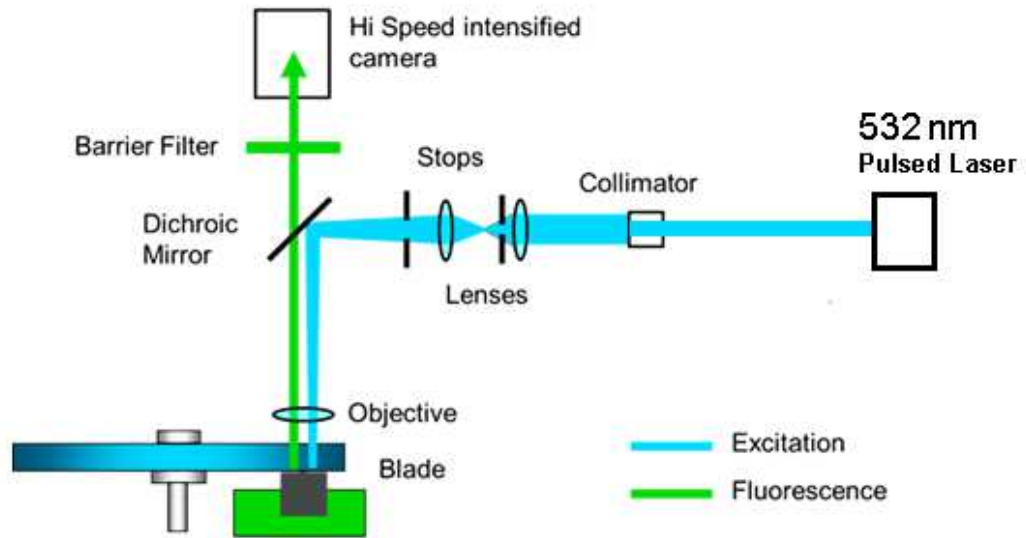
Figure 44. Laser Induced Fluorescence EHD optical set-up.

The water film thickness measured using the EHL rig presented a number of practical difficulties with regard to accurate film thickness measurement using fluorescence: *i*) the wiper/glass contact is upside down so that water falls away from the glass, *ii*) water flies outwards due to the centrifugal force, *iii*) the load is not stable, when low loads on EHD.

To avoid these problems, an inverted fluorescent microscope and a platform for holding the glass disc were built to measure the water film thickness. This allowed the glass to be oriented correctly with respect to the contact (*i.e.*, below it) and had the advantage of being able to fit within the CETR tribometer.

The wiper was therefore loaded against the glass disc using the CETR's loading system while the glass disc was placed on the platform and was driven by CETR motor using a belt-pulley arrangement in Figure 45a, b and c.
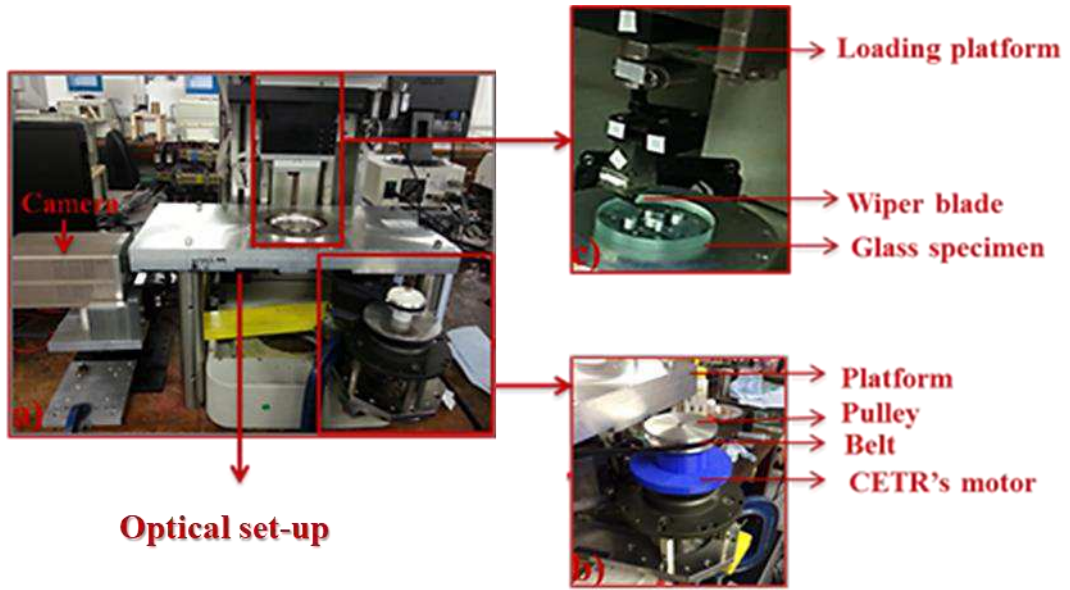
Figure 45 a) CETR tribometer set-up, b) belt-pulley connected to CETR's motor and c) wiper/glass contact.

Here, the microscope was placed on an XYZ stage to allow for the positing and focusing of the contact. A Zeiss 5X Neofluar infinity corrected objective was used to observe the fluorescent intensity distribution of the wiper contact at various loads and speeds. The optical set-up is shown in Figure 46.
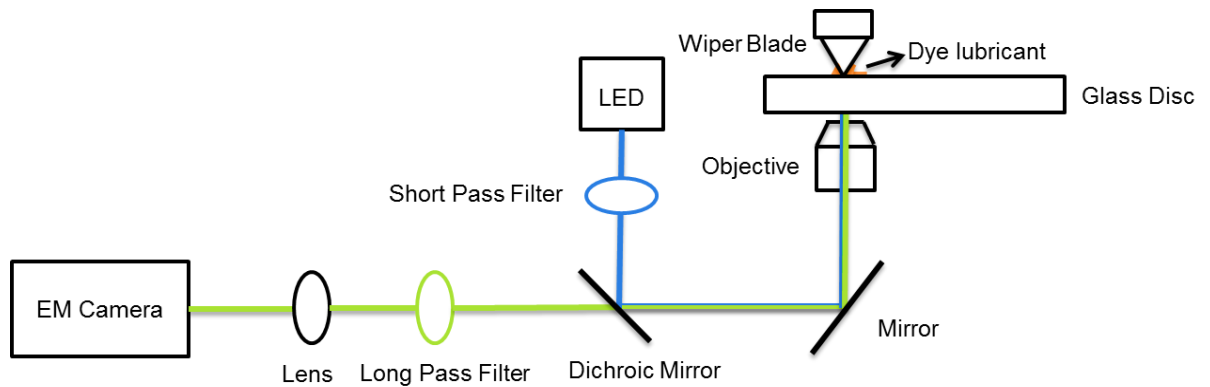
Figure 46. Optical set-up and wiper contact.

A blue light emitting diode (LED) of 490 nm wavelength from Mightex Systems (USA) was used to excite the dye. A short pass filter (Edmund Optics, UK) allowed only wavelength less than 490 nm to pass through the dichroic mirror. The fluorescent light emitted from the contact was collected by the objective after passing through the dichroic mirror. A tilted mirror was employed to align and reflect the emitted light to dichroic mirror, 509 nm (Edmund Optics, UK). A long pass filter (Edmund Optics, UK) restricted any light, which was not produced by the excited fluorescent dye. Moreover, an achromatic lens was placed in front of the camera at a specific distance to refocus the image into the camera.

The images were captured by using a QunatEM: 512SC camera as 16-bit tagged image files, in a 512 × 512-pixel array. This camera can acquire images at high speed as well as in low-light. A Matlab program was written to analyse the images and plot the intensity distribution maps with scale bar.

3.6.3 Normalization

The excitation field of the light emitting diode was unstable over time, due to dust crossing the beam path and settling on the optical parts. This affected the already low level of emission coming from the very thin film when performing thickness measurements in the surrounding of the contact zone. In addition to this, the excitation field of the light emitting diode has a Gaussian distribution. Therefore, a flat-field correction was necessary to counteract the non-uniform intensity distribution of the excitation field [75]. Therefore, to determine the intensity of the excitation field, a specimen with a constant thickness and hence uniform distribution of fluorophores was used. Specifically, a small droplet of dye solution was placed on a clean glass disc and covered by a cover slip to obtain a uniform film. When the microscope was used to view this uniform film the obtained fluorescence images contained only the emissions from the thin film of dyed solution, which resulted in a non-uniform intensity distribution. These imperfections (aberrations) were then removed from the image using a custom Matlab programme. Figure 47 shows an example of this process.
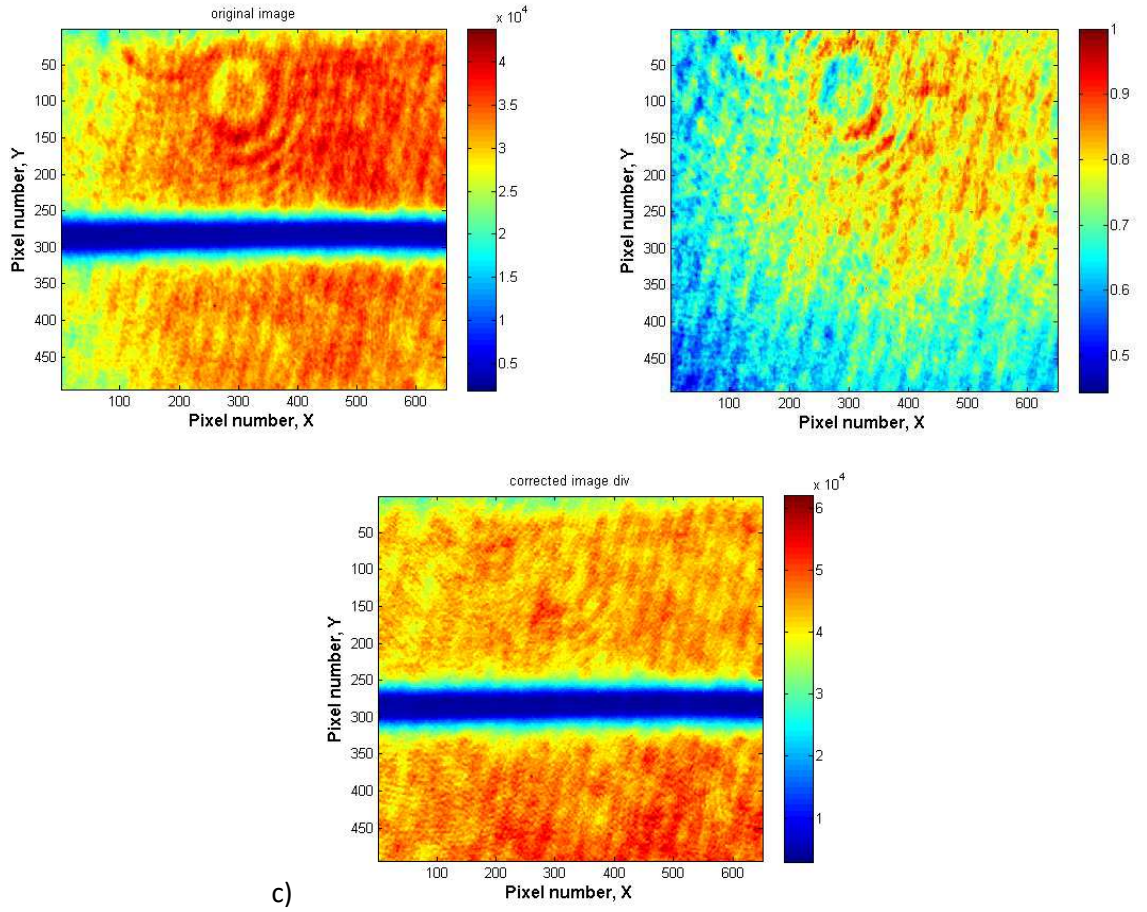
Figure 47. a) Contact image before normalisation, b) Flat-field correction Image, c) Contact image after normalisation.

Here, Figure 47a shows a raw intensity image in which both film thickness variations and aberration are visible, Figure 47b shows the cover slide image in which only the aberrations are visible, and Figure 47c shows the normalised image in which the majority of the aberrations have been removed. The intensity images (I_{AN}) were created after the background noise (I_{BG}) was subtracted from every image and divided by maximum intensity of the flat field correction (I_N).

$$I_{AN} = \frac{I_{BN} - I_{BG}}{\max(\max(I_N - I_{BG}))} \tag{25}$$

where I_{BN} is the intensity image taken before normalisation. After each image was normalised, the intensity maps were correlated with the film thickness maps using a calibration curve, as presented in subsection 3.6.4.

3.6.4 Calibration

In order to measure the residual film on the glass after the wiping action, a calibration curve is necessary to convert the intensity maps into film thickness maps. This was made possible by comparing the theoretical film thickness with the intensity profile obtained experimentally across the centre of contact as shown in Figure 48. The theoretical film thickness gap outside the contact was calculated by using Hertzian point contact equation given by:

$$\mathbf{h} = \frac{\mathbf{a}\mathbf{p_{max}}}{\mathbf{E^*}}\left[-\left(\mathbf{2} - \frac{\mathbf{r^2}}{\mathbf{a^2}}\right)\mathbf{cos^{-1}}\frac{\mathbf{a}}{\mathbf{r}} + \sqrt{\left(\frac{\mathbf{r^2}}{\mathbf{a^2}} - \mathbf{1}\right)}\right] \tag{26}$$

where a is the contact radius, p_{max} is the maximum pressure, r distance from the centre of contact and E^* is the contact modulus. To simulate the gap region outside the rubber/wiper contact, called as wiping zone, a glass ball was loaded against the glass disc.
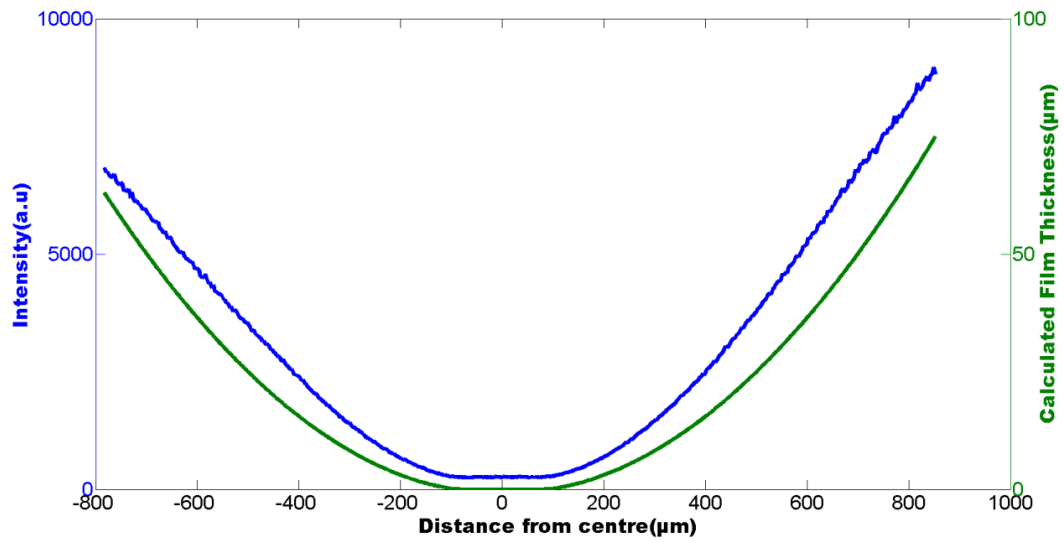
Figure 48. Comparison between calculated film thickness and intensity outside the glass ball disc contact obtained experimentally.
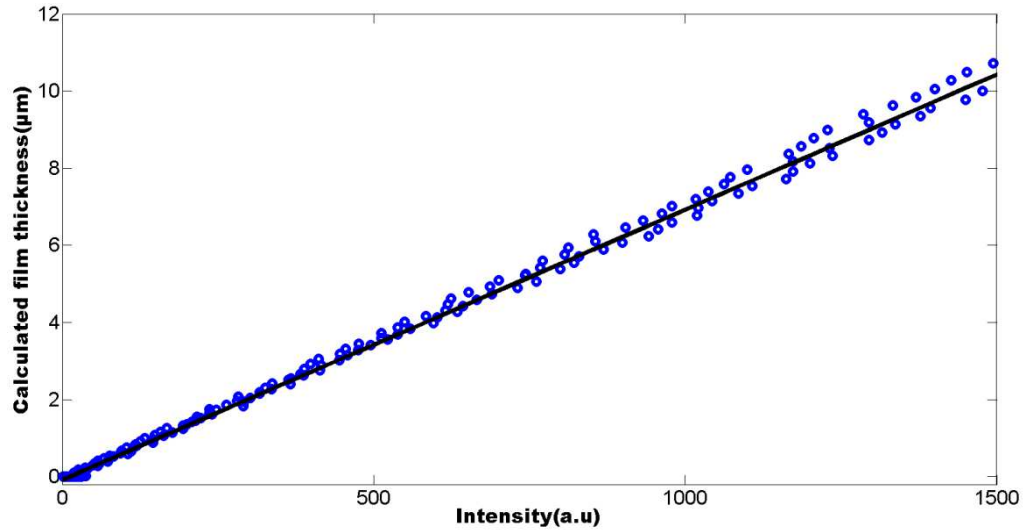
Figure 49. Calibration curve of intensity versus calculated film thickness.
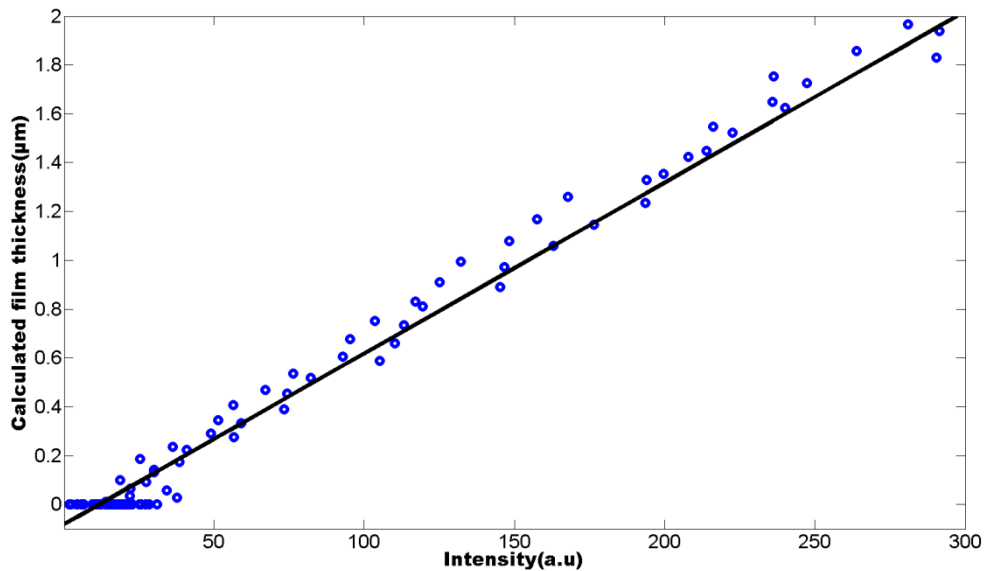
Figure 50. Intensity versus calculated film thickness – zoomed in version of Figure 49, showing minimum measurable film thickness limitation.

In order to obtain repeatable and accurate results, a calibration curve was obtained prior to each testing session. It can be seen that the glass ball had a defect, which caused a slight non-symmetry of the calibration plot, which may be due to a minor misalignment of the the disc specimen. The next step in the calibration procedure was to plot the measured intensity against the calculated film thickness and a linear fit was made to the data to obtain a calibration curve (Figure 49). From the calibration curve, the minimum measurable film thickness was found to be about 200 nm (Figure 50). After, obtaining

intensity value from the images, the calibration curve was then used to create maps of film thickness.

3.7 Summary

This chapter provides a detailed description of all the rigs and materials used during this project, including the technique used for film thickness calibration. A new inverted microscope was built and the drive motor of the tribometer was reconfigured into a belt drive which provided torque to a bearing incorporating a glass disc. The placement of an optical microscope set-up underneath of the newly made platform enabled the wiper contact to be viewed and the film thickness measured using a LIF technique.

Chapter 4

Sample Preparation

4 Sample Preparation

In this chapter, different methods used to prepare the samples are described. These include the application of surface monolayers to modify surface energy, the roughening of the rubber specimens using sandpaper and the roughening of the glass specimens using an etchant.

4.1   Glass coatings preparation for measuring friction, contact angles and noise

A range of surface coatings were applied to the glass, in order to set-up the experiments close to reality; these included: Hochglantztrockner (HGT-hydrophobic), Ceroxide (hydrophilic), Self-assembled monolayers (SAMs), including octadecyltrichlorosilane (OTS), bare glass, and without coating. A hydrophobic coated windscreen is very helpful for the drivers because water can be removed quickly, when it is raining heavily. The HGT and ceroxide are commercial solutions used by drivers to clean the windscreens. HGT is used to break the water film formed on the windscreen because this promotes faster removal of dirt from windscreen. Ceroxide is a polishing powder used in automotive industry to polish the windscreen for a better visualisation of the road.

OTS SAMs is a surface preparation usually carried out in chemical laboratories and is not normally present on windscreens. It is used here in order to accurately control the energy of the glass surface. For these coatings and the bare glass, the contact angles were measured, and the surface energies calculated by using the approach presented in Methods chapter.

4.1.1 Bare glass preparation

Before the coatings were applied, all glass disc specimens were cleaned in solvents. This involved sonicating for 20 minutes in toluene using an ultrasonic bath, followed by 20 minutes sonicating in iso-propanol (to remove residual toluene), before being dried thoroughly in a warm air stream.

4.1.2 HGT preparation

HGT commercial solution is diluted 1:100 in water (dilution factor recommended by the manufacturers) before it is applied on the glass specimen. The HGT solution is then left on the glass in order to produce a hydrophobic coating. After 5 minutes, the HGT solution is aspirated and the glass specimens is dried with a Kimwipe. Alternatively, the glass cover slip may be allowed to dry naturally in air, or by blowing nitrogen.

4.1.3 Ceroxide preparation

The ceroxide is a powder, which is applied on a wet paper or cloth. The ceroxide is rubbed against the glass specimen until the powder covers the entire glass surface. The glass specimen is then rinsed in water in order to remove the excess ceroxide and produce a hydrophilic coating.

4.1.4 OTS preparation

Due to the uneven nature of the glass surface following the HGT preparations, it was decided to use specimens of high surface energy in a controlled repeatable fashion. To produce such specimens, cleaned glass slides were submerged in a solution of OTS and toluene. During submersion, the OTS is known to form a self-assembled monolayer (SAM) on glass, which remains bonded to the surface after the specimen has been dried. The formation of OTS SAM is due to the bonding of the head groups to the glass and crosslinking with each other, forming a solid base. The tail group chains are aligned, forming an effective barrier between the glass and the environment (Figure 51).
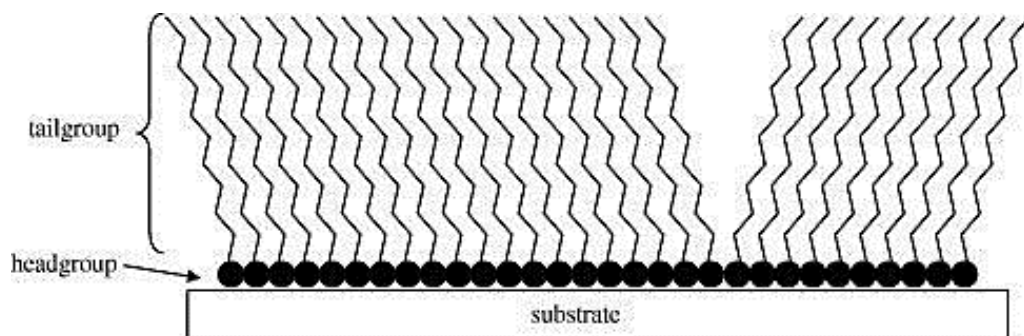
Figure 51. OTS SAM on a hydrophilic substrate. The head groups bond to the substrate and crosslink with each other, forming a solid base. The tail group chains align, forming an effective barrier between the glass and the environment [99].

The OTS SAMs coating technique was validated by comparing the OTS surface energy values with the values of OTS surface energy from literature (see Table 6).

Table 6 Comparing experimental with literature results [99]**.**

Surface energy (mJ/m^2)	OTS monolayer WU [100]	OTS monolayer OWRK [100]	OTS monolayer Fowkes [100]	OTS monolayer
	25.38±0.12	23.50±0.12	26.23±0.16	23.09

Initial friction tests showed that the occurrence of friction induced vibration was strongly dependent on the surface energy of the sample. For instance, both clean glass with high surface energy and glass with a full OTS monolayer with low surface energy showed a low propensity to squeak, whereas HGT with intermediate surface energy showed a high propensity to squeak.

In order to investigate this behaviour in greater detail, it was decided to produce a range of glass specimens with an accurately controlled variation in surface energies. SAMs preparation were used to control surface energy by varying concentration and reaction time; specifically, the glass discs were dipped into OTS solution with two different concentrations 0.1 and 1 mM with dipping durations from 20 s to 30 min (Figure 52).
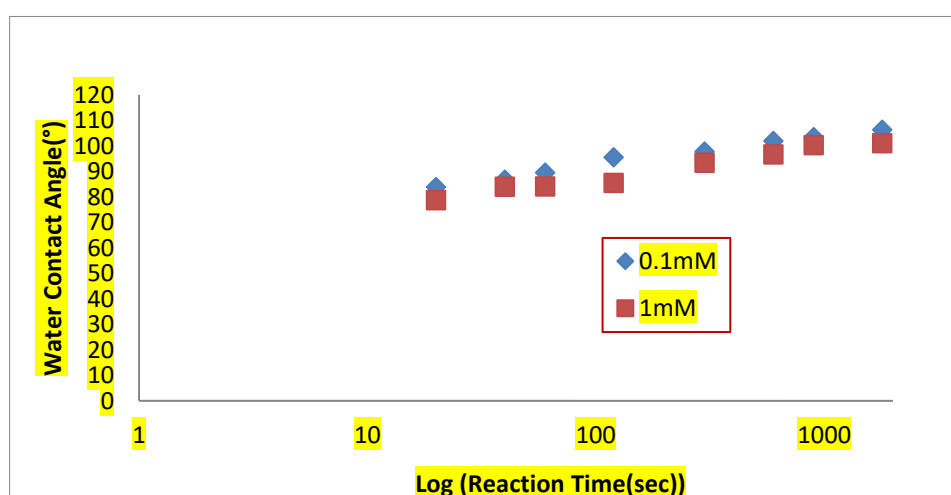
Figure 52. OTS SAM's preparations with different concentrations versus water contact angle.

After the glasses were coated, the contact angles were measured three times and the surface energies for different OTS monolayers were calculated and measured by using two different solvents (water, ethylene glycol (Table 7)).

Table 7 Contact angles and surface energies measurements for OTS coatings with two different solvents.

Sample Name	Time (s)	Water contact angle average of three measurements (°)	Standard deviation Water contact angle	Ethylene glycol (°)	Standard Deviation Ethylene glycol	Surface Energy (mJ/m²)
OTS1	2	25.2	0.97	22.5	1.22	78.18
OTS2	5	62.7	0.36	54.1	0.70	40.64
OTS3	10	72.6	0.63	57.5	0.98	30.73
OTS4	20	83.8	1.26	67.3	0.75	23.28
OTS5	40	86.8	1.26	72.2	0.72	20.87
OTS6	60	89.51	1.89	74.08	0.64	19.59
OTS7	120	95.59	0.93	79.28	0.40	16.92
OTS8	300	97.87	1.35	81.35	0.74	16.01
OTS9	600	102.00	1.01	83.28	0.68	15.96
OTS10	900	103.53	0.32	85.51	0.29	14.83
OTS11	1800	106.43	0.47	87.82	0.11	14.34

It can be seen that this method of varying the dipping time and concentration is an effective means of gradually varying the energy of the glass surface. These values of surface energy provide a better understanding of the contact between wiper blade and windscreen. Several investigations of the surface energy and its relationship with noise and friction are presented in Chapter 6 on Friction Induced Vibration.

4.2 Glass and wiper sample preparation for wear testing

In order to study the effect of rubber wear on the wiping mechanisms that occur during operation, the wipers were rubbed against glass, prior to testing, for different lengths of time between 2 and 10 hours at 1.33 m/s (Figure 53).

In certain cases, an additional step to accelerate wear further was implemented, which involved rubbing the rubber wipers against sand paper prior to testing. These wipers are labelled pre-worn wipers. The burrs that form on these pre-worn wipers for different sliding distances are shown in Figure 54. Friction tests were then performed under wet conditions (using tap water) after the wipers were worn in this way to mimic the wear process in actual wiper blade systems (see Chapter 5).
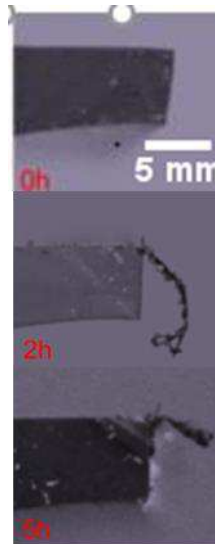
Figure 53. Wiper blades worn for different lengths of time from 2 to 10 hours at 1.33m/s.

| 2.1m | 4.2m | 6.3m | 63m | 126m | 252m |
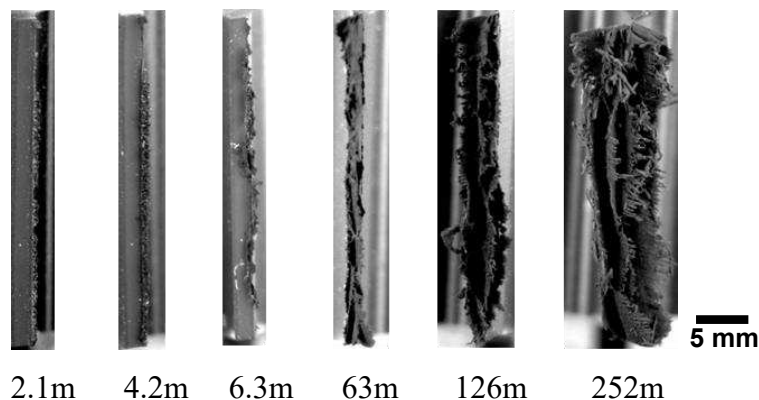
Figure 54. Effect of wear for different sliding distances.

It was also necessary to characterize the effect of glass roughness on the wiping performance. This required a glass specimen with carefully controlled roughnesses and was achieved by exposing the glass specimens to an etching paste. The etching paste consists of sodium fluoride and hydrogen fluoride, which changes the characteristic roughness and translucent qualities of frosted glass over time. As with the OTS, the length of exposure was used to control the degree of surface modification (the resulting range of surface roughness is shown by the optical profilometer images in Figure 55. This enabled friction tests to be carried out on glass surfaces with roughness from 0.5 nm to 5 µm.
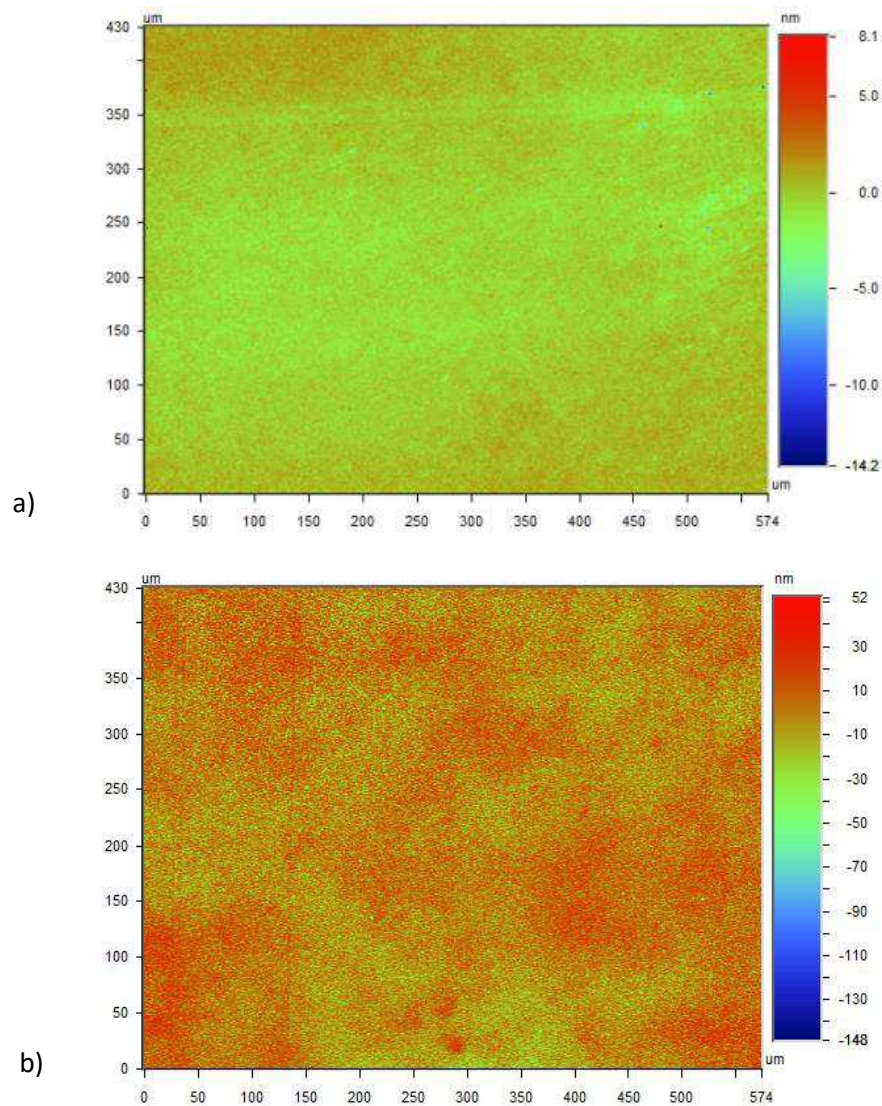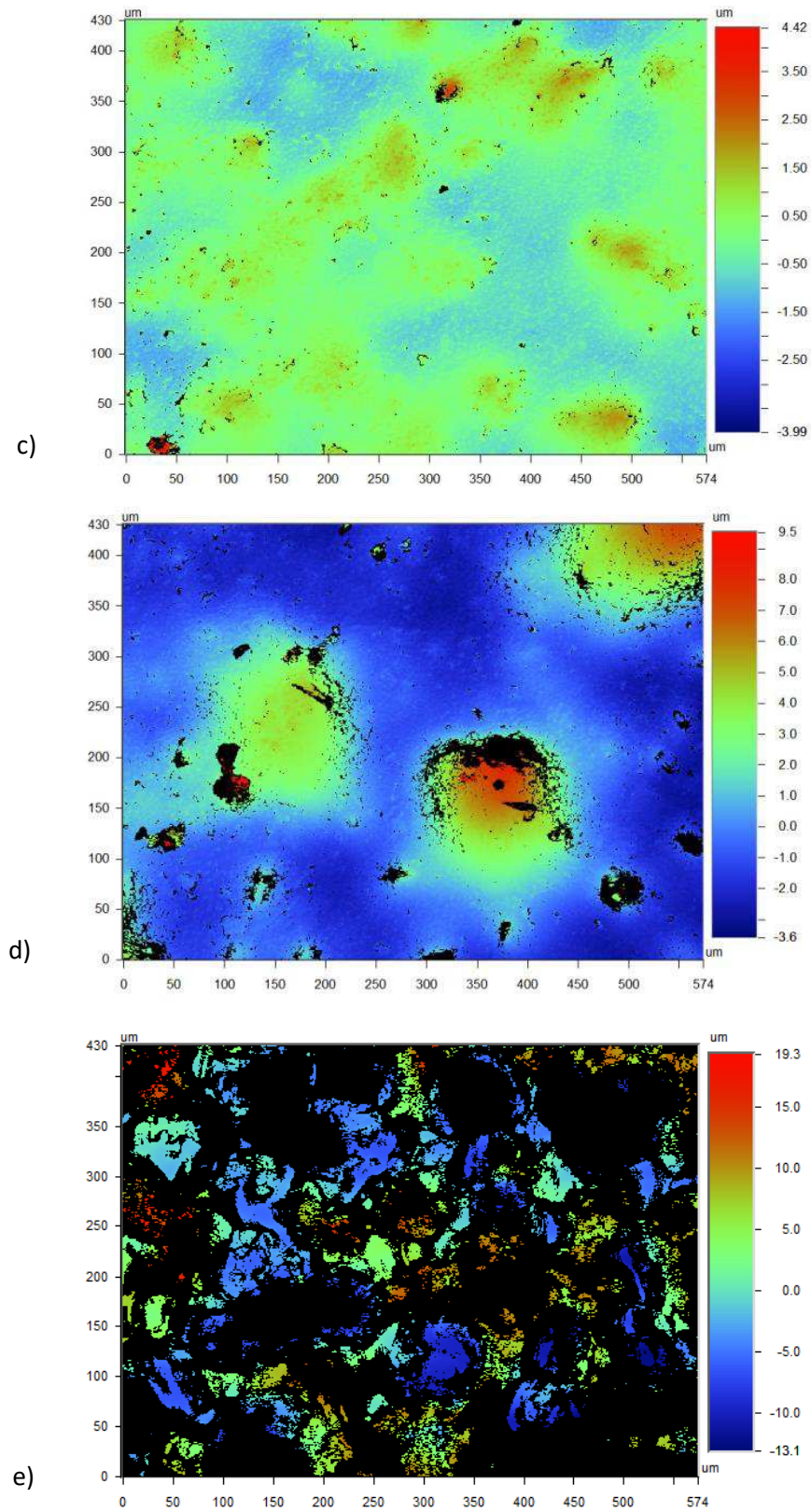
Figure 55. Etched glasses with different roughness a) smooth glass-0.4 nm, b) 10 nm, c) 500 nm, d) 1 µm and e) 1.5 µm.

Chapter 5

Friction Results

5 Friction Results

In the research described in this section, the friction response of the rubber wiper to different glass coatings, surface energy and geometry was studied. To do this, coefficients of friction of a steady-state sliding interface between the windscreen wiper rubber and glass surface were measured for a range of speeds and loads.

In addition, the static friction behaviour was investigated, and the effects of start-up speed and stationary duration on friction are quantified and explained. Finally, the effect on friction of wear was investigated by performing tests during which wiper deformation was monitored, in real-time, using a microscope and video camera.

5.1 Repeatability

The first experimental step in this project was to establish repeatability, which was an issue due to instability of load and cleaning procedure used. The latter was found to be the dominant factor limiting repeatability. To solve this issue, the cleaning process of the glasses was extended to include 5 minutes cleaning by plasma prior to cleaning in toluene and isopropanol in an ultrasonic bath for 40 minutes. Friction tests were repeated five times to assess repeatability (Figure 56). Each test uses a new blade and glass slide. For these tests, a normal load of 17 N/m was applied, and friction coefficient was measured. Each point on Figure 56 represents an average of friction values obtained over a 10 seconds period. The average values of five tests and error bars in Figure 57 show that the tests results are repeatable with error less than 0.1 N.
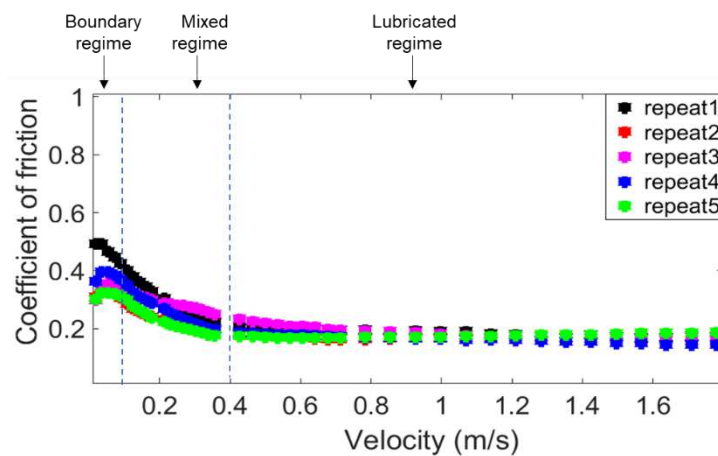
Figure 56. Coefficient of friction versus velocity for five tests carried out using five new wiper blades.
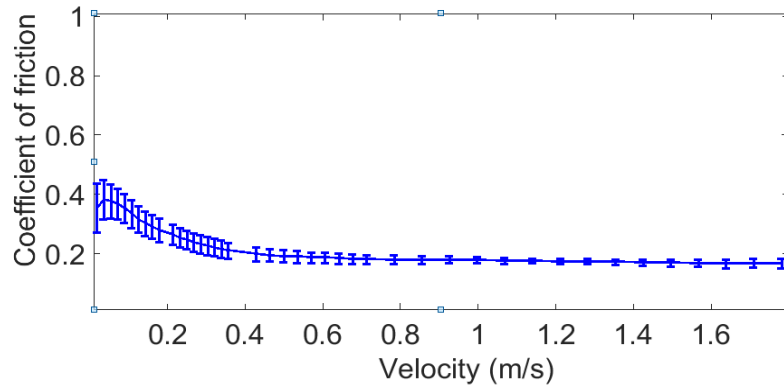
Figure 57. Average of five tests carried out with error bars using five different wiper blades and glass specimens.

There are several possibilities for the low speed instabilities causing the spread in friction in the boundary regime, observed in Figure 56. Partially, it is due to the loading system instabilities of the tribometer due to the feedback system not being able to follow the undulating surface sufficiently rapidly. Another possibility is that using a new specimen for each test introduces unavoidable differences in surface roughness. This is supported by the observation that the spread in friction reduces as the sliding speed increases, since a water film is progressively separating the components and removing the effect of surface irregularities.

5.2   Static friction results

All the other results in this chapter are of kinetic friction, obtained under steady-state conditions. However, it is important to study static friction since static friction, which occurs onset of sliding after a few nanometres of elastic deformation, since it can lead to friction that is higher than would be expected under steady state conditions. Static friction tests were carried out, in which friction was measured when sliding was initiated. These measurements were performed in order to understand the effect of velocity and pre-sliding waiting time on the magnitude of the static friction peak. The following conditions were set: speeds ranging from 0.0000178 to 0.0534 m/s, and pre-sliding waiting times from 0.1 s to 20 s at a constant load of 17 N/m.
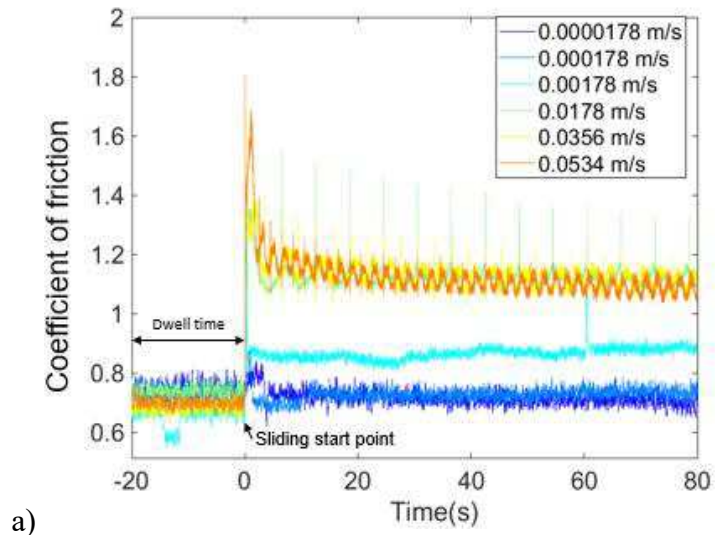
a)
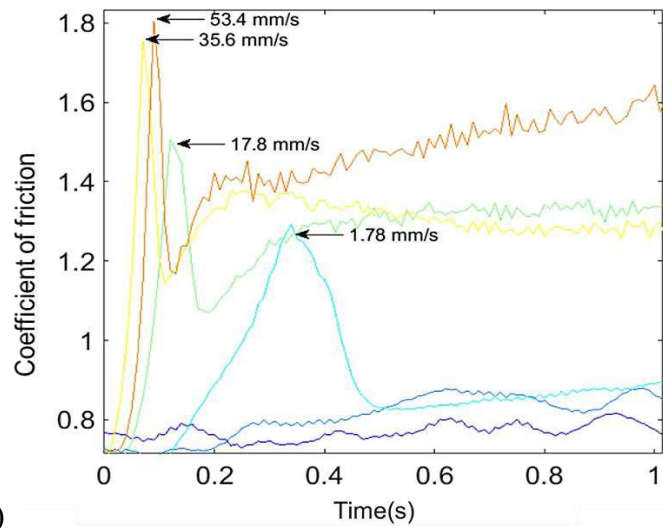
b)
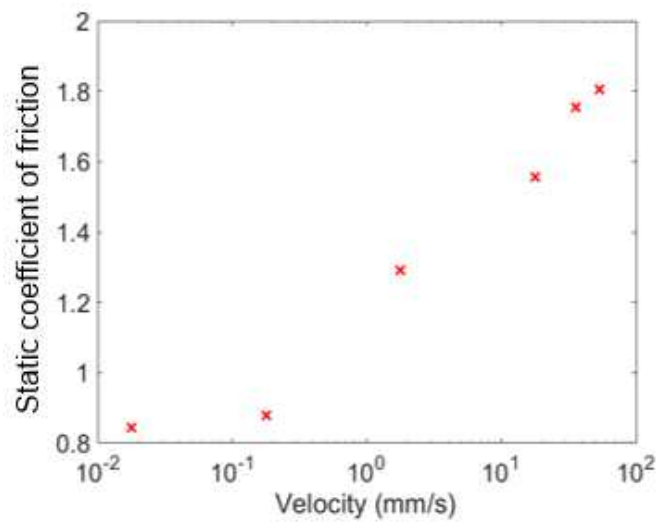
c)

Figure 58. a) Static friction versus velocity, b) zoom in the Figure 58a) representing static friction peaks b) Static friction peak versus velocity.

Static friction tests were first performed for speeds ranging from 0.0000178 to 0.0534 m/s and the results are shown in Figure 58a and b. The variation in friction with time shows the typical static friction peak occurring at the onset of sliding, however, it is also evident that there is a variation between curves obtained at different sliding speeds (note: a slight cyclic variation in friction at the frequency corresponding to the rotation of the disc is also observed due to the experimental errors described above).

Furthermore, at low speeds, there is no change in friction as sliding commences, whereas at higher speeds it can be seen that static friction increases nearly linearly with speed. This behaviour can be seen more clearly in Figure 58c, which plots the magnitude of the static friction versus velocity. At first sight, the absence of a static friction peak occurring at low velocity could be attributed to the rubber only experiencing small displacement, which causes only deformation and no sliding. However, this cannot be the case, if the sliding distance for each test speed is considered (for instance, during the 80 second test at a sliding speed of 0.000178 m/s, the glass surface moved 14.2 cm relative to the holder of the wiper specimen, which is greater than the maximum possible elastic deformation of a specimen). This shows that relative sliding between the rubber and the glass must have occurred. Therefore, the absence of static friction for this sliding speed must be due to the pre-sliding deformation causing the interface between the rubber and glass to break in a gradual fashion (see Figure 59).
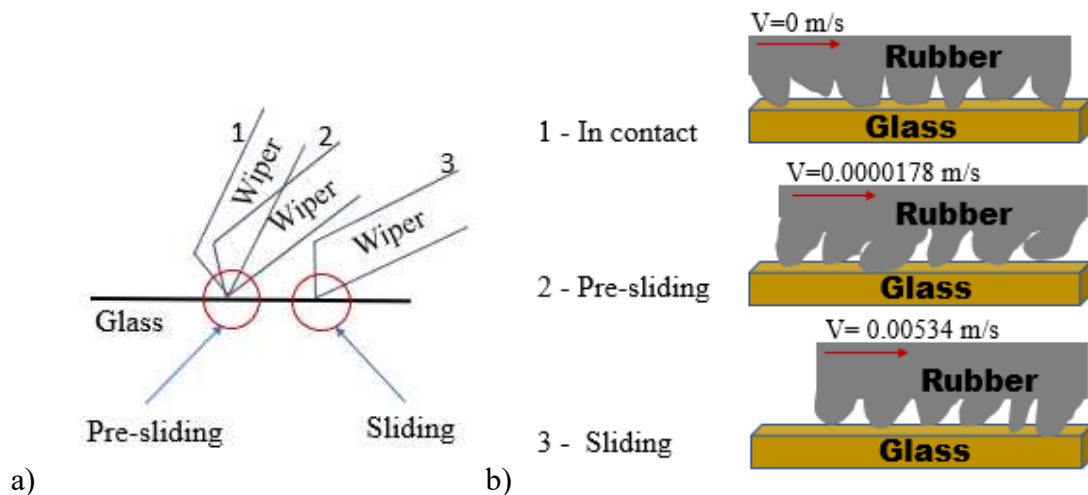
Figure 59. Simple schematic diagrams showing static friction mechanism at: a) macroscopic and b) microscopic level.

Since the static friction peak is associated with the detachment of polymer chains from the counterface surface [30], the increase in static friction with velocity can be attributed to the viscoelastic variation with velocity shown in Figure 9.

As shown by Grosch [26], this dependence of friction on speed follows a similar relationship to the dependence of the loss modulus, shown in Figure 5. This is because the friction force (under normal circumstances) is related to the internal friction of the rubber. In the specific case of static friction, this behaviour can be attributed to elastic deformation of the soft material or local bonding of the asperities that occurs prior to sliding.

a)

b)

c)
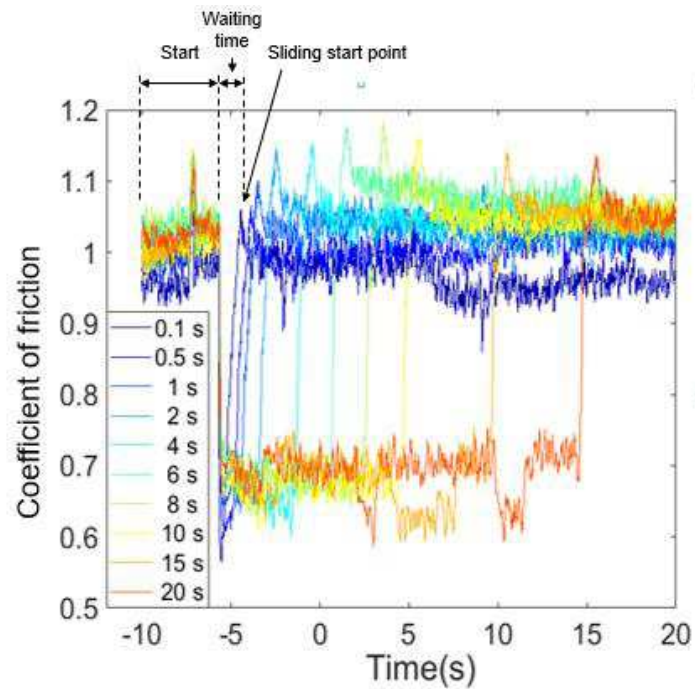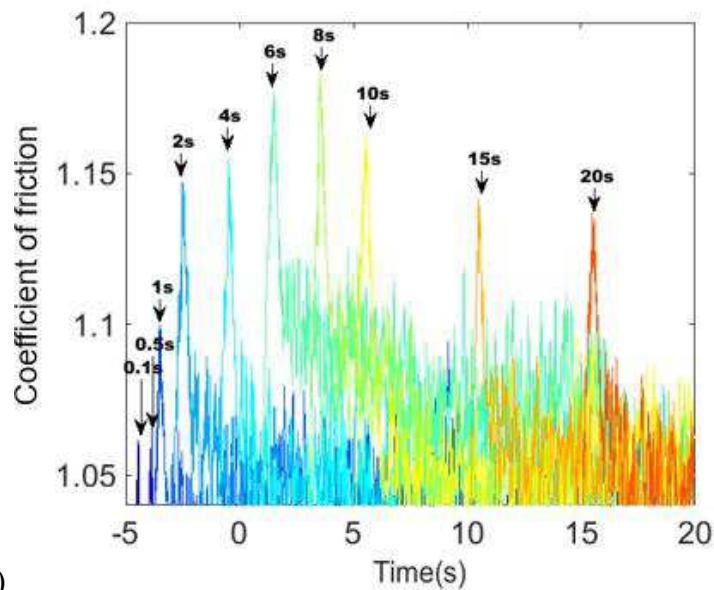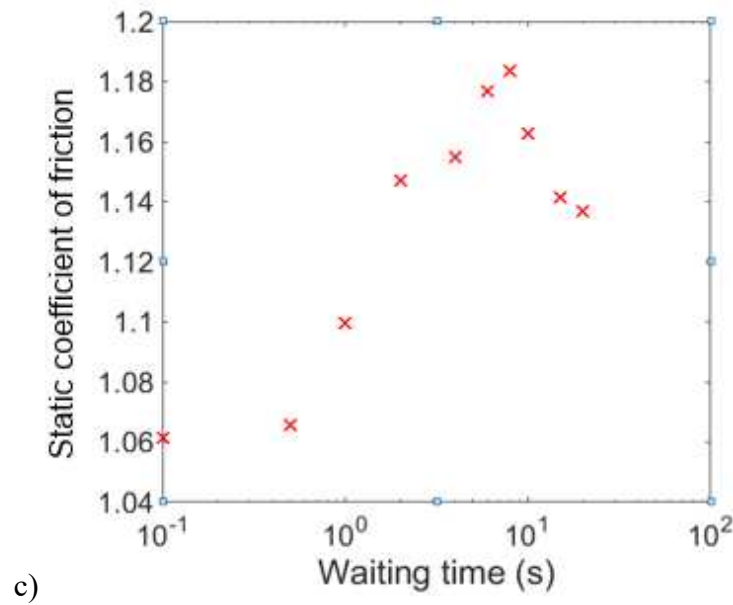
Figure 60. a) Static friction versus time, b) zoom in the Figure 60a) representing static friction peaks and c) Static friction versus waiting time.

Figure 60a and b show the dependence of static friction on waiting time (relaxation time) of the rubber. This data was obtained in the following steps: *i*) sliding surface together under load, *ii*) pausing the sliding motion for a specific length of time, *iii*) resuming sliding.

It can be seen from Figure 60 c, which plots the maximum value of static friction, that the magnitude of the static friction peak is dependent on how long the contact has remained stationary. Friction increases with waiting time and then drops off. This is believed to be due to the gradual increase in surface contact that occurs over time (*i.e.,* short waiting times do not allow the rubber to make a complete bond with the glass surface). The apparent flattening of the curve can then be attributed to the waiting time extending beyond the time necessary to make a complete bond between the surfaces. This behaviour is equivalent to that for metals, except they exhibit shorter times to form intimate contacts.

5.3   Wet and dry friction behaviour of different surface treatments

In liquid lubricated systems, three regimes can exist: boundary, mixed and hydrodynamic. In tribology, these three regimes are plotted all together as Stribeck curves [58], as described in Chapter 2.

In order to obtain a Stribeck curve, friction measurements were performed over a range of speeds. This was done for different glass coatings. The range of surface coatings applied to the glass and tested include: Hochglantztrockner (hydrophobic), Ceroxide (hydrophilic), Self-assembled monolayers (SAMs), including Octadecyltrichlorosilane (OTS), and are describe in the Sample preparation chapter. Cleaned glass without coating was also tested. The data shown in Figure 61a and b are for an uncoated wiper blade rubber when it was tested at a normal load of 17 N/m in wet conditions against a glass specimen with a range of coatings. Figure 61 shows that friction was reduced with an increase in speed according to a typical Stribeck curve under wet conditions (Figure 61a). This negative gradient of the friction is important as it can contribute to "stick–slip", resulting in audible noise under certain conditions which is discussed in detail in Chapter. 6. Figure 61 also shows that surface coating has little effect on wiper friction, at high speeds when a thick liquid film is present as it separates the surfaces; however, a variation in boundary friction attributed to the coatings is seen clearly at low speeds. Friction versus speed behaviour is completely different under dry conditions as shown by Figure 62. Here, there is an initial increase in friction with speed, possibly due to the deformation of the rubber, followed by a more constant region. It can also be seen that the friction for the OTS coating approaches that of the bare glass as the coating becomes worn.

a)

b)
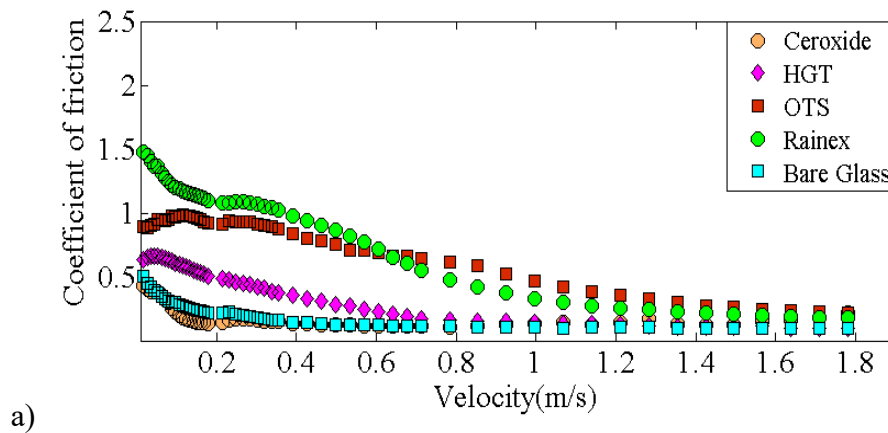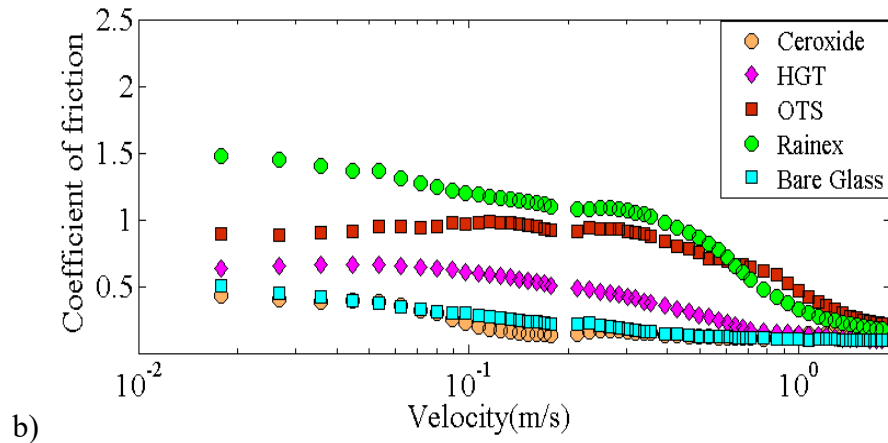
Figure 61. a) Coefficient of friction versus velocity and b) coefficient of friction versus log (velocity) for non-coated rubber specimen, with a normal load of 17 N/m in wet conditions for 5 different coated glasses.

a)

b)
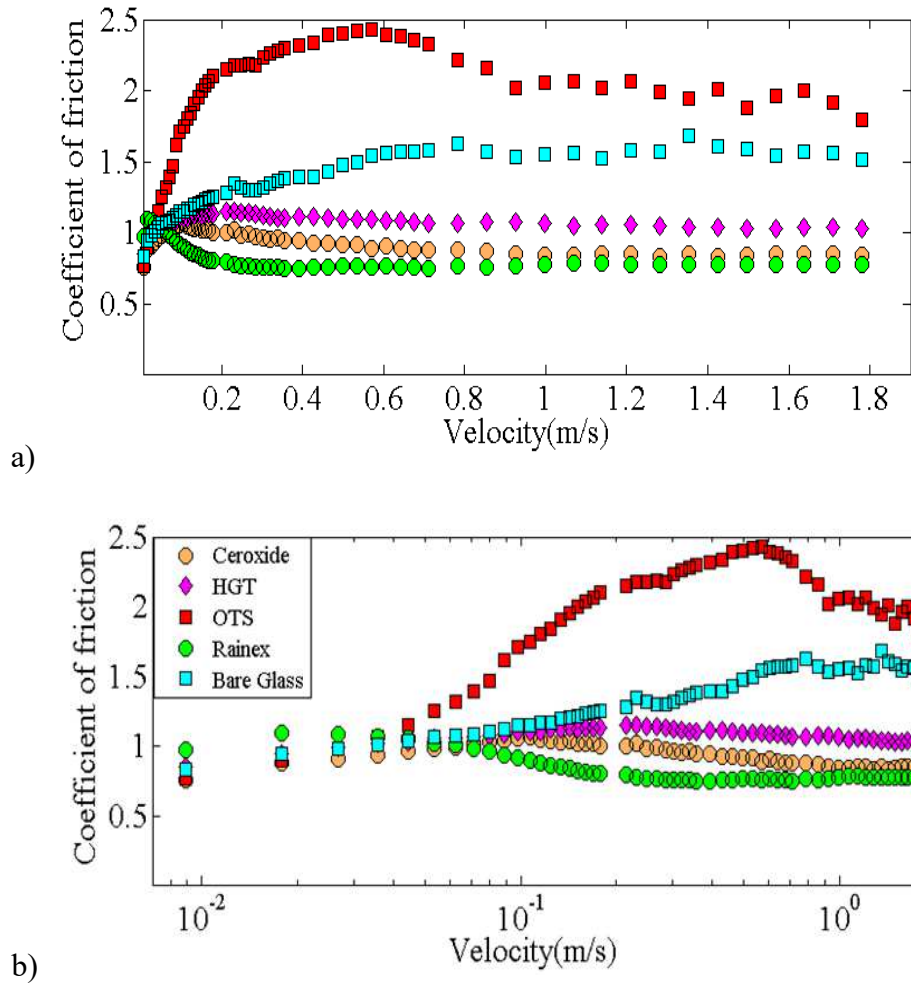
Figure 62. a) Coefficient of friction versus velocity and b) coefficient of friction versus log (velocity) for specimen YL-naked, with a normal load of 17 N/m in dry conditions for 5 different coated glasses.

In dry conditions, the hydrophobic surface treatment generally showed higher kinetic friction than that for the hydrophilic and the untreated surfaces which may be due to higher adhesion. This high friction behaviour becomes less prevalent at high speeds, which may result from increased removal of the wax coating at these speeds, or viscoelastic effects. OTS and HGT surface treatments generally show higher kinetic friction than for the ceroxide and the bare glass, due to higher adhesion and progressive removal of the wax coating at these speeds. The performance of coated specimens was seen to alter during prolonged sliding in dry conditions.

5.3.1 Effect of surface energy

The maximum friction coefficients taken from curves presented in section 5.3 are plotted against the surface energy of each coating in Figure 63. Under dry conditions and at very low speed, friction does not correlate with surface energy. This is understandable, since under these conditions, there is no liquid separating the surfaces and other effects such as surface adhesion dominate.
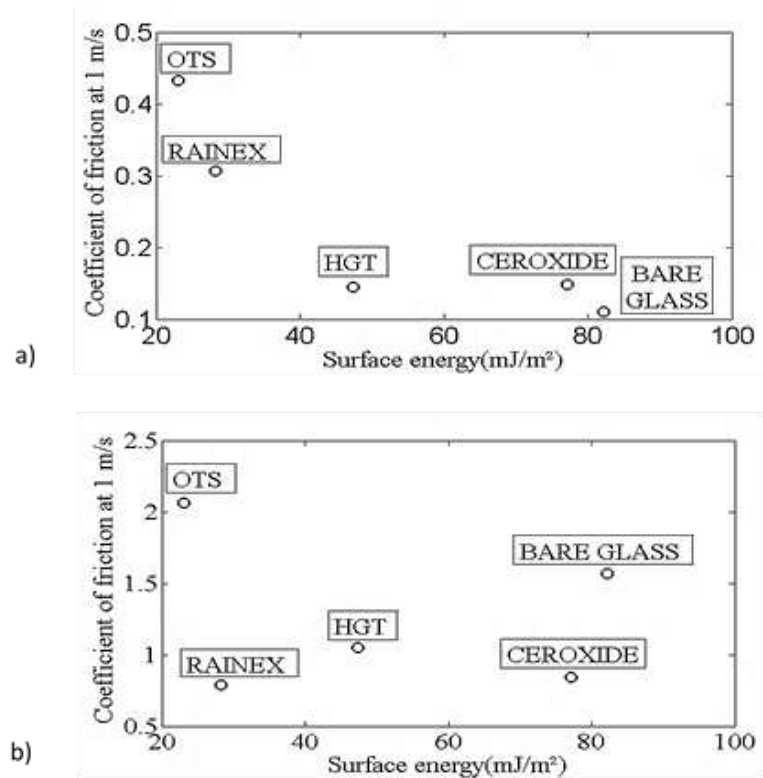
Figure 63. a) Average of coefficient of friction at 1m/s versus surface energy, for YL wiper not coated against glass coated with OTS, HGT, Ceroxide and bare glass in wet and b) dry conditions, with a normal load of 17 N/m.

101

Under mixed and hydrodynamic lubrication conditions, it can be seen that the friction reduces with increasing surface energy. This behaviour can be attributed to the hydrophobic nature of the low energy surfaces preventing liquid from being entrained into the contact, leading to starvation. Conversely, when the surface energy is high, lubricant is entrained effectively into the contact separating surfaces and resulting in low friction. More specifically, Reynolds' equation, which predicts the pressure separating surfaces in hydrodynamic lubrication, requires the lubricant to wet the surfaces (the no-slip boundary conditions) in order produce a lubricant film. This boundary condition, and therefore the ability of the contact to produce a low friction lubricant film, is impeded by the hydrophobic surface treatment. This hypothesis is shown schematically in Figure 64 below. The detrimental effect of hydrophobic surfaces on friction is most pronounced in the mixed regime, since it is here that friction is most sensitive to changes in film thickness, *i.e.,* a small decrease in film thickness in this regime, caused by the hydrophobicity of the surface, increases asperity contact and markedly increases friction. However, when the surface energy is high, the friction is low, as water molecules are effectively dragged into the contact (see hypothesis shown below Figure 64a and b).
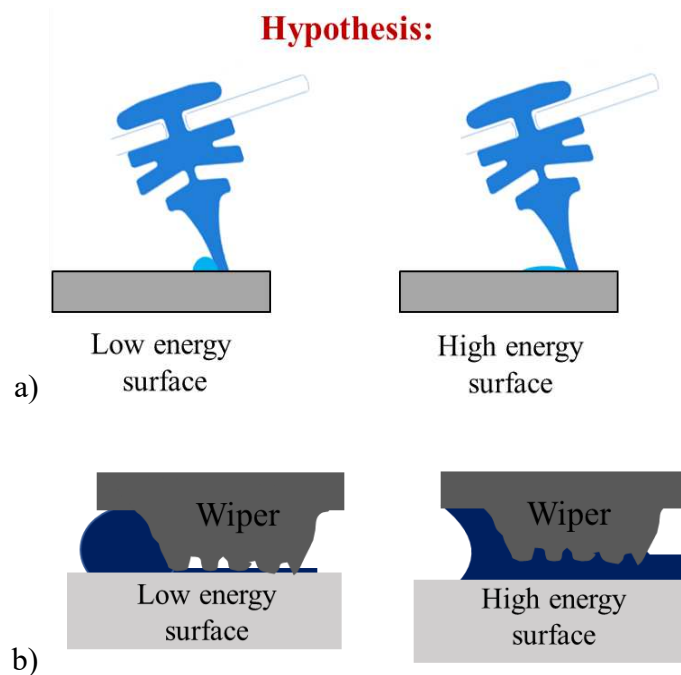
Figure 64. a) Hypothesis regarding the effect of surface energy on friction: behaviour of the wiper blade sliding against a hydrophobic glass (low energy) and hydrophilic (high surface energy) and b) representation of the hypothesis from Figure 64a) at microscopic level.

To further study this behaviour, specimens were tested with a controlled range of surface energies obtained using OTS self-assembled monolayers (with a range of dipping times) and tested over a range of speeds to produce Stribeck curves. The advantage of these tests are that surface energy can be adjusted while other properties, such as surface roughness can effectively remain constant. The results of these tests are shown in Figure 65a.
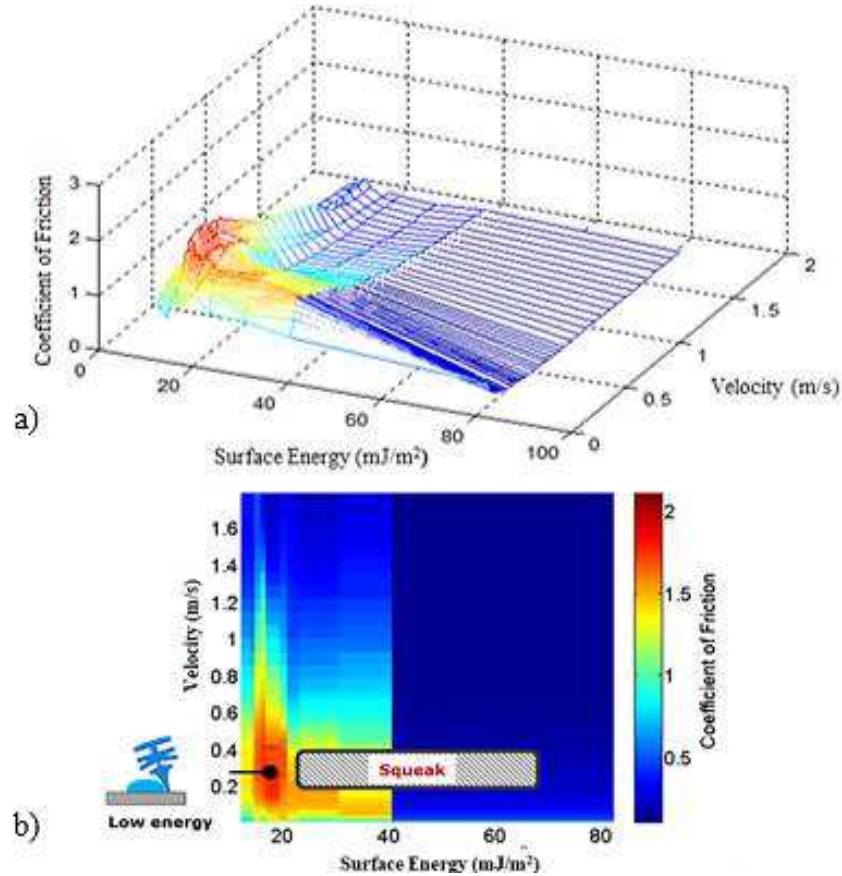
Figure 65. a) Friction measurements for OTS self-assembled monolayers with different surface energies versus velocity and b) critical region where the squeak occurs for OTS self-assembled monolayers with different surface energies versus velocity.

During these tests on SAM surfaces, the occurrence of friction induced vibration was also monitored. As shown in Figure 65b, there is a critical region where the squeak occurs. This region is defined by the negative slope of the Stribeck curve (*i.e.,* the mixed regime) and sufficiently high surface energies to enable water to be entrained into the contact.

5.3.2 Dependence of wiper geometry on friction

One of the requirements of this project was to devise a means of testing the frictional characteristics of rubber wiper materials independently of the wiper geometry. In order to characterize the geometry-independent friction response in this way, friction measurements were carried out using L material in different wiper geometries, such as the YL profile (naked and PPC coated) wiper profiles, triangular (L naked and coated) triangular specimens, L naked strip specimens rolled over bar, glass ball against L naked strip specimens (Figure 66). Two rubber materials Y and L with different mechanical properties are used to manufacture an YL wiper blade, such that the upper part of the wiper blade is made up of Y material while the lower part of the wiper blade (lip) is made up of L material. A glass ball on rubber strip configuration was tried, but this was abandoned since its viscoelastic behaviour is not representative of an actual wiper/windscreen contact.
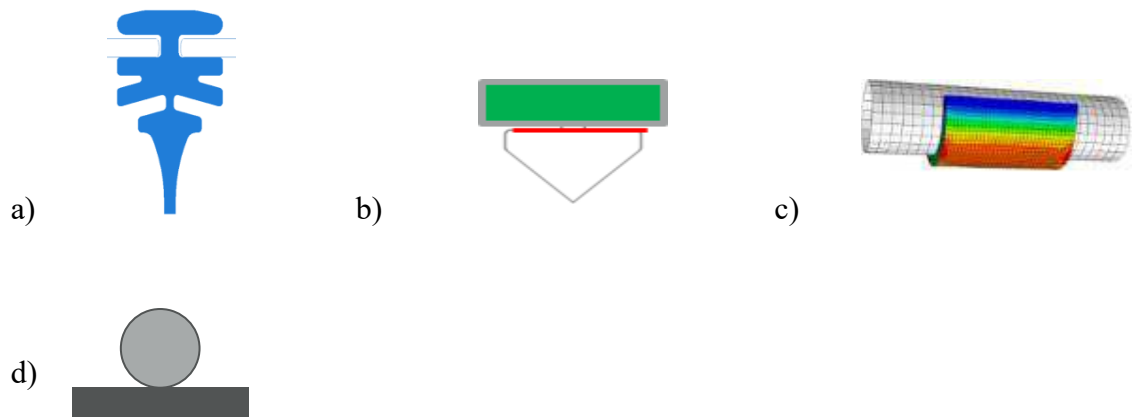
Figure 66. a) Normal wiper blade profile b) triangular specimens c) strip specimen adhered onto glass rod discs and d) glass ball against strip specimen.

The different geometries shown in Figure 66a-c were tested under dry and wet conditions with a load of 17 N/m as shown in Figure 67. Here, it is interesting to note that friction appears to be largely independent of material geometry. This may be explained as follows. Under dry and low speed conditions there is no liquid being entrained between the components surfaces so the wedge shaped geometry is not critical, and friction is governed by the surface properties of the rubber.

a)

b)
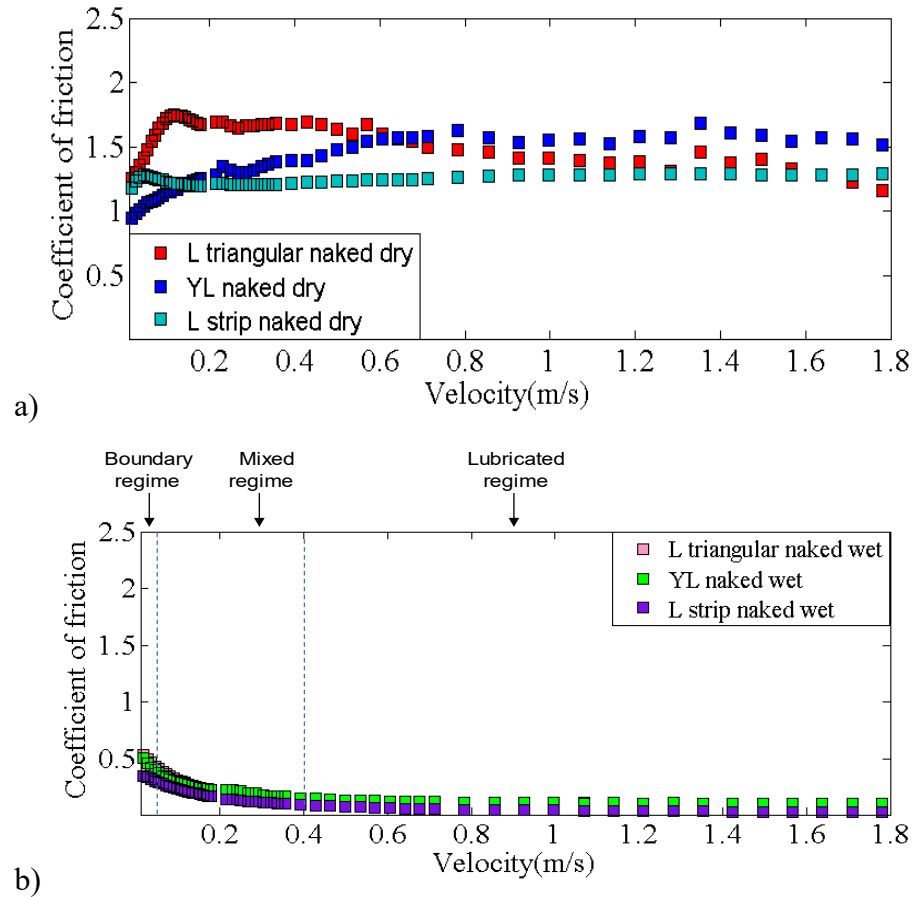
Figure 67. L triangular naked specimens and YL wiper blades naked in dry conditions (old and new wiper blades) and b) wet conditions.

Conversely, at high speed, when the surfaces are separated by a full hydrodynamic film of liquid, there may be differences in friction between the specimens, however, the magnitude of the friction is so low (the only losses are due to the shearing of the thick water film), that the absolute value of the differences are small and difficult to observe. An additional reason for the similarity between friction is that, in the full film regime, friction varies very little with film thickness (*i.e.,* the curve is approximately flat in this region).

Under mixed and boundary conditions, differences in friction can be observed between the specimens, which is understandable since friction is sensitive to changes in film thickness in this regime. This is an important result since it suggests that the friction of different wiper materials can be assessed before complete wiper profiles are manufactured.

a)

b)
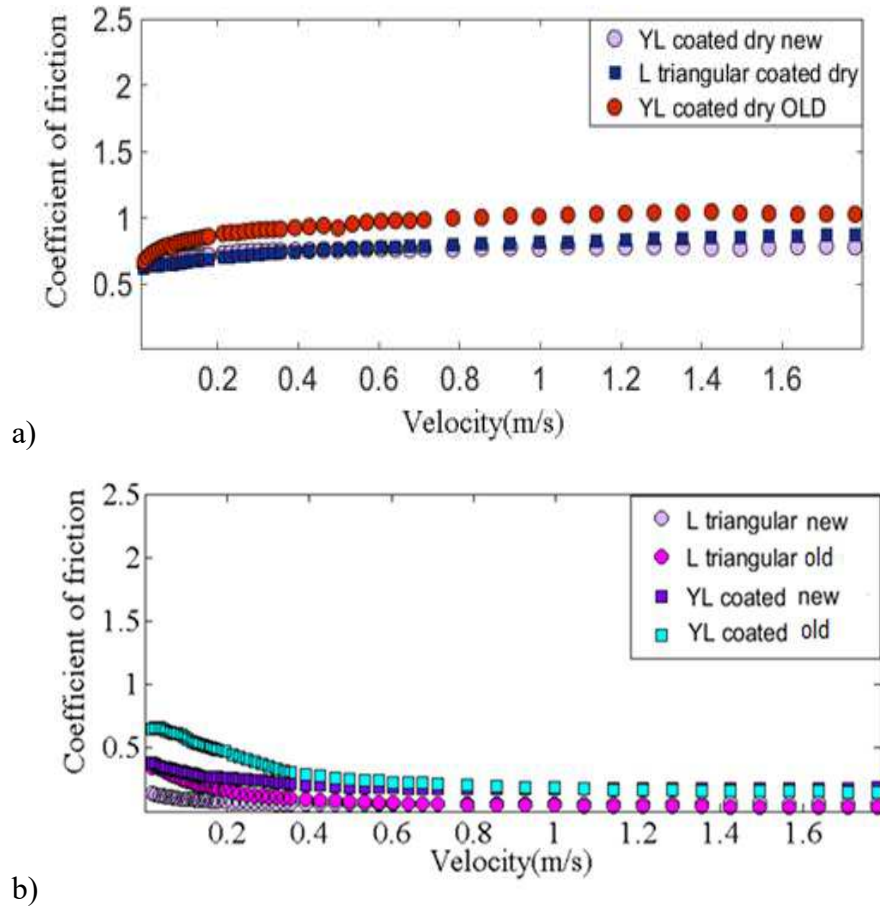
Figure 68. a) L triangular PPC coating specimens and YL wiper blades PPC coating in dry conditions (Old and New) and b) wet conditions.

Figure 68 shows tests which were run in order to assess the effect of components with different material properties of friction, but the same geometry. Specifically, fresh and aged L rubber samples, are compared. Here, a strong effect can be observed. The higher friction of the aged sample can be attributed to a higher elastic modulus, since, over time, crosslinking occurs, which reduces flexibility of the elastomer molecules [30]. The higher stiffness will increase the contact pressure so that thinner films will be required to produce hydrodynamic pressure to balance the applied load (see Figure 69). These thinner lubricant films give higher friction since both asperity contact, and lubricant shear rate are increased. In particular, the higher stiffness limits the ability of the rubber asperities to conform to the glass surface. It can also be seen from Figure 68 that, when surfaces have a PPC coating applied to them, the friction response is no longer independent of geometry. It is suggested that this is because the PPC coating (small spheres attached to the component surface) increases the roughness of the surfaces, however, further testing is required to study this.
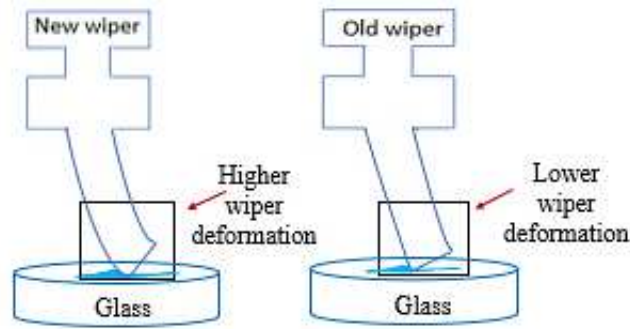
Figure 69. Simple schematic diagram showing ageing mechanism increasing friction in wet conditions.

5.4 Drying friction

For a contact involving a compliant elastomer component, there is a third environment that can occur in addition to the dry and wet conditions investigated above. This condition is named the "tacky" or "drying" regime and exhibits unusually high friction and squeak noise. This behaviour has in a few instances been attributed to meniscus effects as shown in Figure 70. [9]. Specifically, a lack of liquid due to the drying process leads to the formation of a meniscus between the two components (or possibly menisci between individual asperity contacts).

The menisci produce a negative pressure which briefly pull the surfaces together and hence increase the contacting surface area and therefore the friction force. It should be noted that this is only a theory and there has been no direct evidence that tacky friction is caused by meniscus effects.
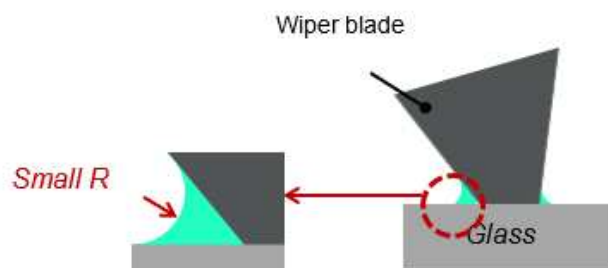
Figure 70. Simple schematic diagram shows capillary mechanism increase friction under tacky conditions.

The tacky friction phenomenon can be encountered, when the wiper system is not turned off by the driver after a rain has stopped so that the rubber wipers are still sliding when there is insufficient water present.

As shown by the experimental results in Figure 71, the peak in friction has a higher value than for the same contact under dry conditions. Then as the remaining water is removed from the contact, (*i.e.,* from ~10 seconds onwards), friction approaches that for the steady-state dry condition. Despite its obvious importance, this maximum friction is difficult to measure.

The main reason for this is that it is questionable whether the tacky condition is reached simultaneously at every point along the length of the wiper blade. In fact, due to the variation in speed along the specimen, it is likely that drying occurs non-uniformly.

Air applied-reducing water volume
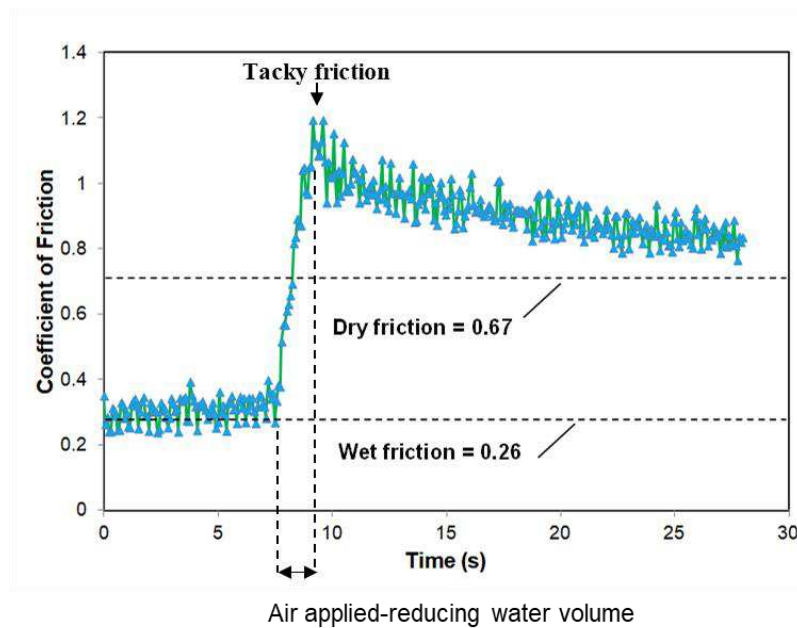
Figure 71. Friction vs. time for rubber wiper specimen FXG sliding at against untreated glass under drying conditions (steady-state friction values for dry and submerged friction are also given for reference). The normal load is 17 N/m, and the sliding speed is 0.25 m/s.

In order to control this tacky friction peak in friction (see Figure 71), tests were performed when the surface tension of the distilled water was varied from 74 ± 1.9dyn to 36.4 ± 2.7dyn cm^{-1} by adding a surfactant. The logic of this is that altering (reducing) the surface tension of the liquid will reduce the meniscus pressure and hence limit the increase in contact area under drying conditions (that is if indeed meniscus effects are responsible for tacky friction). These tests were performed at 34 N/m and 0.5 m/s, while steadily reducing the volume of water through evaporation. Figure 72 shows that drying friction peaks are much lower when a low concentration of surfactant is included in the water. This shows that tacky friction can indeed be controlled (for windscreen wiper

manufacturers, the most effective way of doing this would be to change the rubber formulation to reduce its surface energy). In addition to this, the removal of the friction peaks by the surfactant in Figure 72 are evidence to support the unproven theory that tacky friction is caused by meniscus effects.
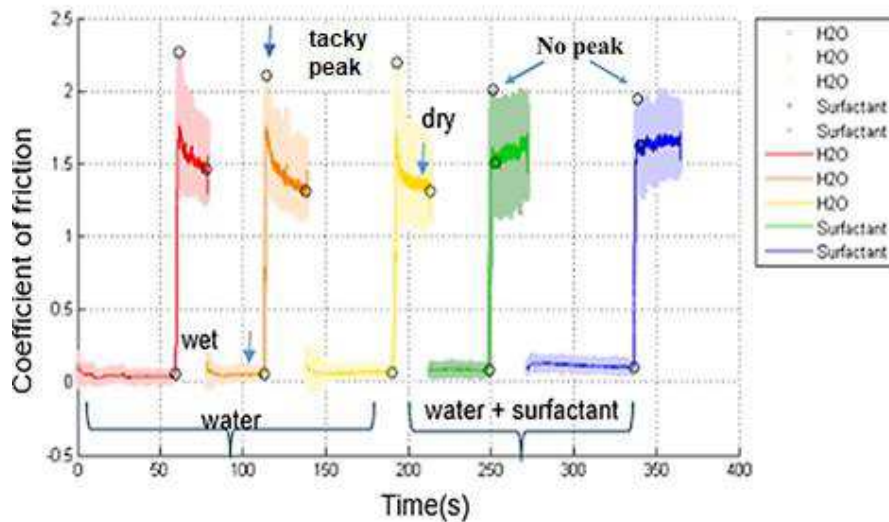
Figure 72. Friction versus time, showing tacky peak and effect of detergent.

It is also evident that there is a slight increase in the value of dry friction in Figure 72. This is most probably due to the fact that the surfactant is forming a film on the glass, while the water is evaporating.

5.5   Wear tests

Tests were also conducted to study the effects of wear on wiper friction. Here, a number of approaches were taken. Various degrees of wiper wear were achieved by rubbing the wiper blades against glass for different lengths of time between 2 and 10 hours at 1.33 m/s, prior to etch test. In addition to this, to mimic severely worn conditions, wiper blades were rubbed against sand paper, prior to testing, in order to accelerate wear. The burrs that form on these pre-worn wipers are shown in Figure 76. Also, an additional approach was to use an etching paste to obtain various roughness of the glass slide. As described in sample preparation chapter, the paste consists of sodium fluoride and hydrogen fluoride, which changes the characteristic roughness and translucent qualities of frosted glass over time. This enabled friction tests to be carried out on glass with different roughness from 0.5 nm to 5 μm. In certain tests, wiper deformation was monitored, in real-time, using a microscope and video camera, while friction was measured (Figure 73).

a)   b)
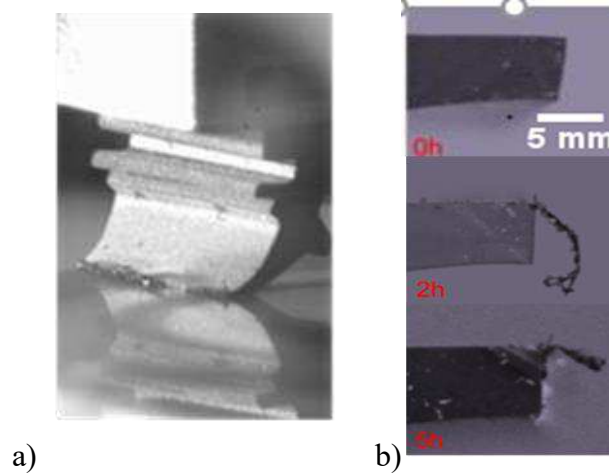
Figure 73. a) Wiper wear test and b) wiper blades worn for different lengths of time from 2 to 10 hours at 1.33m/s.

The Stribeck curves in Figure 74 shows that the friction increases with pretest rubbing time. Analysis shows that this behaviour is due to a combination of rubber wear and the formation of a transfer film on the glass surface (note: from Figure 73 it can be seen that as the wiper has worn the edge of the lip becomes disrupted and also a film of rubber is formed on the glass surface). Figure 74 also shows that the effect of this mild wear is most pronounced at low speeds, whereas, at high speeds, there is little difference between the specimens. This again can be attributed to the independence of friction on film thickness in the full film regime.
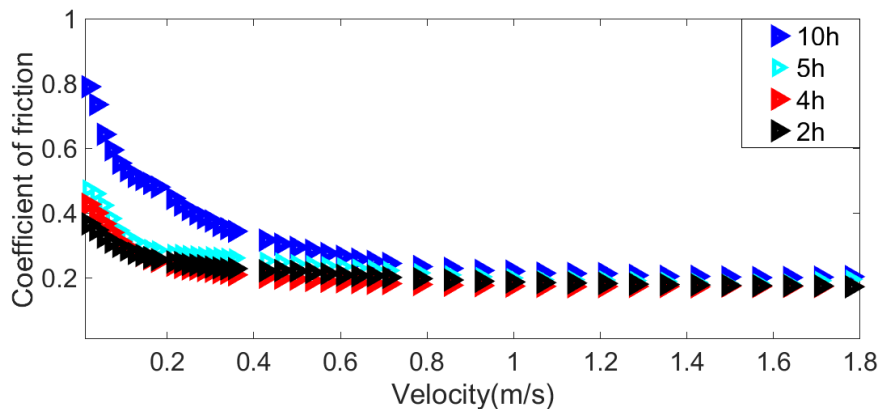
Figure 74. Coefficient of friction versus velocity for wiper profiles (pre-worn wipers for different lengths of time from 2 to 10 hours at 1.33m/s) in wet conditions.

In the case of severely pre-worn wipers, the hydrodynamic film is disrupted by the formation and removal of burrs (Figure 75). Specifically, friction increases when burrs are formed and subsequently decreases when they are removed (252 m sliding distance).

110

This is because the burrs formed do not have the same smooth wedge-shaped geometry as the non-worn specimens and therefore hydrodynamic load support is reduced (leading to thinner films and more surface contact). Furthermore, the increased roughness of the worn wipers means that a greater film thickness is required to separate the rubbing surfaces, so that the onset of full film lubrication is postponed until higher speeds. It is also possible that the fraying of the worn surfaces results in a larger contact area, which would increase adhesion. This behaviour can be noticed by comparing the microscope image of the specimens before and after testing (Figure 76). For instance, the wiper that was pre-worn for 252 m of sliding initially shows the highest friction but then falls to below the 63 m specimen. Examination of Figure 76 reveals that a large burr has been removed from the rubber profile and is very likely responsible for the change in friction performance (this is in perfect agreement with observations made by Schallamach regarding the formation and detachment of rubber wear debris discussed in the literature review chapter). It can also be observed that the surface topography of the worn rubber surfaces in photographs in Figure 76, appear to be very similar to those predicted by Gent in Figure 14 of the Literature Review Chapter. In both figures wear results in parallel ridges lying perpendicular to the sliding direction, which is indicative of tearing during sliding wear.

The etched glass results in Figure 77 show that friction increases with roughness. This may be due to an increase in contact adhesion between the asperities of rubber and glass surface due to the breakdown of the water film separating the surfaces, *i.e.*, the lambda value of the contact has been increased (Figure 77). It can also be seen that there are differences in hydrodynamic friction between all of the different specimens except the 0.5 and the 10 nm roughness specimens, which confirms that the water film thickness is in nanometric range between 10 and 200 nm.

By comparing the friction values in Figure 75 and Figure 77, it can be seen that roughening the glass has a greater effect of increasing friction that roughening the rubber wiper. This is because the rubber is significantly more compliant compared to the glass, and its roughness features are therefore more easily flattened by the contact pressure. The values of coefficient of friction at 0.18 m/s are scattered in Figure 75 due to the instability of the low speed motor.
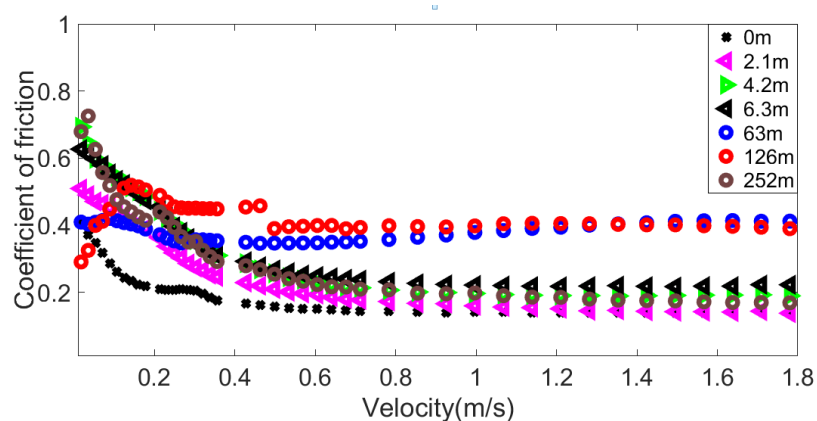
Figure 75. Coefficient of friction versus velocity for wiper profiles (pre-worn wipers using sand paper) in wet conditions.

Before measuring friction

After measuring friction
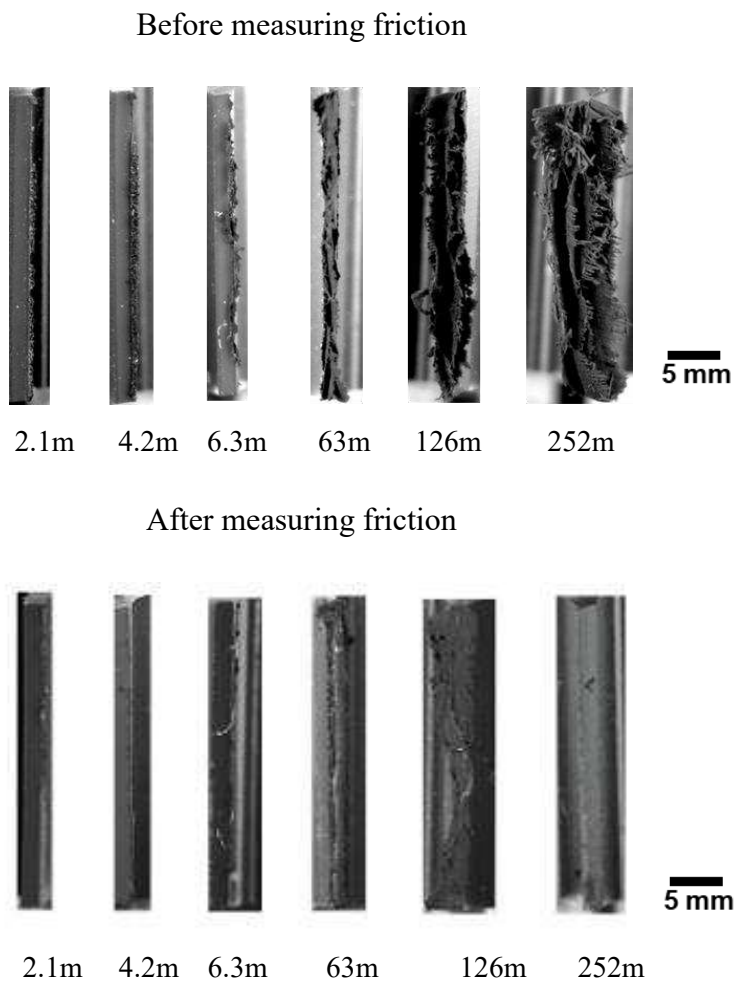
Figure 76. Microscope images showing pre-worn blades before and after measuring friction.
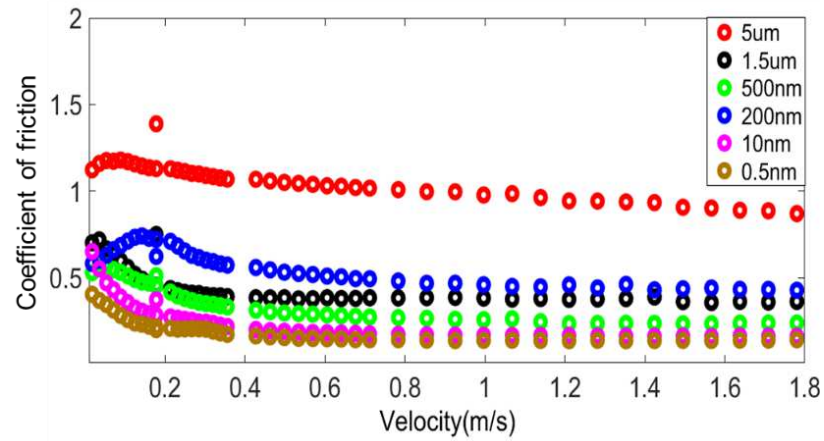
Figure 77. Friction versus velocity for etched glass.

To summarize the results in this section, two types of wear mechanism are evident, which agrees with previous work by Roberts [101]. For smooth surfaces (Figure 73a), adhesion/smearing is observed, which is characterized by tacky surfaces and the transfer of material from the rubber to the glass. This can be attributed to either extrusion of low molecular weight polymer additives or degradation of the polymer. This degradation may result from either thermal or mechanical stress [101], or alternatively, for low speeds, it has been attributed to mild abrasion. For rough surfaces on the other hand (Figure 77), abrasion of rubber results from mechanical failure due to excessively high local frictional stresses which are most likely to occur on rough surface peaks.

Furthermore, it can be seen from Figure 76 that the severely worn wiper has formed frayed ridges, which run parallel to the sliding direction. This is a similar pattern to those described by Gent and Pulford [48] for abrasion of rubber in a constant direction, and is suggested to be due to the cumulative growth of cracks caused tearing of the elastic material, which occurs in a repetitive fashion similar to fatigue. A summary of the overall mechanism by which wiper blades wear is produced is presented in Figure 78.
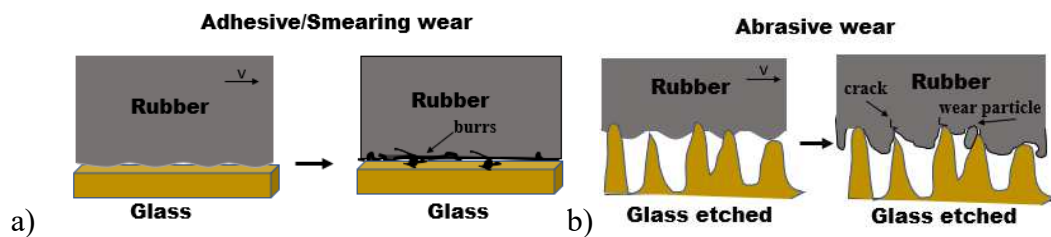
Figure 78. Wiper blade wear mechanisms: a) adhesive and b) abrasive.

5.6   Summary

This chapter has described research that was carried out to study the friction behavior of wiper-glass interfaces. Specific attention was paid to effect of non-steady state conditions, since these have not previously been studied in detail.

Key findings include:

- Static friction can reach considerably higher levels that kinetic friction and therefore must be considered with selecting motor requirements. It was also shown that static friction has a strong dependence on both waiting time (relaxation time) of the rubber and sliding speed. Specifically, static friction increases linearly with speed, while changes in wiper no addition change in friction was observed after a waiting time of 8 seconds suggesting that this is the relaxation time of the material.

- Friction is largely independent of wiper geometry for naked specimens under wet and dry conditions. However, friction does depend on geometry for coated specimens under wet and dry conditions. It was also shown that ageing has a strong effect on friction.

- Friction reduces with increasing surface energy in the mixed and full film regime, and this has been attributed to increased wetting of the surfaces (at low surface energies the water is prevented from entering the contact). This effect is not present under dry and boundary lubrication conditions when there is no liquid separating the surfaces.

- Tacky friction peaks were reproduced and results showed the studies show that their magnitude could be significantly reduced by including a low concentration of surfactant in the water. This result provides evidence to support the theory that tacky friction peaks arise due to meniscus forces. It also raises the possibility of modifying the surface energy of the rubber in order to limit this unwanted effect.

- Following gradual wear, friction increases, which has been attributed to a combination of wiper damage (which increases roughness and reduces lambda value) and the formation of a transfer film.

- Following rapid wear, friction variations result from the formation and removal of burrs. The wear mechanisms observed in this study agree with those found in the literature for both high and low wear conditions.

- Comparing test results from etched glass specimens with those from worn rubber profiles showed that friction is more sensitive to the roughness of the glass surface. This behavior is attributed to higher compliance of the rubber compared with the glass. Tests on the etch glass also showed that the thickness of the water film must be in the nm range (since changes in glass roughness of this order affected friction values). Further study of water film thickness is carried out in Chapter 7.

Chapter 6

Friction Induced Vibration Results

6 Friction Induced Vibration Results

In this chapter, an investigation into the noise emitted from a wiper/glass contact is described, which was carried out in order to elucidate the mechanisms of noise generation and understand the effect of different parameters. To this end, friction, sound, and high-speed video measurements were recorded and analysed to locate the source of the noise, characterise the oscillatory motion and the role of the water meniscus.

In addition to this, experimental data are compared to the finite element model, described in section 6.6 and the mass-spring-damper model described in Chapter 2. The overall purpose of this section of the project is to develop a list of criteria that can be used by companies to enable them to produce windscreen wipers that do not squeak.

First, friction coefficient and sound measurements are presented. Then, simultaneous measurements of squeak using the microphone set-up and the laser Doppler vibrometer are compared to determine whether the frequency of emitted sound coincides with the frequency of the vibrating wiper (*i.e.*, to ascertain which component is producing the sound). Next, high speed camera video recordings are analysed to understand the motion of the wiper and water during the emission of squeak. Following this, the results of the wiper/glass contact using a finite element model are compared with the experimental data. The chapter ends with a list of practical recommendations on how to prevent wiper squeak that have arisen from the findings.

6.1   Reproducing Friction Induced Vibration using tribometer

The first step in this investigation was to reproduce the friction induced noise that is typically emitted from a windscreen wiper system using the lab-based experimental set-up. A range of speeds, loads and different test conditions were adjusted until loudly audible friction induced vibration could be heard. It was found that this occurred most when a commercially available windscreen wax was applied to the glass specimens after cleaning, which was rubbed against the rubber wiper at low speed. This is in agreement with previous observations, noted by drivers and windscreen wiper manufacturers, that the prevalent friction induced noise increases under these conditions.

6.2 Laser Doppler Vibrometer measurements

Once the friction induced vibration could be reproduced reliably under laboratory conditions, the next step was to use the Laser Doppler Vibrometer (LDV) to ascertain whether the vibration of the wiper could be detected and if so, to measure its frequency. To do this, the LDV was positioned with its beam incident on a thin strip of reflective tape bonded to the wiper specimen (Figure 79a). This tape was necessary in order for the vibrometer to detect a reflected signal back from the specimen (the approach was taken once additional measurement had proved that the presence of the tape did not prevent the emission of friction induced noise). The LDV's laser spot was positioned at several different locations along the lip of the wiper: A, B, C, D, and F (see Figure 79b) and velocity measurements made. Very little difference was observed between the measurements at these different locations, which may suggest that that the wiper is vibrating in plane (further confirmation of this is given in Figure 93). For this reason, the results shown here are only those obtained from point C in the centre of the wiper.

a)   b)
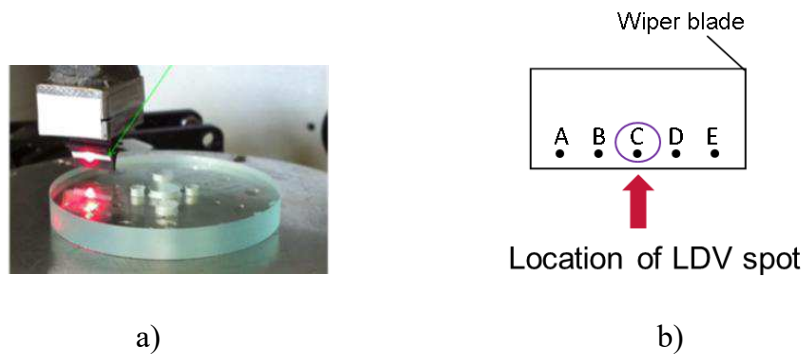
Figure 79. a) LDV beam incident position on the reflective strip on the blade and b) Diagram of wiper blade specimen showing locations of focused laser spot, for use during LDV.

Figure 80 shows an example of the raw data from the LDV, obtained while the rubber wiper was rotating against the glass and producing an audible squeaking sound. This velocity versus time signal shows some cyclic fluctuations are occurring as the glass disc is rotating. To study these in greater detail, Figure 81 shows a zoomed in plot of data in Figure 80, from 0.44 to 0.53 seconds (note: the axis has now been changed off from disc rotations to time in seconds), which appears to show that for this test, the wiper is oscillating only at certain positions on the glass disc surface.

Furthermore, the individual oscillations of the wiper can be seen to have a period of approximately 5 kHz, which was believed to correspond the frequency of the emitted sound. However, it is difficult to interpret the signal in this way without looking directly at its frequency content. Therefore, in order to do this, a Fast Fourier Transform (FFT) was performed on the time signal to view the individual frequency components. The results from this are shown in Figure 82, which are FFTs taken of the time signals shown in the two previous figures. It can clearly be seen from Figure 82 that there is a large peak in the data at around 5 kHz, which is likely to correspond to the audible noise. In order to further confirm that the peaks in the frequency signal were indeed due the presence of the emitted noise, two consecutive tests were carried out. The only difference between these two tests was that the first used waxed glass to produce audible friction induced vibration while the second used bare glass and was silent. The FFTs of the LDV signal from these two tests are shown in Figure 83. It can clearly be seen that the high frequency vibration of the wiper only occurs when the audible noise is heard.
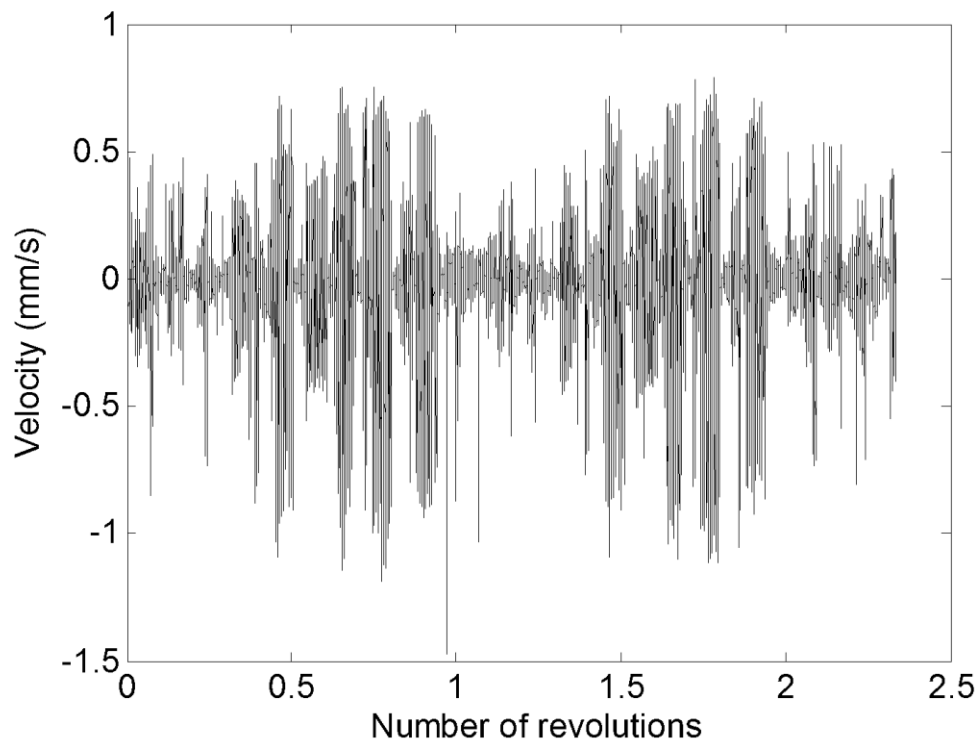
Figure 80. Velocity versus time for naked wiper blade PQ, rotating at 70 rpm (0.125 m/s), under 7 N/m loading. Note: time for one rotation is 1.1667 s.

119
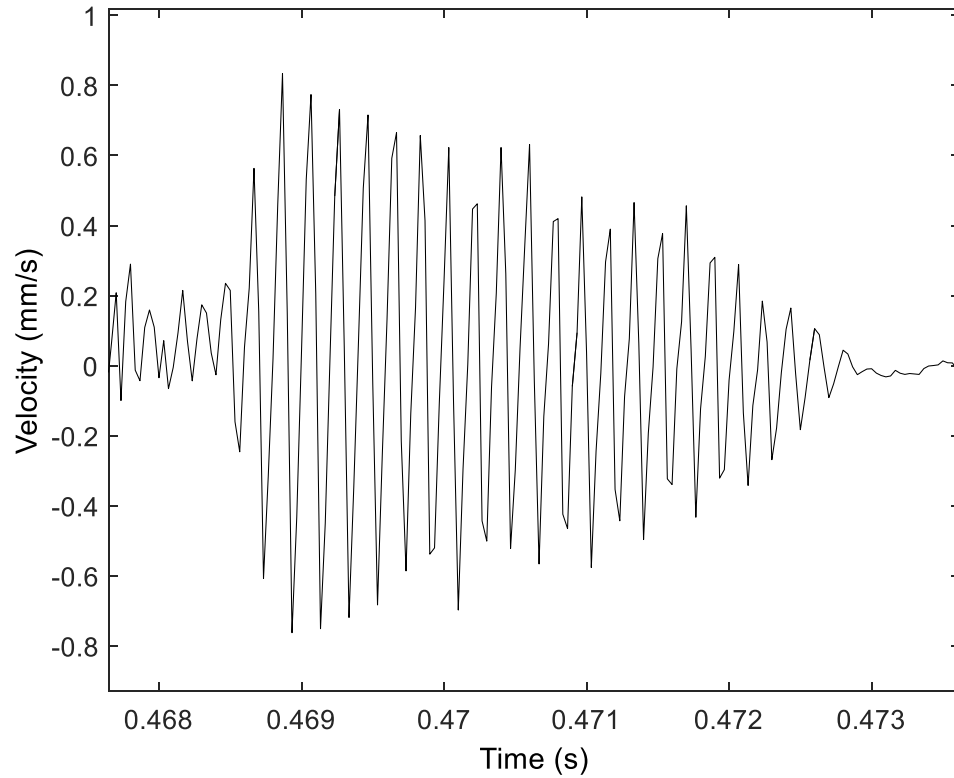
Figure 81. Zoomed in plot of the signal shown in Figure 80.
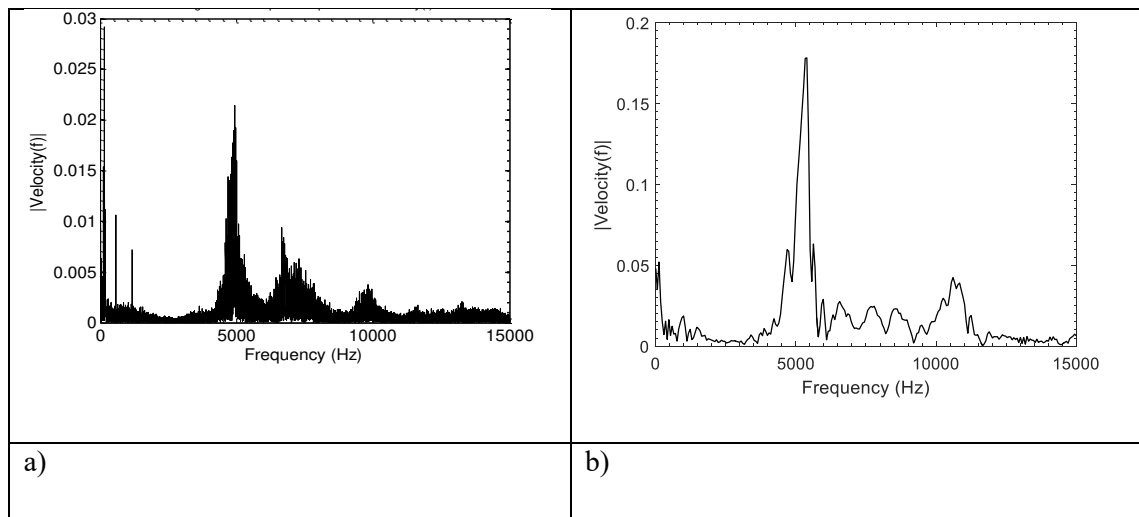
Figure 82. Fast Fourier Transform of the data shown in a) Figure 80 and b) Figure 81.

a)

b)
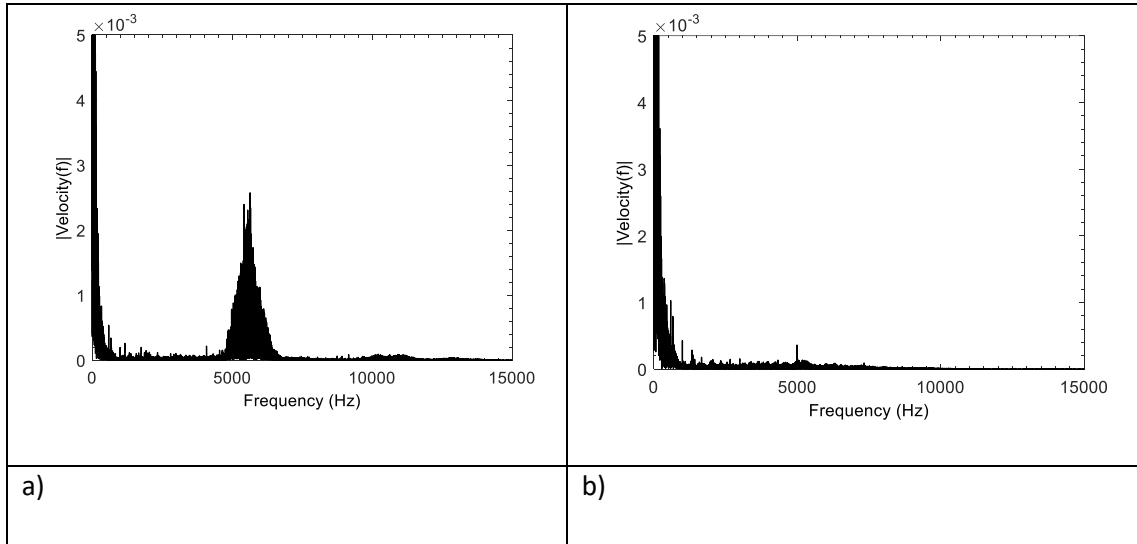
Figure 83. Fast Fourier Transform of LDV signal obtained when friction induced was a) audible, b) inaudible.

6.3   Microphone measurements

Simultaneous measurements of friction and vibration were performed under a range of conditions, in order to determine the frequency range of squeak and to understand the effect of the lubrication regime on noise generation. Friction measurements were performed using a UMT2- CETR tribometer shown in Figure 84, while the microphone was mounted very close to the contact to monitor the emitted noise.
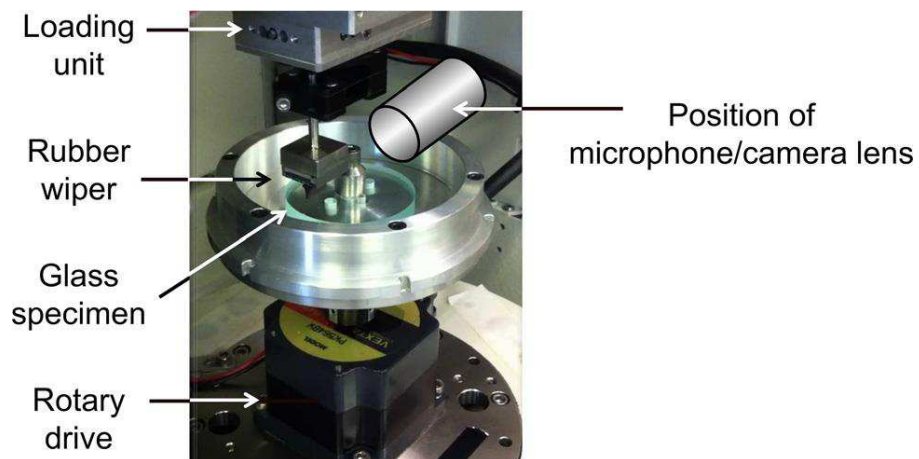
Figure 84. Photograph of apparatus used to simulate the contact between wiper and glass.

121

The first tests to be carried with the microphone were in order to validate the measurements made using the LDV. These tests involved setting up the contact under conditions which caused the emission of friction induced noise and measuring the signal using both the microphone and the LDV. Figure 85 shows FFTs from both of these measurements, obtained during one of these tests, where it can be seen that here is very close agreement. This validates both sets of measurements and shows that the emitted sound is indeed produced by the vibration of the wiper.
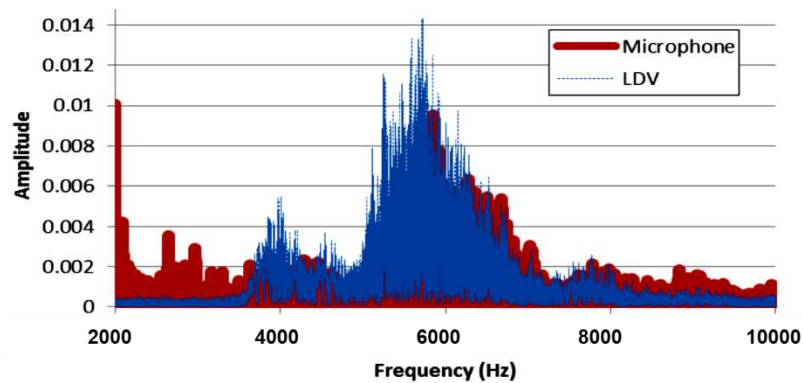
Figure 85. Squeak measured by Microphone and LDV at the same time.

In order to analyse the noise further, the microphone data was plotted in the form known as a spectrogram. This is a frequency versus time plot, where the colour corresponds to the amplitude of the signal. This plot is produced using Matlab software and is effectively a series of FFTs, performed on consecutive portions of a time signal. An example of such a spectrogram is shown in Figure 86.

One unwanted feature of this plot is the presence of the continuous line at around 1200 Hz. After several control tests were performed (*i.e.*, tests in which the sound was recorded while the glass was rotated but with no contact being made with the rubber wiper), it was ascertained that this frequency component was due to interference from the tribometer's motor. To rectify this problem, a post processing filter was used, which performed an FFT and then suppressed the frequency component.
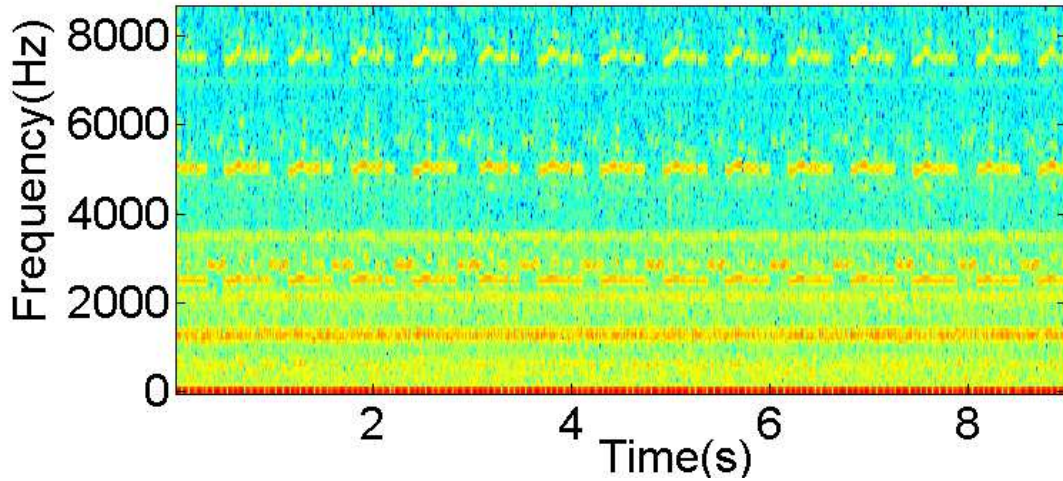
Figure 86. Spectrogram of recorded noise from friction induced vibration test.
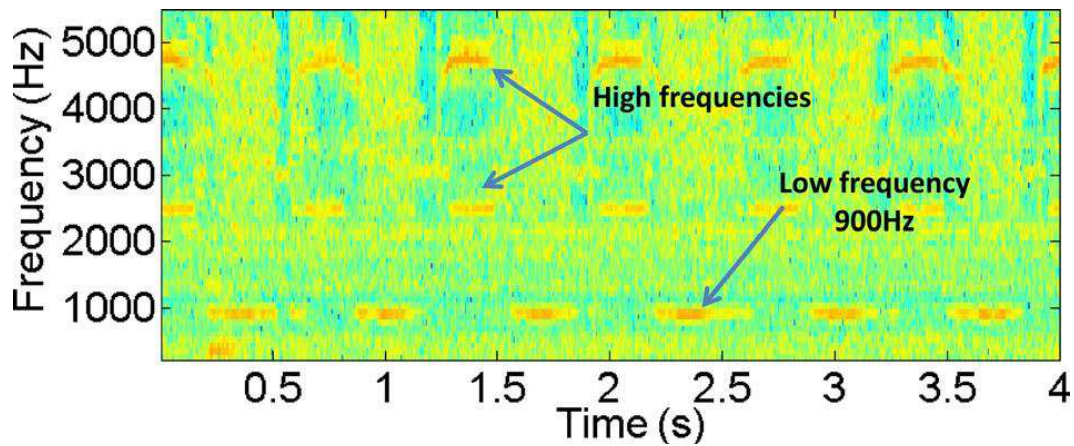
Figure 87. Spectrogram of friction induced noise with motor interference removed.

Figure 87 shows an example spectrogram, in which the motor interference has been removed, from a friction induced vibration test. During this test, which involved a combination of untreated rubber and waxed glass with water present at the inlet, friction induced noise was clearly audible. Two distinct frequencies can be distinguished at approximately 900 and 2400 Hz. It should be noted that these frequencies have changed from those of the LDV tests shown previously. This difference is attributed to the presence of the reflective tape that was required for the LDV tests and is believed to increase the frequency of the emitted sound due to its stiffening effect.

During the large number of tests carried out under similar conditions, the noise frequencies detected were always close to one of these two values (though not usually during the same test as shown in Figure 87. These two frequency values have also been observed by other researchers [84].

123

Furthermore, as shown Figure 87, the emitted noise does not occur at both frequencies simultaneously. This suggests that vibration may be occurring due to the excitation of specific bending modes of the specimen (see section 5.5). It can be seen in Figure 87 that the high frequency component just below 5000 Hz appears to be a harmonic of the 2400 Hz component, since it is exactly double the frequency. Such harmonics suggest that the vibration is not purely sinusoidal in nature.

The variation of friction coefficient with sliding speed for the wiper glass contact, loaded with 17 N/m with water at the contact inlet, is plotted in Figure 88. This shows the typical Stribeck behaviour, with "mixed" friction falling from a high value in boundary regime, where the load is supported solely by asperities to a lower value in the hydrodynamic regime, where a liquid film separates the surfaces.

These observations are in agreement with those made in other studies on wiper lubrication regimes [59]. Since a combination of untreated rubber and waxed glass was used, friction induced noise was clearly audible during this test. This sound was recorded and processed in MATLAB to isolate the component between 2 and 3.5 kHz. The result is plotted alongside friction in Figure 88. It can be observed that the largest amplitude of sound occurs within the mixed lubrication regime, where the gradient of the friction versus speed curve is negative. This supports the negative damping theory suggested by Le Rouzic *et al.* [84], presented in Chapter 2.
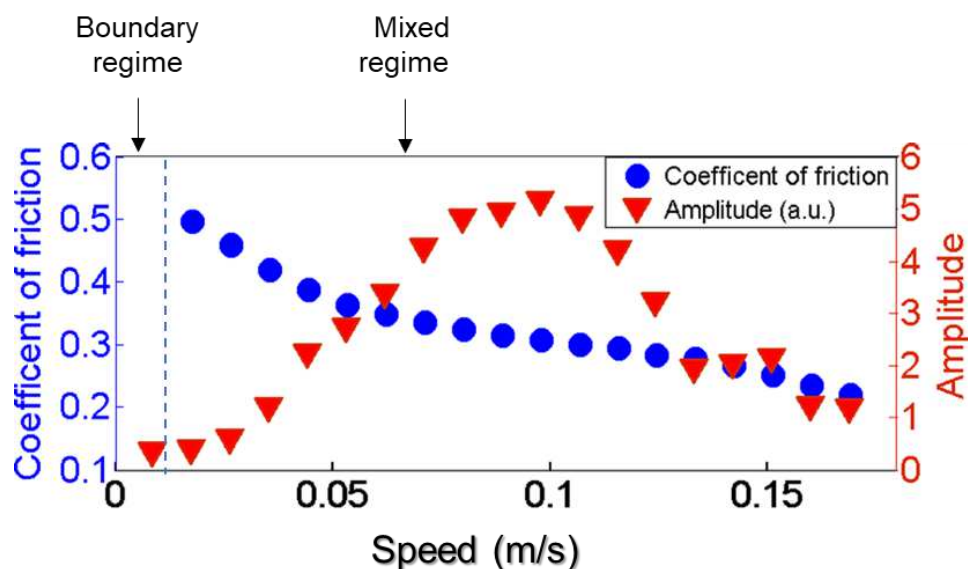
Figure 88. Friction coefficient and noise amplitude versus velocity, for glass–wiper contact, in the presence of water with an applied load of 17 N/m.

To study the role of surface condition more closely, friction tests were carried out on glass specimens with a range of surface energies. Glass specimens were produced with a range of surfaces energies, using the OTS dipping methods described in sample preparation chapter.

As shown in Figure 89, the surface energy and resulting water contact angle can be varied from 14.34 to 82.21 mJ/m^2 by adjusting the dipping time and the OTS solution concentration. Friction tests, in which the occurrence of friction induced noise was noted, were then carried out on each of these specimens. As shown in the Figure 89, friction induced noise only occurred for glass surface energies between 23.28 and 78.18 mJ/m^2. It is not immediately obvious why this is the case, however, a tentative explanation is that below a certain surface energy, the water contact angle is too high to allow liquid to reach the contact which prevents Stribeck curve like behaviour.
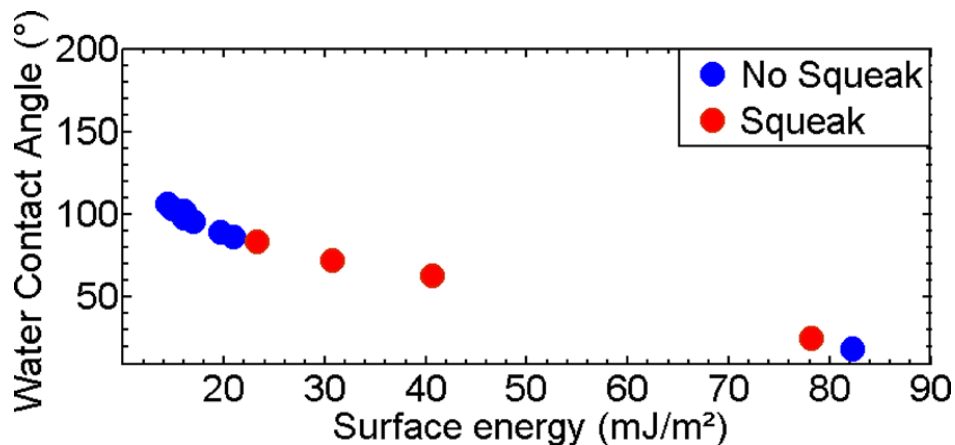
Figure 89. Water contact angle versus surface energy of glass specimens.

The points represent specimens that produced friction induced vibration during sliding tests. In each of these tests, the applied load was 7 N/m and the sliding speed was 0.17 m/s. Figure 89 also shows that no friction induced vibration occurs for bare glass when the surface energy is very high (*i.e.*, when the water contact angle is low). This may be due to the formation of an adsorbed film of water on the glass surface under these conditions, which reduces friction.

Until now, all results that have been presented are from tests in which the volume of water on the glass is constant. This is in line with all the other research into wiper vibration, which have ignored the presence of the water meniscus in the generation of the audible noise.

In order to study for the first time, the effect of water on the vibration, a test was then carried out in which the volume of water in contact with the wiper lip was progressively increased. To vary the quantity of water present at the contact inlet, the contact was initially run dry and then a micropipette was used to administer water in doses of 25µl. This variation in the quantity of water present has a marked effect on the audible sound, as shown by Figure 90, where the dominant frequency of emitted noise (obtained by MATLAB processing of the microphone signal) is plotted against the volume of water present.
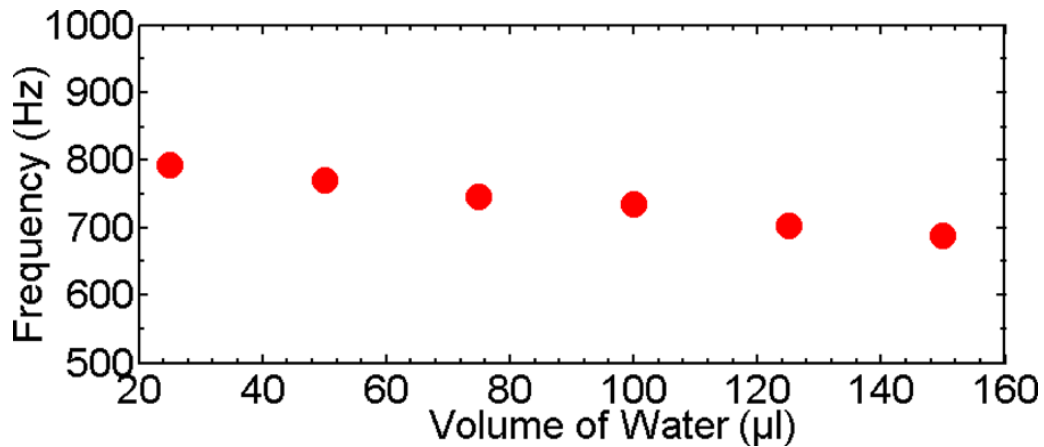
Figure 90. Dominant frequency of emitted noise versus volume of water present at wiper lip.

Here, the frequency of sound decreases as the mass of water at the lip increases. This behaviour has not been reported previously, however, there are two obvious explanations. First, the removal of water may be starving the contact of lubricant, causing a change in the gradient, λ, of the friction versus speed curve. According to equation (6) from Chapter 2, this will affect the damping.

However, this theory was discounted since, even the smallest volume of water applied was sufficient to fully flood the contact. Instead, the relationship between sound frequency and meniscus size can be attributed to the role of water in determining the natural frequency of the vibrating system, *i.e.*, adding water to the contact increases the vibrating mass. This hypothesis is supported by the fact as shown in Figure 90, frequency increases monotonically with volume and therefore follows approximately a $\omega = (k/m)^{1/2}$ relationship.

6.4 High speed camera results

In order to further investigate the effect of the water further, the high-speed camera was focused on the meniscus during tests when audible noise was generated. As shown in Figure 91, large oscillations are observed in the water during the occurrence of friction induced vibration and the patterns produced correspond to the frequency of noise. These disturbances in the water appear to be capillary standing waves, similar to Faraday waves [102], which occur due to the interaction between gravity and the acceleration of an oscillating liquid container [103].

The high-speed videos taken during wiping were then processed in MATLAB to extract the frequency of oscillation of both the wiper and the meniscus. This was done by tracking the intensity variation with time of pixels showing water and pixels showing rubber. Fast Fourier transforms of these intensity variations showed that both the water and the wiper oscillate at the same frequency. It is therefore suggested that the oscillations in the water are driven by the vibrating wiper. Furthermore, this observation that the water follows the motion of wiper supports the hypothesis that the water modulates the frequency of vibration by adding mass to the wiper lip. The fact that the frequency of water waves equals the frequency of wiper is contrary to conventional theory for Faraday waves, which predicts that standing waves have a frequency that is half the excitation frequency [102].

However, for small scale meniscus excited at a high frequency, standing capillary waves can be produced at a frequency equalling the excitation frequency [104]. This phenomenon occurs when the meniscus is sufficiently small that gravity effects are negligible and can be explained by analysing the Mathieu equation [104].
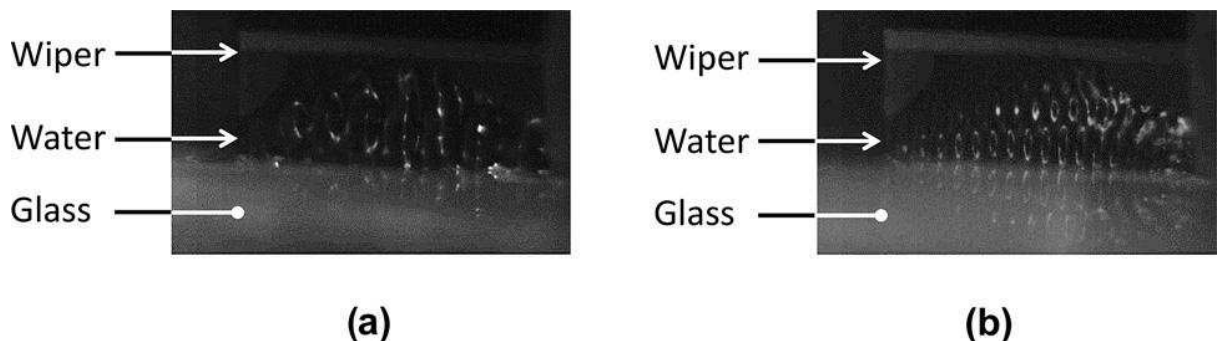
Figure 91. Photographs of meniscus during the emission of: a) 900 Hz noise and b) 2400 Hz noise.

Another high-speed camera test was performed to characterize the motion of the rubber wiper. Figure 92 shows a single image from a video of the wiper lip. In this test, the end face wiper has been painted white to ensure it is visible at high frame rates (30 kHz).

As summarized in the image, the wiper lip oscillates backward and forward while noise is emitted. Also shown is the motion of the water waves, which propagate from the wiper edge. The frequency of lip vibration was then compared with that of the audible sound and was found to coincide. Figure 92 shows that the wiper tip has a forward and backward oscillatory motion.
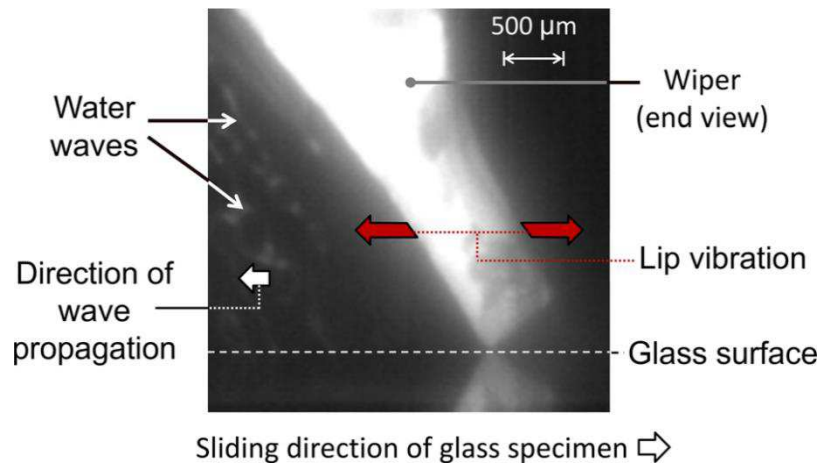
Figure 92. Single frame from high-speed video, showing oscillatory motion.

It is possible that in addition to this, the wiper exhibits a torsional mode of vibration, in which the displacement is not constant along the wiper length (*i.e.*, points along the length of the wiper may not vibrate in phase). To investigate this possibility, videos were acquired during friction induced vibration, in which each end of the wiper was in focus. The video was then processed to show the intensity variation with time of pixels at each end of the wiper. The results from this analysis are shown in Figure 93, where the vibrations of the ends of the wiper are observed to be approximately in phase. This seems to demonstrate that no torsional modes of the wiper are being excited and justifies the two-dimensional (2D) assumption made in the FE simulation.
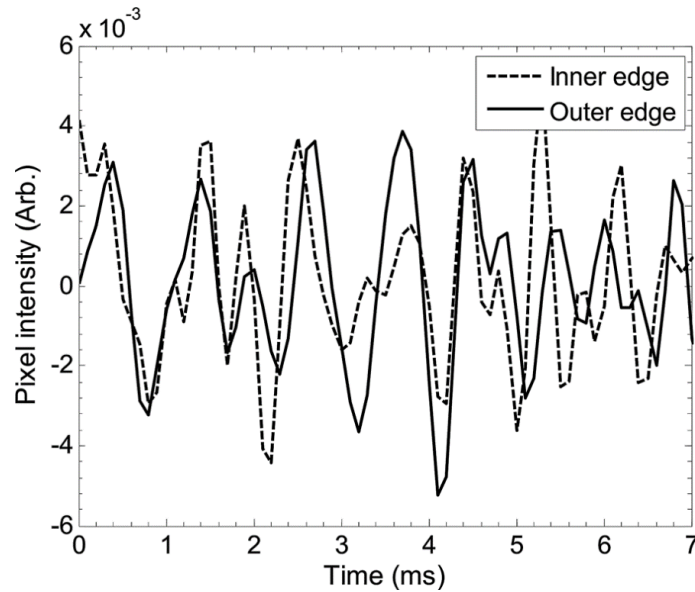
Figure 93. Variation of intensity with time for pixels at each end of the rubber wiper.

Although, the above analysis suggests that torsional modes of vibration are negligible in our experiments, the question remains as to whether such modes are prevalent in the assembled wiper blade structure. Furthermore, the occurrence of these, and other larger-scale three-dimensional modes, may in practice interact with the vibration modes measured in the current study, thus rendering our 2D analysis unrepresentative. However, the frequency components around 1000 and 2500 Hz are close to those found in actual automotive applications (where similar, distinct frequencies can be heard). This suggests that larger-scale oscillations of the wiper structure are decoupled from the high frequency vibrations measured in my study and this supports the validity of the 2D analysis performed.

Tests were also carried out on glass specimens of varying thicknesses. Results from these tests showed that the frequency of the emitted sound was independent of glass thickness. This supports the view that it is the vibration of the excitation of rubber wiper that drives the emitted sound. However, it is believed that the glass must transmit the vibration in order for sound to be audible (if only the rubber vibrated, then it is unlikely that vibrating wipers would be audible to those inside vehicle, as is known to be the case). It is therefore suggested that the glass acts as a sounding board to transmit noise to the driver.

6.5   Finite Element (FE) prediction of wiper vibrational modes

To predict the wiper vibrational modes (the eigen-frequencies) a finite element mode was developed using the commercial software package ABAQUS. The first two bending modes and corresponding eigen frequencies of the rubber wiper as predicted by the ABAQUS FE simulation are shown in Figure 94. It is striking how these eigen-frequencies are in close proximity to those measured experimentally (see Figure 87). Most FE simulations predicted two modes of vibration, the first close to 1000 kHz and the second between 2000 and 2500 kHz identical to those obtained experimentally. FE simulations were also run on profiles with different material properties. These simulations predicted that rubber wipers with sufficiently high viscoelastic damping would have natural frequencies outside the audible range. These predictions were confirmed when experimental friction tests on such specimens showed no audible friction induced vibration. Moreover, the effect of material, boundary conditions and geometry of the wiper blade on noise were simulated using ABAQUS and are presented in section 6.6.1.
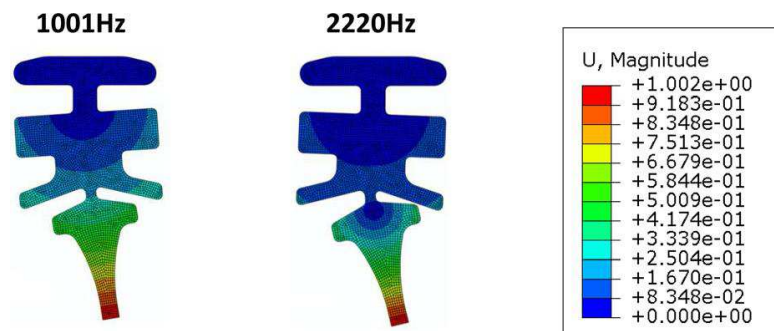
Figure 94. ABAQUS prediction of first two bending modes of rubber.

Figure 95 shows an example of an image taken using the acoustic camera. This image was acquired when the camera was directed at the UMT2 test rig as it rubbed a section of wiper rubber against a piece of waxed glass, (using a setup similar to that shown in Figure 84). During this test, audible friction induced noise could be heard. In Figure 95, the bright colours show the emitted sound, while the black sketch marks show the outline of the rig. It can be seen that the camera is able to detect and image the sound caused by friction induced vibration. However, due to the small size of the wiper specimen and the oblique angle between the camera and the glass specimen, it is not possible to locate the source of the emitted sound.
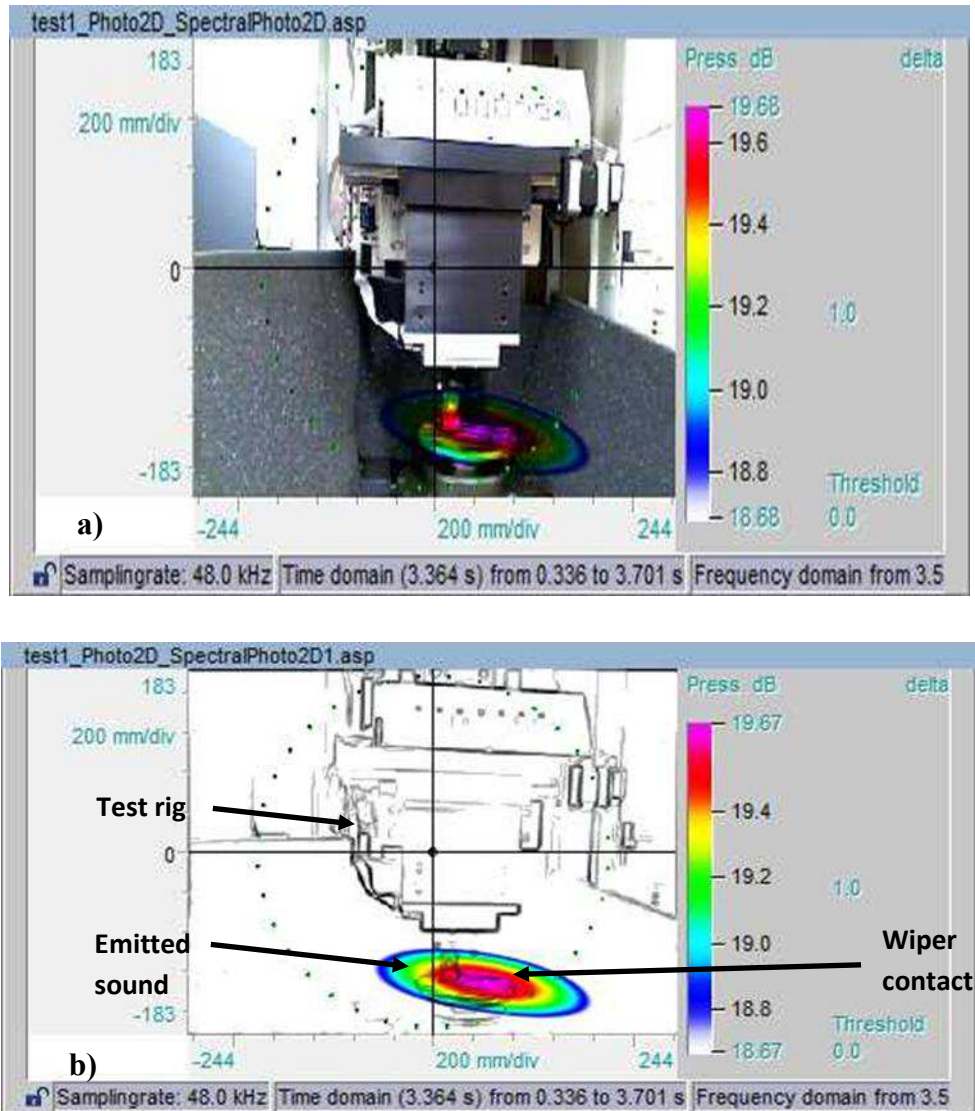
Figure 95. Sonic images of test rig as wiper/glass contact is emitting friction induced noise. (Bright colours show the emitted sound). a) Sonic image superimposed on photograph of rig, b) Sketch of the sonic image superimposed on photograph of rig.

In order to ascertain more accurately the location where sound is emitted, the acoustic camera was focussed on a different type of contact. In this latter test, the contact was produced by manually rubbing a length of wiper rubber against a glass door panel. A low sliding speed was implemented to promote FIV and this was confirmed by the audible presence of squeak. An example video frame from this test is shown in Figure 96. Here, it is interesting to observe that the sound is emanating from the glass at the edge of the panel, rather than from the contact itself.

This is a clear demonstration that the audible noise is produced by the vibration of the glass material and agrees with the fact that windscreen wiper noise is audible from inside a vehicle (if it was only the rubber that was producing the noise, then it would not be audible from within the vehicle).
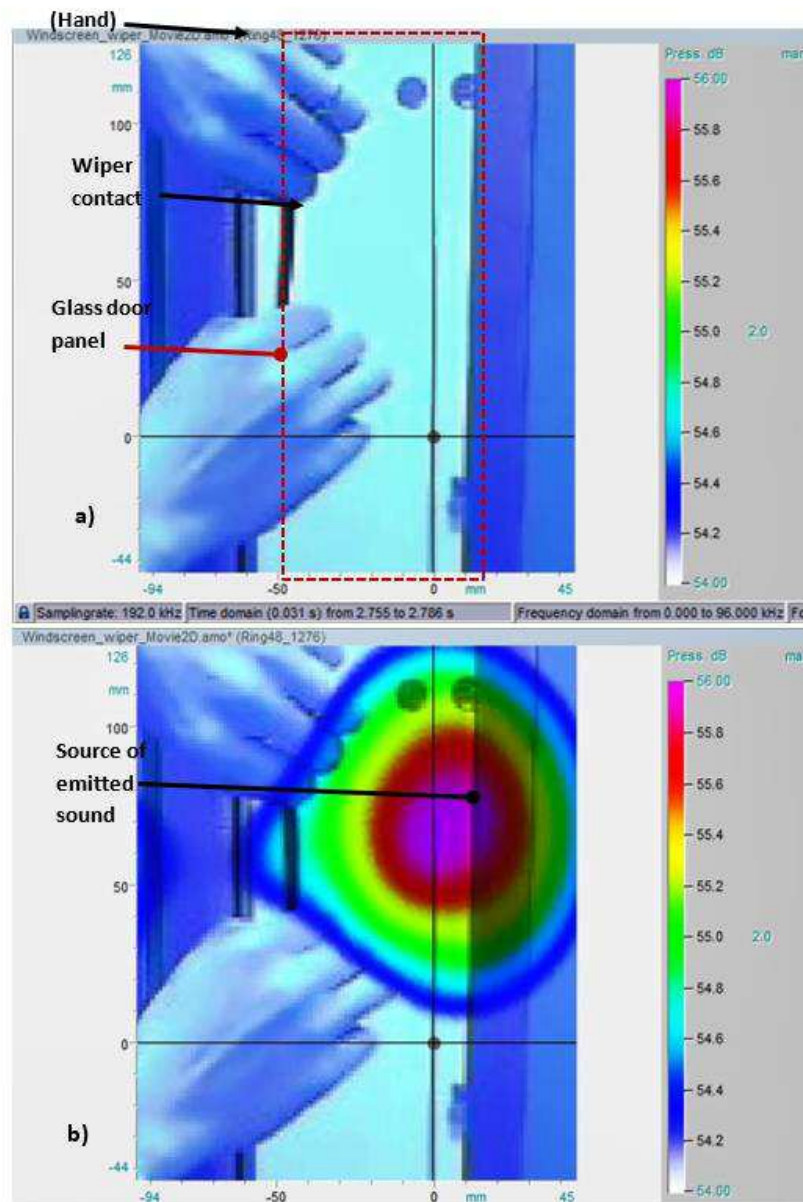
Figure 96. Sonic image superimposed onto photograph of glass door when rubbed by a section of wiper rubber, a) no audible noise, b) audible friction induced vibration.

6.6 ABAQUS simulation

In the study of friction induced vibration described in section 6.5, it was shown that the friction induced noise occurs only when the natural frequency of the wiper profile, predicted by ABAQUS software, is excited. It follows from this that ABAQUS can be used prior to production to determine the natural frequencies of different wiper configurations in order to produce a profile with a natural frequency outside the audible range.

In this section, ABAQUS is used to characterise the effect of different parameters on the natural frequencies of wiper. Specifically, the effect of boundary conditions, geometry and wiper material on Eigen-frequencies are predicted. In this model, the maximum value of predicted frequencies was set at 20,000 Hz because humans can only hear frequencies from 20 Hz up to 20,000 Hz. For this study, wiper blades with various profiles, geometry and materials properties were inputted in the ABAQUS model (see Table 8).

Table 8 Various profiles, geometry and materials properties used inputted in Abaqus model.

Material	Profile	Coating
P, Q, Q_1step, F, X	P68612, P37612, P37614	Not coated

6.6.1 Effect of boundary condition constraints on natural frequency of the wiper blade

In order to study the influence of the boundary constraints on the frequency of the wiper blade, different parts of the wiper blade were fixed using encastre boundary conditions. As depicted in Figure 97, these boundary conditions are identified by a number from 0 to 6.
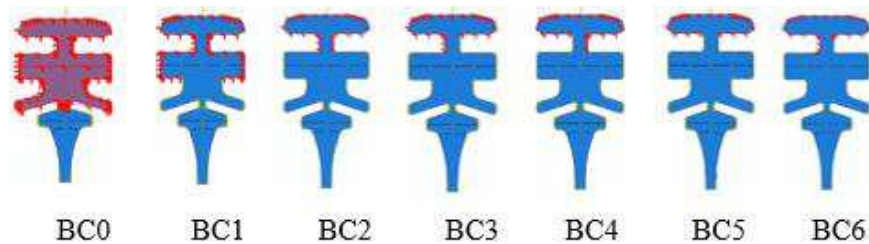
Figure 97. Different types of the wiper blade constraints.

133

The first constraint is called BC0, which has the upper part of the wiper fully constrained and only the lip free to move. The difference between the first and second constraints is that the shoulders of the wiper blades are not fixed in the second constraint named BC0. The third constraint, BC2, has the head and the neck of the wiper blade locked in place. BC3 and BC4 each have half of the neck of the wiper and the head constrained. BC6 has the same constraint as BC3 plus a short portion of the left shoulder, while BC4 has the head and neck fully constrained.
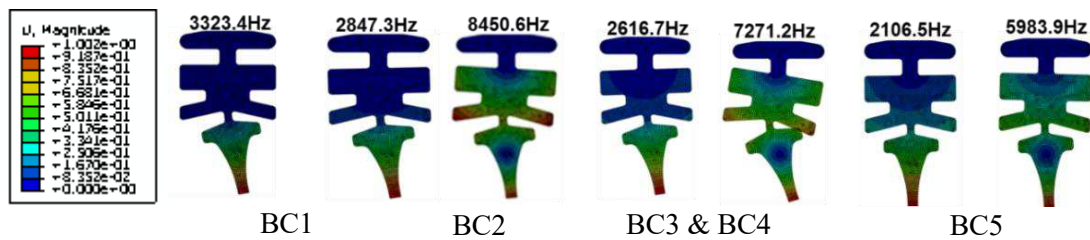
Figure 98. Effect of constraints (boundary conditions) on natural frequency of the FX wiper blade using different wiper profiles.

It can be seen in Figure 98 that by decreasing the constraint of the wiper blade, the frequency for each mode decreases. In order to ascertain whether the frequency values from simulation and experiments are the same, the PQ material used to mimic the squeak was experimentally tested to determine the natural frequency of the profile.

As shown in Figure 94, it is observed that the first and second mode of vibration of the wiper blade is similar with the frequencies values of the squeak recorded experimentally. This agreement suggests that modelling the natural frequency of wiper profile using ABAQUS can indeed help the company to check if the materials and geometry chosen to for a wiper are indeed suitable for low noise operation.

6.6.2 Effect of material on natural frequency of the wiper blade

The wiper profile can be manufactured from a single material or by combining two materials together - the upper material being stiffer than the lower material. This allows the wiper to deform easily and slide over the windscreen without greatly affecting the wiping quality. There are two types of materials that have been combined in the manufacture of the wiper profiles used in this study blade: the first combination type involves the lip of the wiper blade being made by a material (F) and the remainder being

made by another material (X), and the second combination involves the lower section of the lip being made from one material and the remainder of the wiper being made from another (see Figure 99).
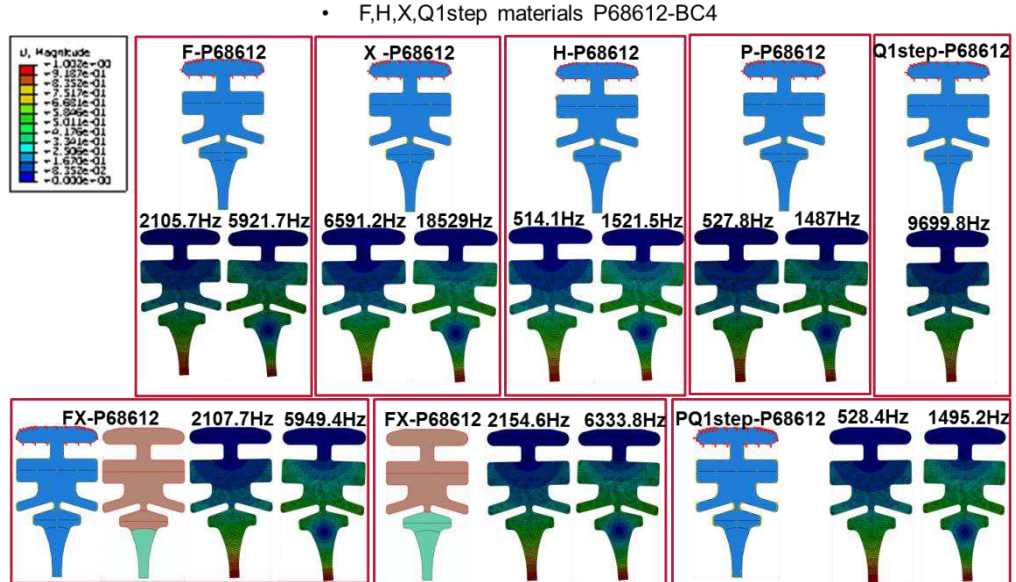
Figure 99. Effect of material on natural frequency of the F, H, X, Q_1 step material wiper blade using P68612 wiper profiles.

As shown in Figure 99, the material has a major influence on the vibration of blade, with the upper material being largely responsible for controlling frequency. The values of frequency predicted for the other two wiper profiles holders are presented in Appendix A. This is as an important finding and demonstrates that material selection is an effective means of preventing wiper vibration.

6.6.3 Effect of geometry (profile) on the natural frequency of the wiper profile

It can be seen in Figure 100 that geometry has a minor influence on the vibration of blade (except when the blade is heavily constrained). More results are presented in Appendix A for PQ material.
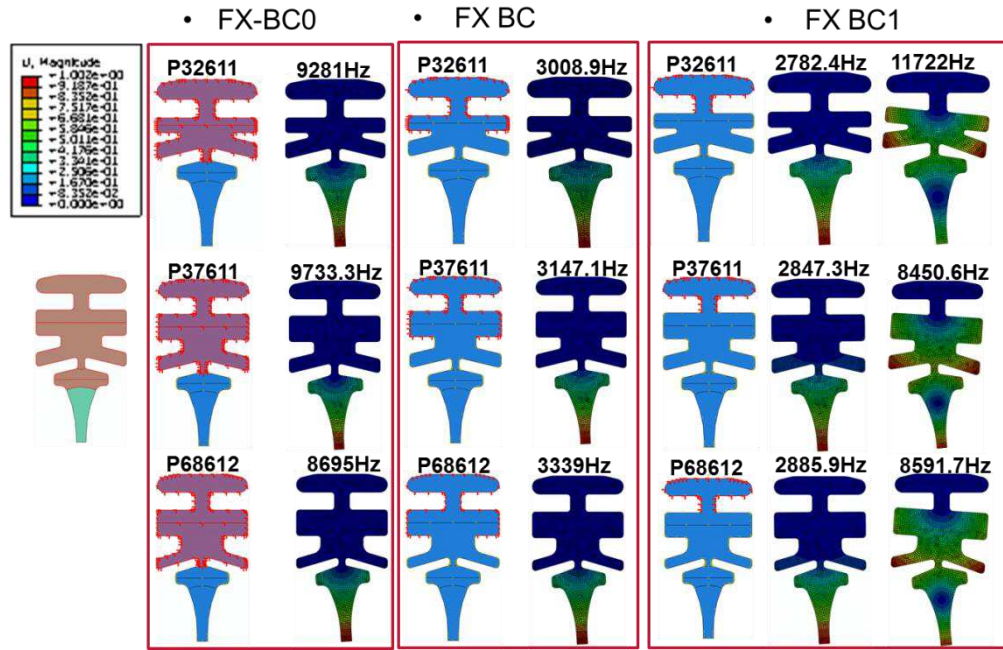
Figure 100. Effect of geometry on natural frequency of the FX wiper blade using different wiper profiles.

6.7 Noise mechanism

An outline of the noise production mechanism is put forward, based on the finding described in this chapter is outlined as follows. As confirmed above, friction induced vibration of blades is initiated due to the negative slope of the Stribeck curve, which gives rise to a negative damping term in the equation of motion of the wiper and hence leads to instability. However, this is only a part of the overall noise emitting mechanism. Specifically, the results show that this instability only results in audible noise if a natural vibration mode of the rubber profile is excited.

Furthermore, this frequency is modulated by the mass of water in contact with the profile (qualitatively following $\omega = (k/m)^{1/2}$ relationship). Sound is subsequently transmitted to the observer through the motion of the glass, which acts as a sounding board to amplify vibration (this is similar to a guitar in which the string vibrates but the sound is emitted from the body of the instrument). A summary of the overall mechanism by which noise is produced is presented in Figure 101.
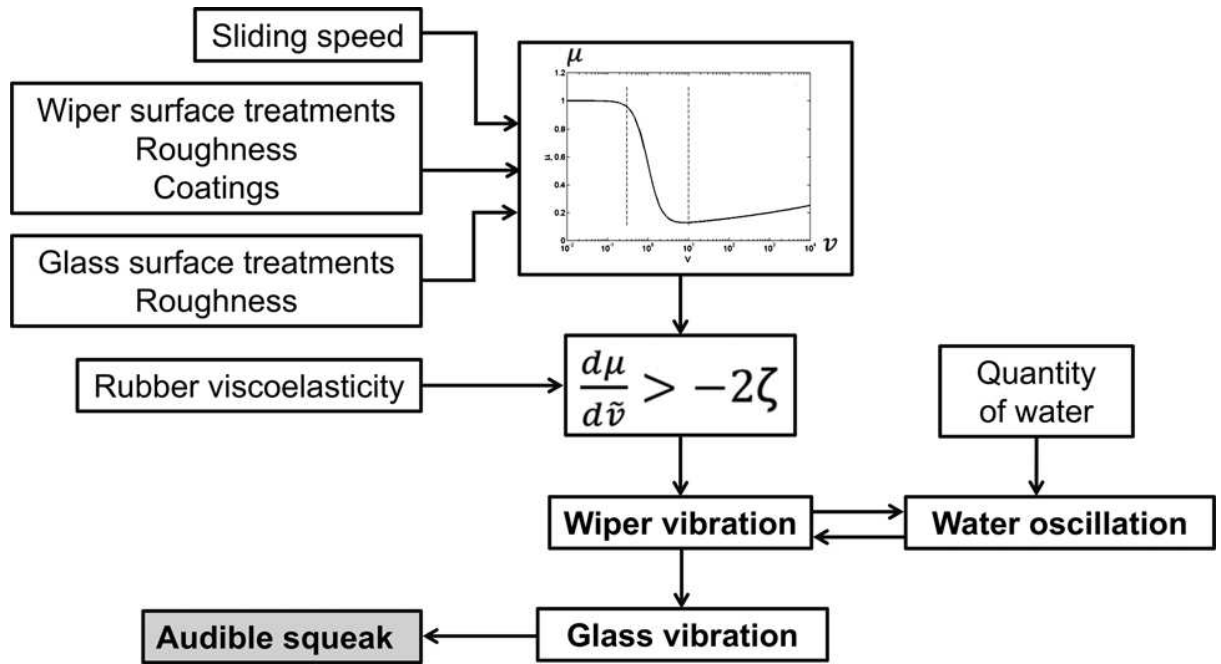
Figure 101. Schematic diagram summarizing the mechanism by which windscreen wiper noise is generated.

6.8   Summary

The research presented in this chapter has aimed to elucidate the mechanisms that govern friction induced vibration in windscreen wipers and how this results in an audible sound. The main findings of this paper can be summarized as follows:

- In agreement with previous research [84], a negative slope of the friction–velocity relationship is required to generate noise.
- Capillary standing waves seem to be observed in the water during the occurrence friction induced vibration.
- The frequency of emitted noise is a function of the mass of water in contact with the blade.
- The rubber wiper vibration, water oscillation, and emitted noise all occur at the same frequency—a frequency that coincides with the first and second natural vibration modes of the wiper-blades as predicted by FE simulation.
- No noise is detected experimentally for blades in cases where the FE method predicts no vibrational modes below 20,000 Hz.
- Agreement is seen between the shape of the vibration modes predicted by FE simulation and those measured using the high-speed camera.

- Noise is only emitted over an intermediate range of glass surface energies.
- The frequency of emitted noise does not depend on the glass thickness.

These observations support the theory [84] that friction induced vibration is caused by the negative slope of the Stribeck curve. However, sound is only heard when this excites a natural frequency of the rubber wiper that is within the audible range. The role of water is to modulate the frequency by adding mass to the wiper lip, while the glass acts as a sounding board to transmit noise to the observer.

This understanding suggests a number of approaches that can be used to eliminate friction induced noise in wiper/glass systems:

- Decrease surface energy of glass (*e.g.*, apply a highly hydrophobic coating) to prevent water reaching the contact.
- Adjust stiffness/geometry of the wiper profile to modify friction–speed curve and reduce negative gradient.
- Increase material damping of wiper blade material to ensure that instability criteria is not met.
- Use FE simulation to predict and control the natural vibration modes of the profiles, prior to production, so that they are not excited by frictional instability.

An ABAQUS Finite Element model was used to characterise how the natural frequencies, or Eigen-frequencies, of a wiper profile, depends on material, profile shape and how the wiper is held in place. Each of these factors, and in particular the material composition, has been shown to affect the resulting natural frequency. This, therefore, provides the manufacturers with means of avoiding unwanted friction induced noise. Importantly, this can be done in the design stage, before the wiper has been manufactured

Chapter 7

Film Thickness Measurements

7 Film Thickness Measurements

In this chapter, water film thickness measurements for wiper profiles with different geometries and defects are presented. Particular attention is paid to the water film left on the glass after the wiping action. This is known as the wiping film or residual film and is important as it reduces visibility and can distract drives.

The aim of this study is to visualise the wiper sealing in order to analyse phenomena such as "hazing" and "hair lines", which have known macroscopic effects, but their mechanisms are still not very clear. An additional aim of this study was to define a sealing limit, *i.e.*, the maximum acceptable film thickness left on the glass after wiping process.

Two different experimental set-ups - an EHD rig and a CETR tribometer (see Methods Chapter) - were modified in order to measure the water residual film. The measurement technique used to evaluate the film thickness inside the contact as well as the residual film for the rubber/glass interface is laser induced fluorescence (LIF). LIF is chosen because of the reduced reflectivity of the rubber, which limits the use of any other technique such as Interferometry. This technique enables determination of the minimum residual film thickness as well as how the thickness is affected by load and speed. Initially, results from calibrated tests are compiled in terms of quantitative film thickness values. Results obtained by using the EHD rig are presented in Appendix B in terms of fluorescence intensity, which gives a qualitative measure of film thickness (Chapter 3 shows how film thickness is proportional to intensity).

7.1 Film thickness results using CETR tribometer

To measure the residual film, a CETR tribometer and an inverted fluorescent microscope were used as follows. The CETR tribometer was used to control the load and measure friction, while the microscope was used to apply the fluorescent technique (see Methods Chapter for details). These tests were carried out on wiper specimens, which had been identified by Bosch as having wiping quality failures such as "hairlines" and "grey hazing" (see Figure 102a and b). The wipers with notch defects are the wipers which have cracks on the lip of the wiper blade.
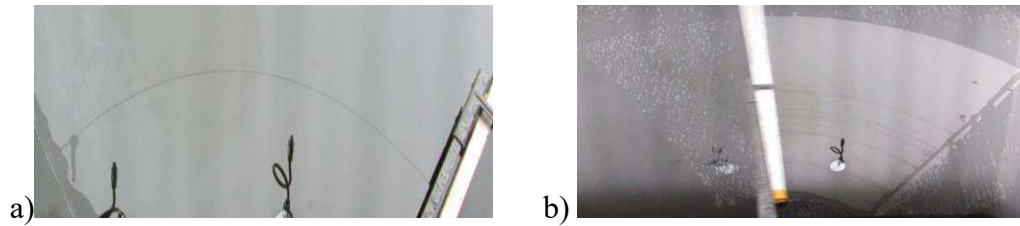
Figure 102. Wiping quality failures identified by Bosch for wipers with a)" hairlines"
and b) "grey hazing".

Also, commercial wipers without defects were used to measure the residual film thickness. These were wipers that were tested by Bosch and showed no visible wipe quality issues such as hazing or hairlines.

Before using the fluorescence microscopy setup to assess rubber wipers with real defects, it was decided to assess the capabilities of the rig by testing samples with artificially produced defects. Such defects were produced by pressing each rubber wiper against the hot wire of a wire cutting machine. The thin (100 μm diameter) wire of the cutter allowed precise localised defects to be produced, of varying size as shown in Figure 103). This figure also presents the fluorescence measurements made when these specimens were tested in the CETR rig. It can clearly be observed that the presence of a notch in the wiper causes the water to leak through the contact and that the flow of water increases with increasing notch radius. It is also interesting to note that instead of flowing over the glass directly, a meniscus forms at the outlet of the contact instead, which acts as a reservoir.

The presence of the meniscus at the exit of the contact may explain the anomalous results observed in previous tests in which the residual film on the glass decreased with increasing speed (in contradiction to hydrodynamic theory). Specifically, the increase in sliding speed may deplete the volume of water in the meniscus of the water and hence cause a decrease in residual film thickness, according to the model developed by Landau and Levich [105] for coating applications. This discovery of the outlet meniscus also suggests that the geometry and surface energy of the wiper could be modified to improve wiping quality.
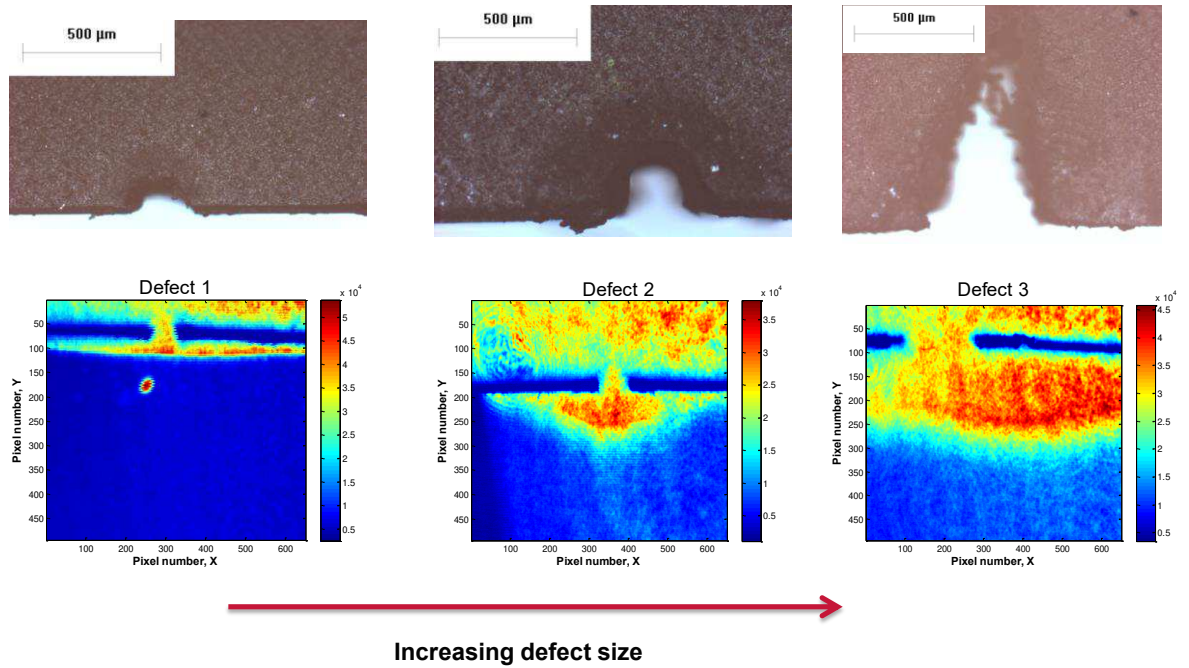
Figure 103. Microscope images of artificially produced defects along with corresponding in-contact fluorescence images.

7.1.1 Effect of load and speed on wiper with notch defects

The new fluorescence set-up on the CETR tribometer was then used to investigate the effect of load on the residual film for wiper profiles that were known to produce "grey hazing" on windscreens. First, the intensity maps were acquired and converted into film thickness maps by using a calibration curve (see Chapter 3).

Thereafter, the film thickness distribution in the y direction was plotted for different loads (see Figure 105) by taking an average along the red dash line (Figure 104). The load was varied from 7 N/m to 30 N/m and the speed was kept constant at 0.18 m/s. These figures show that the hazing is observed on the windscreen are caused by notch defects in the rubber wiper (the notch is evident for the two lower load conditions). It can be seen that the residual film thickness left by the notch defect varies between 300 nm to 1.5 μm.
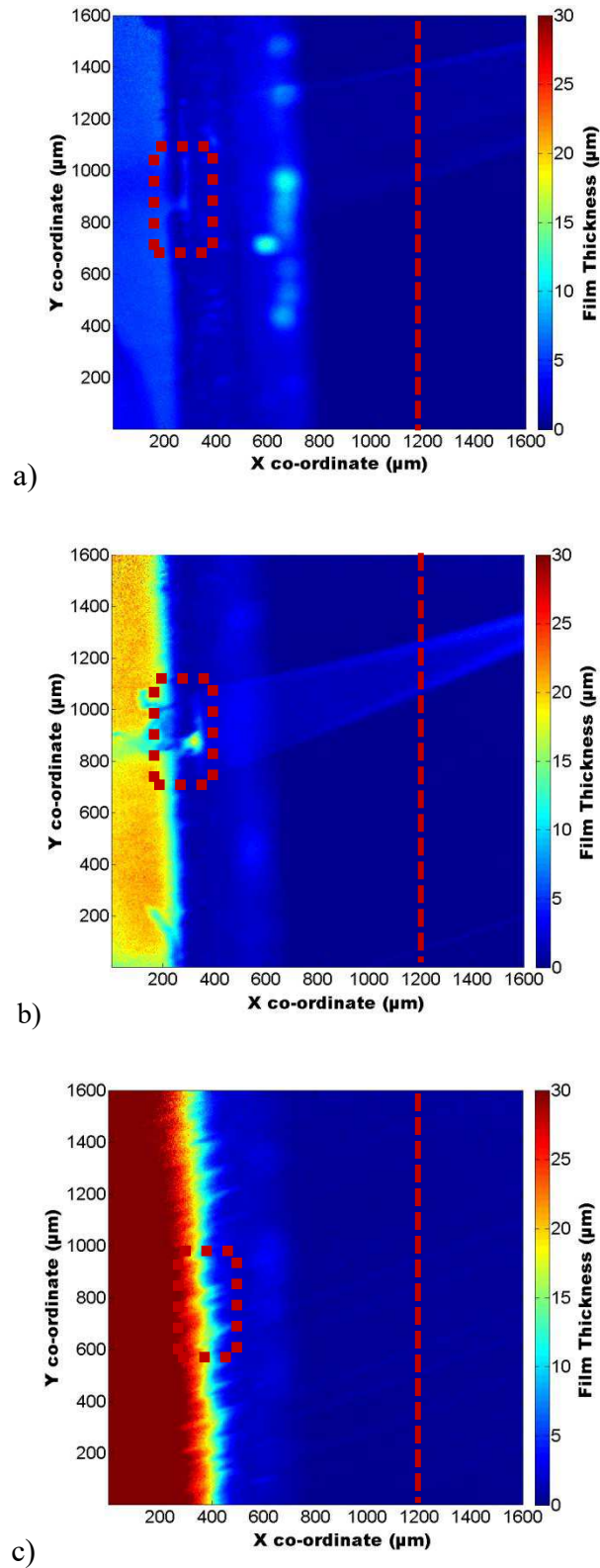
Figure 104. Residual film thickness maps of wiper with notch defect, lubricated with water by varying the load a) 7 N/m, b) 17 N/m and c) 30 N/m. Notch defect identified by red dashed rectangle.

The results in Figure 105 show that the notch defect has no influence on wiping quality at higher load, whereas for lower loads the residual film increases with load. It is suggested that this increase in film thickness with load is associated with a change in the shape of the defect at higher load (see Figure 106), specifically, the defect width is increased in between 7 and 17 N/m, but is then closed by the higher load of 30 N/m, (see Figure 104). This closing up of the notch defect at higher load is in agreement with observations made on automotive windscreens, in that hairlines are seen to decrease at high load.
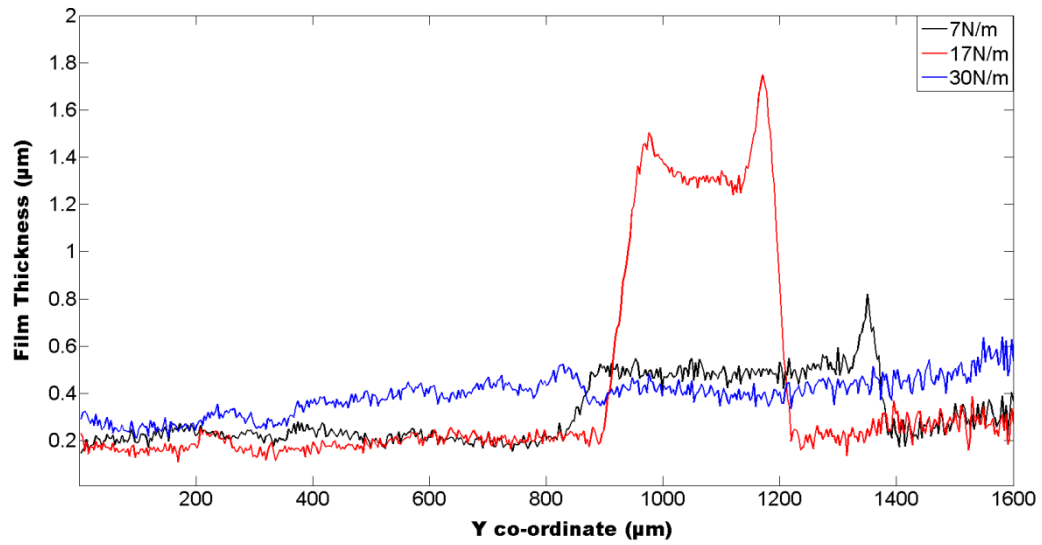
Figure 105. Variation of residual film thickness of wiper with notch defect with load.
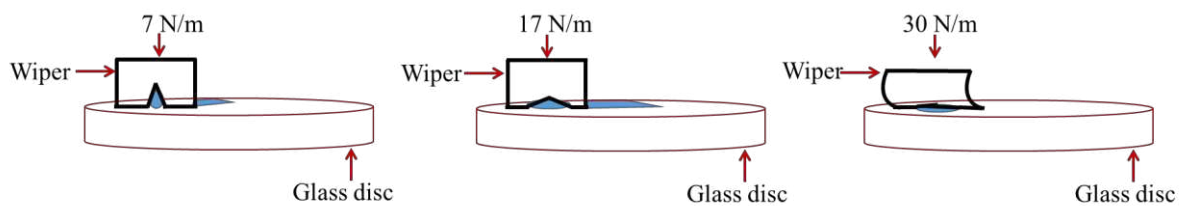
Figure 106. Schematic of notch defect deformation with load variation.

The effect of speed on residual film thickness was also studied for wiper blades with a notch defect. The speed was varied from 0.06 to 0.37 m/s at a uniformly distributed load of 17 N/m. Maps of wiping film thickness and residual dye on the back of the wiper are shown in Figure 107.
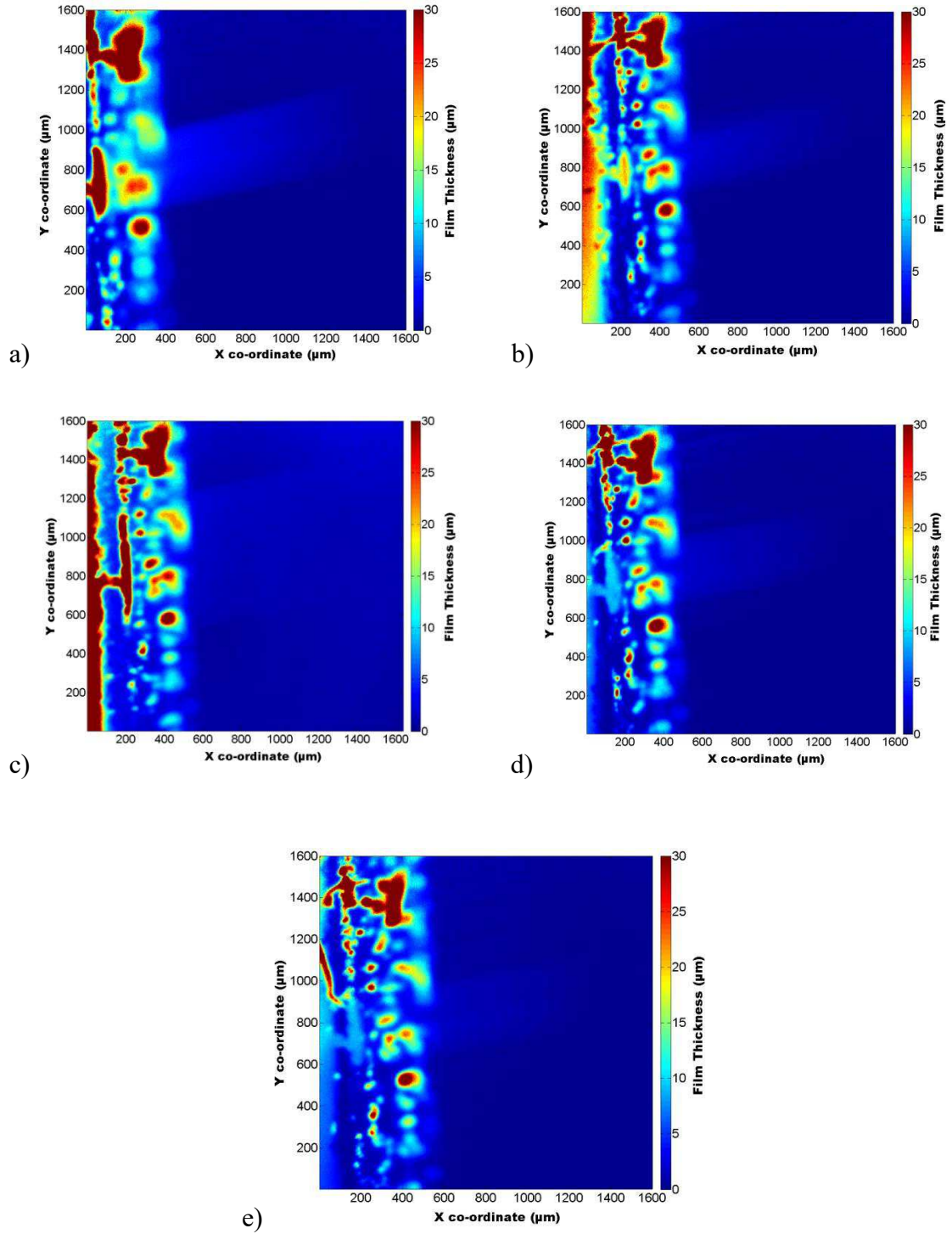
Figure 107. Film thickness maps of wiper contact and residual film with notch defect, lubricated with water by varying velocity a) 0.06 m/s, b) 0.18 m/s, c) 0.25 m/s, d) 0.31 m/s and e) 0.37 m/s.
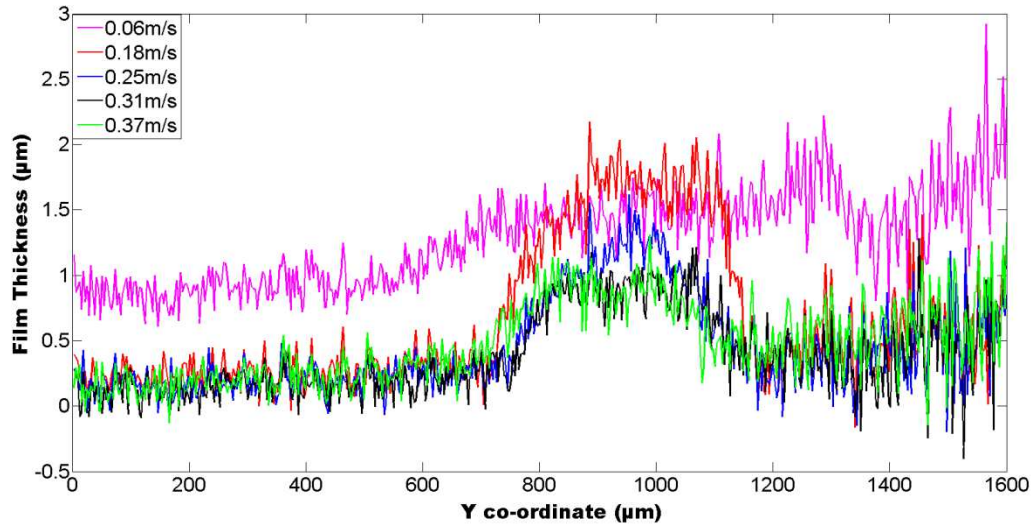
Figure 108. Variation of residual film thickness of wiper with notch defect with velocity.

The residual film decreases with speed when the wiper has a defect (Figure 108). This behaviour is contrary to conventional elasto-hyrdodynamic theory, but may be explained by the Landau and Levich [105] model, whereby the residual water thickness reduces with speed as it is spread more thinly over the glass.

7.1.2 Influence of wipers with high coating particles coverage on wiper quality

Another type of wiper was tested under different loads from 9 to 25 N/m at a constant speed of 0.02 m/s. This wiper had a coating which was known to cause hairlines - *i.e.* a wipe quality failure with numerous fast disappearing fine stripes. With this wiper, the wiping quality was found to be highly dependent on load (see Figure 109). The wiping quality is poor when the load increases due to the changes in contact pressure. The fluorescent images of the contact reveal that the rubber particles caused by shortcomings in the manufacturing process are responsible for the poor wiper quality. It can also be seen that some particles from the coating were removed from the lip of the blade during wiping and transferred to the glass surface, while other particles remained at the contact which hindered the wiping process.
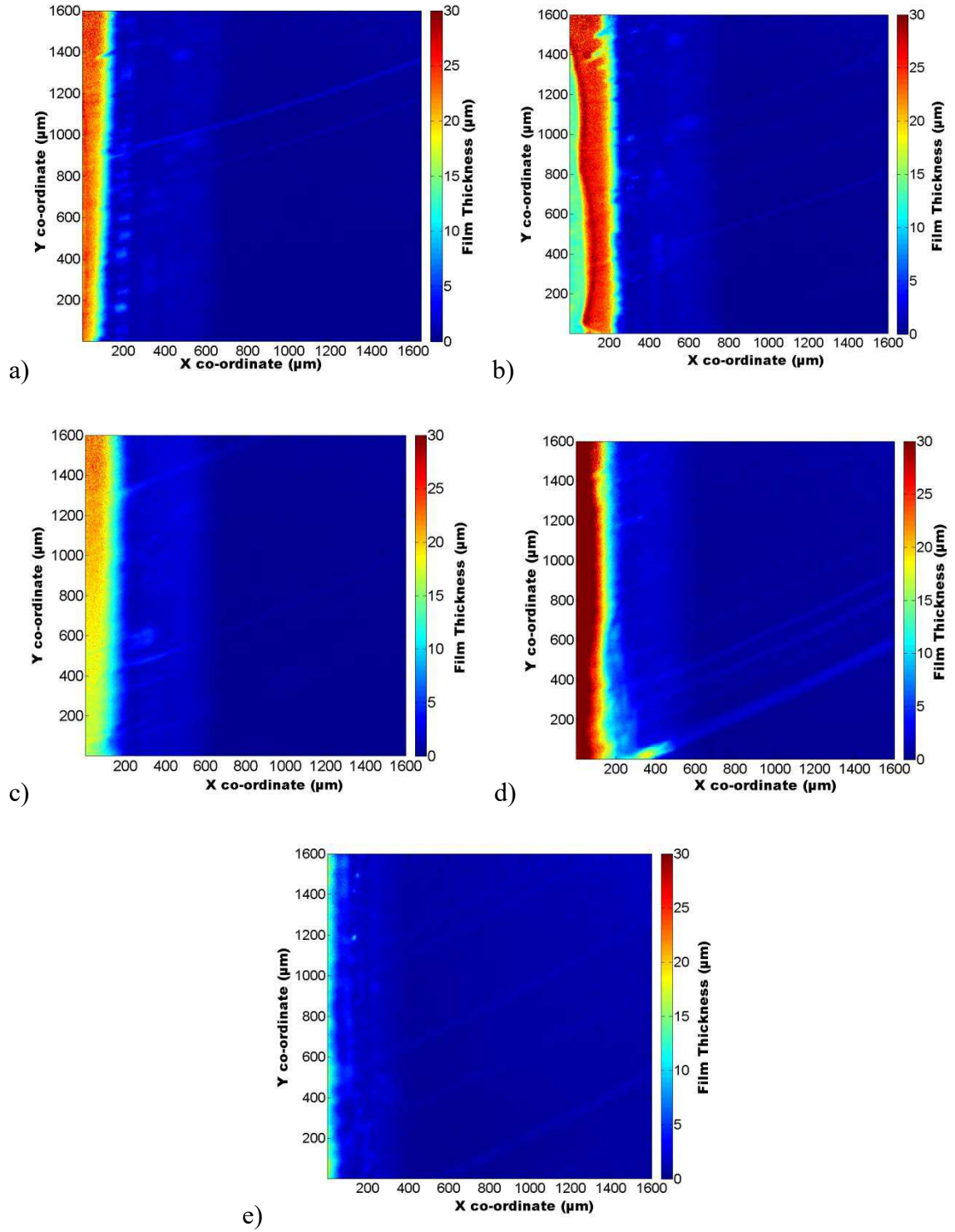
Figure 109. Film thickness maps of wiper contact and residual film of wiper with higher coverage particles, lubricated with water at varying loads of a) 9 N/m, b) 12 N/m, c) 17 N/m, d) 22 N/m, e) 25 N/m.
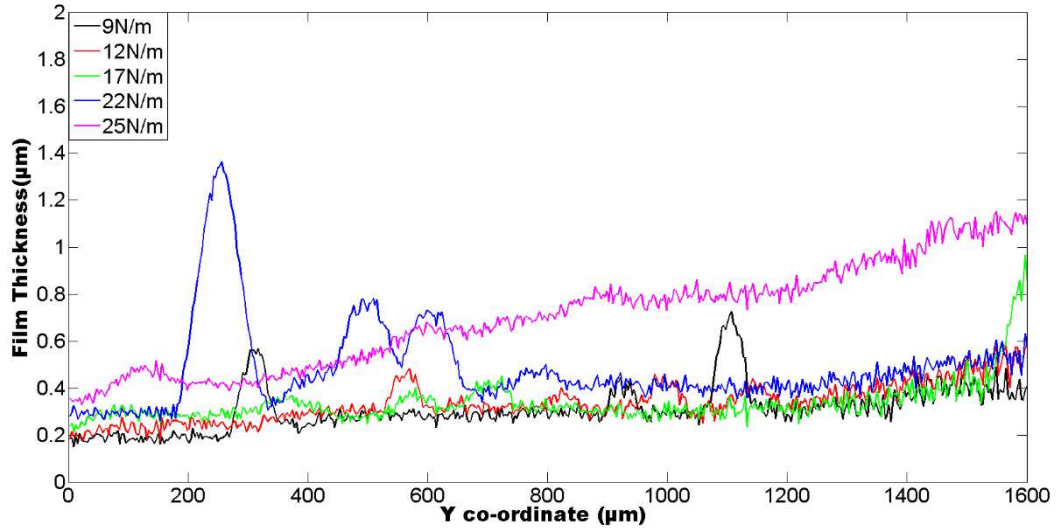
Figure 110. Variation of residual film thickness of wiper with higher coverage particles.

The results in Figure 110 show that the wiping quality is poor when the load is increased for wipers with high coating particles coverage due to the changes in contact pressure.

7.1.3 Sealing limit for wipers without defects

The effect of load on a wiper without defects was studied in order to define the sealing limit (maximum acceptable residual film thickness). The results for loads varied from 9 to 22 N/m at a speed of 0.02 m/s are presented in Figure 111.

a)   b)

c)
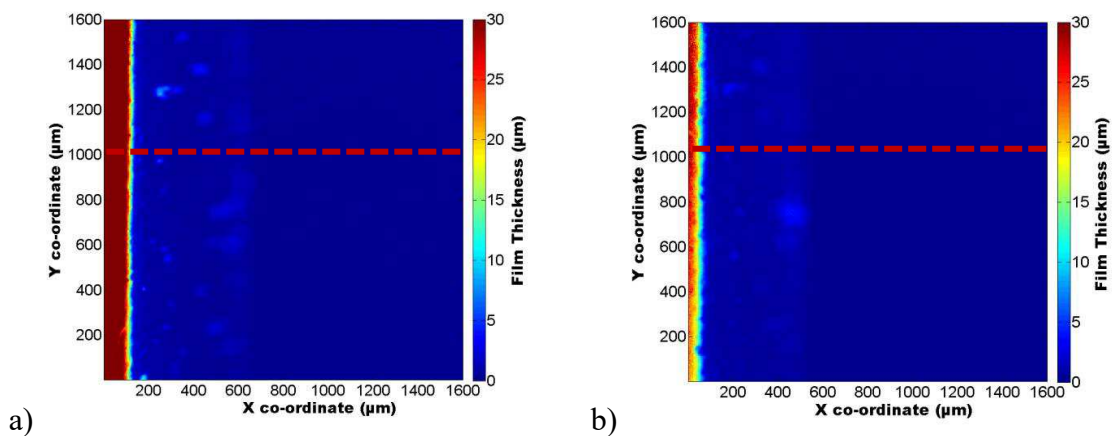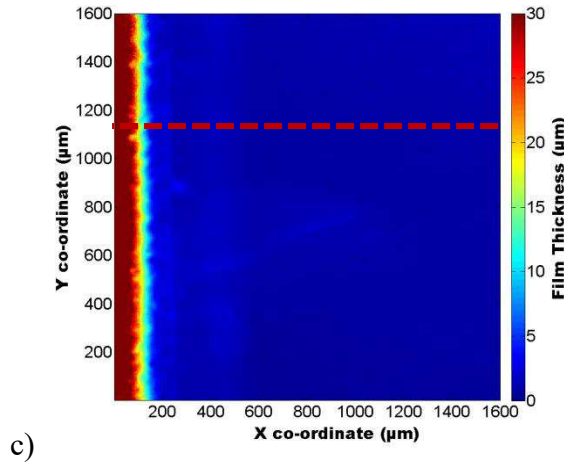
Figure 111. Film thickness maps of wiper contact and residual film without defects, lubricated with water at varying loads of a) 9 N/m, b) 12 N/m and c) 17 N/m.

In Figure 112, the film thickness distribution in the direction parallel to sliding is plotted for a load of 9 N/m by taking an average along the red dash line from Figure 111 a. The residual film thickness was found to be less than 200 nm, which is equal to the lower limit of calibration. Since this wiper is known to produce no detectable defects when used in service on an automotive windscreen, this measurement indicates that the maximum acceptable film is just above 200 nm. This information is important for windscreen wiper manufacturers since it can be used as an estimate of the allowable defects on the rubber surface. This also agrees with the friction measurements obtained for glass surfaces with different roughness (section 5.5), which showed the film thickness to be between 10 and 200 nm. It is also interesting to the note that height of the roughness of the wiper blades themselves (measured in Chapter 4 to be ~500 nm), is considerably larger than this measured water film thickness. At first sight, this may suggest a very low lambda value, however it should be noted that the roughness in the contact is likely to be considerably less than this, due to the compliant nature of the wiper.
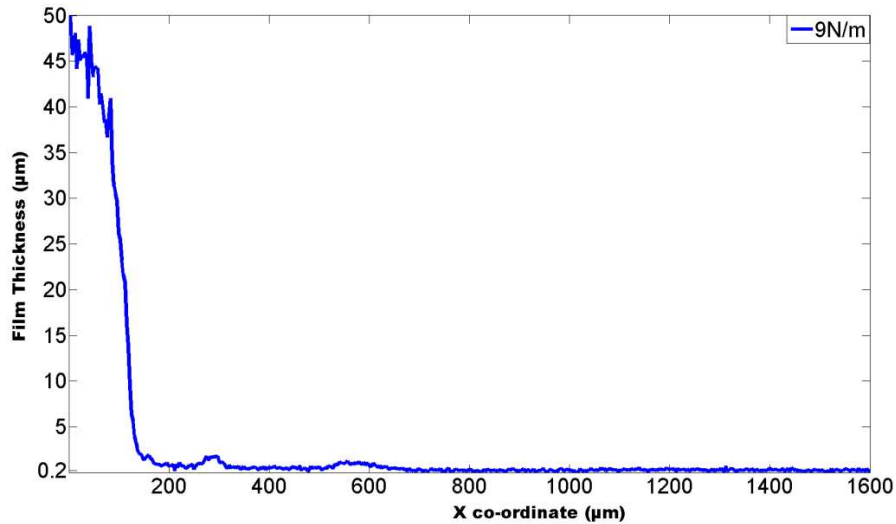
Figure 112. Residual film thickness of wiper without defects; lubricated with water at 9 N/m, load.

7.2 Summary

A laser induced fluorescence technique was used to investigate the film thickness inside/outside the contact for a commercial wiper and triangular specimen. This technique was used in combination with two different sliding test rigs - an EHD and CETR tribometer - in order to characterize water film thickness qualitatively and quantitatively.

The laser induced fluorescence technique was used to measure the residual film thickness for wipers which were known to produce poor quality wiping (*i.e.* they left marks on the windscreen known as hazing or hairlines). Results showed that these two wiping problems arose respectively due to notch or particle defects present on the wiper. Measurements showed that the residual hazing film thickness caused by the notch defect was approximately 900 nm, while that of the hairlines caused by the hairlines was 1 μm.

The effect of speed and load on these wiper quality defects were also studied, Here, it was seen that the notch defect has no influence on wiping quality at higher load, whereas for lower loads the residual film increases with load. Also, the residual film decreases with speed when the wiper has a notch defect. Moreover, it was shown that the wiping quality for wiper with higher particle coating is highly dependent on loading.

The sealing limit was assessed from calibrated film thickness results for commercial wipers without defects and gave a value below 200 nm. The actual residual film thickness for wipers without defects is expected to be less than this, however, it was not possible to determine it more precisely due to limitations in the fluorescence measurement technique described in the methods chapter. Nevertheless, work presented in this chapter has proved useful providing a means of assessing the mechanisms behind wiping quality issues and has also provided estimates of film thickness values, which will aid manufacturing and quality assurance processes.

Chapter 8

Conclusions and Future Work

8 Conclusions and Future Work

8.1 Summary of main findings

The aims of this research were to gain insights into the friction and wear behaviour of windscreen wiper contact in order to save energy, reduce the cost, improve wiping quality and avoid friction induced vibration. These aims were achieved by developing a range of experimental techniques to analyse the effect of glass coatings, contact conditions, roughness and surface energy, and to measure friction, vibration characteristics and water film thickness, both inside and outside the wiper blade contact.

In the initial experimental stage of the project, the windscreen wiper friction behaviour was reproduced in the laboratory under controlled conditions and specific attention was paid to the effect of non-steady state phenomena since these have not previously been studied in any detail. The second stage of the experimental investigation involved elucidating the mechanisms that govern friction induced vibration in windscreen wipers in order help the company to avoid the production of audible sound. The final stage was to provide a means of assessing the mechanisms behind wiping quality issues and estimate film thickness values, in order to aid manufacturing and quality assurance processes.

Key findings from the friction testing section of the project include:

- Static friction can reach considerably higher levels than kinetic friction and therefore must be considered when selecting motor requirements. It was also shown that static friction has a strong dependence on both waiting time (relaxation time) of the rubber and sliding velocity. Specifically, static friction increases linearly with speed and waiting time, while changes in wiper no addition change in friction was observed after a waiting time of 8 seconds suggesting that this is the relaxation time of the material.

- Friction is largely independent of wiper geometry for naked specimens under wet and dry conditions. However, friction does depend on geometry for coated specimens under wet and dry conditions. It was also shown that ageing has a strong effect on friction. This is important as it suggests that the friction behaviour of wiper materials can be assessed, during the design process before full wiper profiles have been manufactured.

- A finding of practical importance is that friction reduces with increasing surface energy in the mixed and full film regime, and this has been attributed to increased wetting of the surfaces (at low surface energies the water is prevented from entering the contact). It was also shown that this effect is not present under dry and boundary lubrication conditions when there is no liquid separating the surfaces.

- Tacky friction peaks, which are a problem in automobile applications under drying conditions, were reproduced and results showed that their magnitude could be significantly reduced by including a low concentration of surfactant in the water. This result provides evidence to support the theory that tacky friction peaks arise due to meniscus forces. It also raises the possibility of modifying the surface energy of the rubber in order to limit this unwanted effect.

- The wear process of wipers has now been understood in greater detail. Following gradual wear, friction increases, which has been attributed to a combination of wiper damage (which increases roughness and reduces lambda value) and the formation of a transfer film. However, following rapid wear, friction variations result from the formation and removal of burrs.

- A new etching method was devised in order to control the roughness of the glass specimen. Comparing results tests on etched glass specimens with those from worn rubber showed that friction is more sensitive to the roughness of the glass surface, due to its high stiffness. Tests on the etch glass also showed that the thickness of the water film is in the nm range.

The second aim was to elucidate the mechanisms that govern friction induced vibration in windscreen wipers and how this results in an audible sound. The main findings from this section of work are presented below:

- In agreement with previous research [84], a negative derivative of the friction–velocity relationship is required to generate noise.

- Capillary standing waves, similar to Faraday waves, have for the first time been observed in the water during the occurrence friction induced vibration.

- The frequency of emitted noise during friction induced vibration was discovered to depend on the presence of water in contact with the wiper, which reduces the natural frequency of the system.

- During friction induced vibration, the oscillation of the wiper and the water, and emitted noise all occur at the same frequency—a frequency that coincides with the first and second natural vibration modes of the wiper-blades as predicted by FE simulation.

- No noise is detected experimentally for blades in cases where the FE method predicted only vibrational modes above 20,000 Hz.

- Agreement is seen between the shape of the vibration modes predicted by FE simulation and those measured using the high-speed camera.

- Noise is only emitted over an intermediate range of glass surface energies, due to the varying presence of water in the contact.

- The frequency of emitted noise does not depend on the glass thickness.

These observations support the theory [84] that friction induced vibration is caused by the negative slope of the Stribeck curve. However, it also shows for the first time that sound is only heard when this vibration excites a natural frequency of the rubber wiper that is within the audible range. The role of water is then to modulate the frequency by adding mass to the wiper lip, while the glass acts as a sounding board to transmit noise to the observer.

This understanding suggested a number of approaches that can be used to eliminate friction induced noise in wiper/glass systems:

- Decrease surface energy of glass (*e.g.*, apply a highly hydrophobic coating) to prevent water reaching the contact.

- Adjust stiffness/geometry of the wiper profile to modify friction–speed curve and reduce negative gradient.

- Increase material damping of wiper blade material to ensure that instability criteria is not met.

- Use FE simulations to predict and control the natural vibration modes of the profiles, prior to production, so that they are not excited by frictional instability.

The final aim of the project was to provide a means of assessing the mechanisms behind wiping quality issues and estimate the film thickness values.

A laser induced fluorescence technique was used to investigate the film thickness inside and outside the contact for a commercial wiper and triangular specimen. This technique was used in combination with two different sliding test rigs - an EHD and CETR tribometer, in order to characterize water film thickness quantitatively and qualitatively.

- When the LIF was used in combination with EHD rig, it was shown that the residual film is thicker for triangular specimens than for commercial wiper, while the film in contact is thicker for commercial wiper than that for triangular specimens. These results were explained on the basis that more water flows around the triangular specimen than commercial wiper. The thicker in-contact film for commercial wiper was due to lower contact pressure while thinner in-contact film was attributed to the higher contact pressure on the triangular specimens when subjected to the same load.

- The residual film and in contact film decreased and then increased as load was increased for the commercial wiper, whilst for triangular specimens the residual film and in contact film thickness decreased monotonically with load.

The laser induced fluorescence technique was used to measure the residual film thickness for wipers which were known to produce poor quality wiping (*i.e.* they left marks on the windscreen known as hazing or hairlines). Results showed that these two wiping problems arose respectively due to notch or particle defects present on the wiper surface.

- Measurements showed that the residual hazing film thickness caused by the notch defect was approximately 900 nm, while that of the hairlines caused by the hairlines was 1 μm.

- The notch defect has no influence on wiping quality at higher loads, whereas for lower loads the residual film increases with load. For this defect, the residual film decreases with speed. In contrast to this, the wiping quality for rubber with a high particle coating showed highly dependent on loading.

- The sealing limit was assessed from calibrated film thickness results for commercial wipers without defects and gave a value below 200 nm. The actual residual film thickness for wipers without defects is expected to be less than this, though, it was not possible to determine it more precisely due to limitations in the fluorescence measurement technique described in the methods chapter. Despite this issue, the approximate value of sealing limit, which was found, still provides useful information for the wiper manufactures' quality control purposes.

8.2   Future Work

This section contains suggestions relating to future work, which would be worthwhile pursuing.

8.2.1 Effect of ageing on friction and sealing performance

The large majority of rubber wipers used in this study were in new, pristine condition, however, some initial results showed that aged wiper rubbers performed worse than new ones. To quantify the effects of ageing, it is suggested that specimens be stored for a number of weeks (under a range of conditions: at low and high temperature, and subject to controlled humidity) prior to carrying out friction tests. In addition to this, it is suggested that a study is made into the combined effect of ageing and wear on sealing performance using the pre-worn method, described in Chapter 5.

These findings from these tests should help the company to understand the role of ageing on friction and sealing and to prevent a poor wiping quality issues under more realistic wiping conditions.

8.2.2 Drying friction

It was found that the most dominant factor effecting tacky friction is the surface energy of the glass. Lower surface energies resulted in significant decrease in the tacky peaks. This is now understood to be due to lower adhesion resulting in smaller convex regions at the base of the contact, allowing smaller menisci to form.

It is suggested that an FEA model is developed to investigate the influence of factors such as contact angle and rubber profile on tacky friction. This could support future experimental work studying the possibility of modifying the surface energy of the rubber in order to limit this unwanted effect.

8.2.3 Modelling the sealing behaviour of windscreen wipers

Finally, it is suggested that a numerical approach is followed that combines FE modelling and finite difference solutions to Reynolds Equation under both full film and boundary lubrication conditions. This can be validated by the experimental data that was obtained in this study and can be used to predict the water film thickness and friction performance rubber wiper with new materials and geometries.

References

[1] K. Nice, "How windshield wipers work." [Online]. Available: http://www.howstuffworks.com/wiper.htm, How Windshield Wipers Work.

[2] J. S. Murawa and T. W. Cox, "Winshield windscreen wiper blade cleaning system," US 6438789 B1, August 27, 2002.

[3] L. Morello, L. R. Rossini, G. Pia, and A. Tonoli, *The automotive body. Components Design*. New York: Mechanical Engineering Series, Springer, 2011.

[4] C. Hens, "Process and apparatus for bending glass," US 3123459, March 3, 1964.

[5] E. C. Miles, "Windshield glass," US 2924485, February 9, 1960.

[6] "Windscreen Wipers and Washers (Automobile)." [Online]. Available: http://what-when-how.com/automobile/windscreen-wipers-and-washers-automobile/.

[7] "Wiper Blade Testing & development." [Online]. Available: http://www.ardl.com/wiper-blade-testing-development.

[8] "Find the right wiper blades for your car." [Online]. Available: http://www.halfords.com/motoring/bulbs-blades-batteries/wiper-blades.

[9] "Encyclopaedia of Alabama." [Online]. Available: http://www.encyclopediaofalabama.org/face/Article.jsp?id=h-2553.

[10] M. Anderson, "Window-cleaning device," US743801 A, November 10, 1903.

[11] C. W. Carey, *American inventors, entrepreneurs & business visionaries*, Revised Ed. New York: Infobase Publishing, 2002.

[12] "First in auto history." [Online]. Available: http://allontario.ca/2013/05/first-in-auto-history/.

[13] C. Edquist and L. Hommen, *Small Country Innovation Systems*. Cheltenham: Edward Elgar, 2008.

[14] "Windscreen wipers - Trico." [Online]. Available: http://www.trico.eu.com/.

[15] "Windscreen wiper." [Online]. Available: http://www.bosch.com.au/content/language1/html/715_5615.htm.

[16] "Innovations. Always at the forefront of technology." [Online]. Available: http://www.trico.eu.com/About/News/TRICOFirstinIndustryWindscreenWiperBl adeManufacturer.

[17] G. W. Ehrenstein, *Polymeric material*, 1st ed. Munich: Hanser, 2001.

[18] M. L. Williams, R. F. Landel, and J. D. Ferry, "The Temperature Dependence of Relaxation Mechanisms in Amorphous Polymers and Other Glass-forming Liquids.," *J. Am. Chem. Soc.*, vol. 77, no. 14, pp. 3701–3707, 1955.

[19] B. N. J. Persson, "On the theory of rubber friction," *Surf. Sci.*, vol. 401, no. 3, pp. 445–454, 1998.

[20] B. N. J. Persson, "Capillary adhesion between elastic solids with randomly rough surfaces," *J. Phys. Condens. Matter*, vol. 20, no. 31, p. 12, 2008.

[21] B. N. J. Persson, "Elastoplastic Contact between Randomly Rough Surfaces," *Phys. Rev. Lett.*, vol. 87, no. 11, p. 116101, 2001.

[22] B. N. J. Persson, "Rubber friction: role of the flash temperature," *J. Phys. Condens. Matter*, vol. 18, no. 32, pp. 7789–7823, 2006.

[23] G. Palasantzas, "Influence of self-affine roughness on the adhesive friction coefficient of a rubber body sliding on a solid substrate," *Surf. Sci.*, vol. 565, no. 2–3, pp. 191–196, 2004.

[24] D. F. Moore and W. Geyer, "A review of hysteresis theories for elastomers," *Wear*, vol. 30, no. 1, pp. 1–34, 1974.

[25] P. Thirion, "The Coefficients of Adhesion of Rubber," *Rubber Chem. Technol.*, vol. 21, no. 2, pp. 505–515, 1948.

[26] K. A. Grosch, "The Relation between the Friction and Viscoelastic Properties of Rubber," *Rubber Chem. Technol.*, vol. 37, no. 2, pp. 386–403, 1964.

[27] C. Putignano, T. Reddyhoff, and D. Dini, "The influence of temperature on viscoelastic friction properties," *Tribol. Int.*, vol. 100, no. 1, pp. 338–343, 2015.

[28] G. Carbone and C. Putignano, "A novel methodology to predict sliding and rolling friction of viscoelastic materials: Theory and experiments," *J. Mech. Phys. Solids*, vol. 61, no. 8, pp. 1822–1834, 2013.

[29] A. Schallamach, "The Velocity and Temperature Dependence of Rubber Friction," *Rubber Chem. Technol.*, vol. 66, no. 5, p. 386, 1953.

[30] K. Vorvolakos and M. K. Chaudhury, "The effects of molecular weight and temperature on the kinetic friction of silicone rubbers," *Langmuir*, vol. 19, no. 17, pp. 6778–6787, 2003.

[31] D. Tabor, "The Mechanism of Rolling Friction. II. The Elastic Range," *Proc. R. Soc. London. Ser. A. Math. Phys. Sci.*, vol. 229, no. 1177, p. 198 LP-220, 1955.

[32] J. A. Greenwood and D. Tabor, "The Friction of Hard Sliders on Lubricated Rubber: The Importance of Deformation Losses," *Proc. Phys. Soc.*, vol. 71, no. 6, pp. 989–1001, 1958.

[33] B. E. Sabey, "Pressure Distributions beneath Spherical and Conical Shapes pressed into a Rubber Plane, and their Bearing on Coefficients of Friction under Wet Conditions," *Proc. Phys. Soc.*, vol. 71, no. 6, p. 979, 1958.

[34] C. Putignano, J. Le Rouzic, T. Reddyhoff, G. Carbone, and D. Dini, "A theoretical and experimental study of viscoelastic rolling contacts incorporating thermal effects," *Proc. Inst. Mech. Eng. Part J J. Eng. Tribol.*, vol. 228, no. 10, pp. 1112–1121, 2014.

[35] C. Putignano, T. Reddyhoff, G. Carbone, and D. Dini, "Experimental investigation of viscoelastic rolling contacts: A comparison with theory," *Tribol. Lett.*, vol. 51, no. 1, pp. 105–113, 2013.

[36] G. Carbone and C. Putignano, "Rough viscoelastic sliding contact: Theory and experiments," *Phys. Rev. E*, vol. 89, no. 3, p. 32408, 2014.

[37] F. L. Roth, R. L. Driscoll, and W. L. Holt, "Frictional Properties of Rubber," *Rubber Chem. Technol.*, vol. 16, no. 1, pp. 155–177, 1943.

[38] A. Schallamach, "The Load Dependence of Rubber Friction," *Proc. Phys. Soc. Sect. B*, vol. 65, no. 9, p. 657, 1952.

[39] A. D. Roberts, "Studies of lubricated rubber friction: Part 1: Coupling optical observations to friction measurements," *Tribol. Int.*, vol. 10, no. 2, pp. 115–122, 1977.

[40] A. D. Roberts, "Studies of lubricated rubber friction. Part 2: Optical techniques applied to practical problems," *Tribol. Int.*, vol. 10, no. 3, pp. 175–183, 1977.

[41] F. P. Bowden, "Friction of clean metals and the influence of adsorbed films," *Proc. R. Soc. London. Ser. A. Math. Phys. Sci.*, vol. 142, no. 818, pp. 1039–1040, 1951.

[42] M. Barquins and A. D. Roberts, "Rubber friction variation with rate and temperature: some new observations," *J. Phys. D. Appl. Phys.*, vol. 19, no. 4, pp. 547–563, 2000.

[43] B. N. J. Persson, "Theory of rubber friction and contact mechanics," *J. Chem. Phys.*, vol. 115, no. 8, pp. 3840–3861, 2001.

[44] M. Mofidi, B. Prakash, B. N. J. Persson, and O. Albohr, "Rubber friction on (apparently) smooth lubricated surfaces," *J. Phys. Condens. Matter*, vol. 20, no. 85223, p. 8, 2008.

[45] A. Le Gal, X. Yang, and M. Klüppel, "Evaluation of sliding friction and contact mechanics of elastomers based on dynamic-mechanical analysis," *J. Chem. Phys.*, vol. 123, no. 14704, p. 11, 2005.

[46] B. N. J. Persson, "Adhesion between an elastic body and a randomly rough hard surface," *Eur. Phys. J. E*, vol. 8, no. 4, pp. 385–401, 2002.

[47] D. C. Evans and J. K. Lancaster, *The Wear of Polymers*. New York: Academic Press, 1966.

[48] A. N. Gent and C. T. R. Pulford, "Mechanisms of Rubber Abrasion," *J. Appl. Polym. Sci.*, vol. 36, no. 5, pp. 375–378, 1984.

[49] A. Schallamach, "Friction and abrasion of rubber," *Wear*, vol. 1, no. 5, pp. 384–417, 1958.

[50] A. Schallamach, "Abrasion, fatigue, and smearing of rubber," *J. Appl. Polym. Sci.*, vol. 12, no. 2, pp. 281–293, 1968.

[51] L. W. Liu, Y. H. Lee, C. J. Lin, K. W. Li, and C. Y. Chen, "Shoe Sole Tread Designs and Outcomes of Slipping and Falling on Slippery Floor Surfaces," *PLoS One*, vol. 8, no. 7, pp. 1–7, 2013.

[52] T. B. Leamon and P. L. Murphy, "Occupational slips and falls: more than a trivial problem," *Ergonomics*, vol. 38, no. 3, pp. 487–498, 1995.

[53] J. D. Clarke, K. Hallas, R. Lewis, S. Thorpe, G. Hunwin, and M. J. Carré, "Understanding the Friction Measured by Standardised Test Methodologies Used to Assess Shoe-Surface Slip Risk," *J. Test. Eval.*, vol. 43, no. 4, p. 20120334, 2015.

[54] K. Link, "Friction and Tire Traction," Bachelor project, Department of Engineering and Science, Rensselaer Polytechnic Institute Hartford, 2015.

[55] H. W. Kummer, *Unified theory of rubber and tire friction*. Pennsylvania: Pennsylvania State University, College of Engineering, 1966.

[56] Y. Oh and H. Lee, "Characteristics of a tire friction and performances of a braking in a high speed driving," *Adv. Mech. Eng.*, vol. 2014, no. 260428, p. 6, 2014.

[57] S. Ella, P-Y. Formagne, V. Koutsos, and J. R. Blackford, "Investigation of rubber friction on snow for tyres," *Tribol. Int.*, vol. 59, no. 10, pp. 292–301, 2013.

[58] B. Jacobson, "The Stribeck memorial lecture," *Tribol. Int.*, vol. 36, no. 11, pp. 781–789, 2003.

[59] A. Koenen and A. Sanon, "Tribological and vibroacoustic behavior of a contact between rubber and glass (application to wiper blade)," *Tribol. Int.*, vol. 40, no. 10–12, pp. 1484–1491, 2007.

[60] G. Bodai, "Material and frictional behavior of rubber sliding on glass surface," Doctoral Degree thesis, Department of Machine and Product Design Material, Budapest University of Technology and Economics, 2012.

[61] S. C. Richards and A. D. Roberts, "Boundary lubrication of rubber by aqueous surfactant," *J. Phys. D. Appl. Phys.*, vol. 25, no. 1A, pp. A76–A80, 2000.

[62] B. N. J. Persson and M. Scaraggi, "On the transition from boundary lubrication to hydrodynamic lubrication in soft contacts.," *J. Phys. Condens. Matter*, vol. 21, no. 18, p. 185002, 2009.

[63] B. N. J. Persson and M. Scaraggi, "Lubricated sliding dynamics: Flow factors and Stribeck curve," *Eur. Phys. J. E*, vol. 34, no. 10, p. 113, 2011.

[64] O. Reynolds, "Theory of Lubrication and its Application to Mr . BEAUCHAMP," *Philos. Trans. R. Soc. London.*, vol. 177, no. 1886, pp. 157–234, 2011.

[65] J. de Vicente, J. R. Stokes, and H. A. Spikes, "The frictional properties of Newtonian fluids in rolling - sliding soft-EHL contacts," *Tribol. Lett.*, vol. 20, no. 3–4, pp. 273–286, 2005.

[66] J. de Vicente, J. R. Stokes, and H. A. Spikes, "Rolling and sliding friction in compliant, lubricated contact," *Proc. Inst. Mech. Eng. Part J J. Eng. Tribol.*, vol. 220, no. 2, pp. 55–63, 2006.

[67] J. H. H. Bongaerts, K. Fourtouni, and J. R. Stokes, "Soft-tribology: Lubrication in a compliant PDMS-PDMS contact," *Tribol. Int.*, vol. 40, no. 10–12, pp. 1531–1542, 2007.

[68] F. Deleau, D. Mazuyer, and A. Koenen, "Sliding friction at elastomer/glass contact: Influence of the wetting conditions and instability analysis," *Tribol. Int.*, vol. 42, no. 1, pp. 149–159, 2009.

[69] R. Mazda, "An Investigation into 'Tacky' Friction," Master thesis, Department of Mechanical Engineering, Imperial College London, 2014.

[70] L. Sirghi, "Effect of capillary-condensed water on the dynamic friction force at nanoasperity contacts," *Appl. Phys. Lett.*, vol. 82, no. 21, pp. 3755–3757, 2003.

[71] T. Reddyhoff, D. Dini, and H. A. Spikes, "Wiper Blades: Experimental Investigation of Friction," Consultancy Project, Department of Mechanical Engineering, Imperial College London, 2011.

[72] M. Fagervall and M. Nyman, "Optimal windshield cleaning performance Optimal windshield cleaning performance," Master thesis, Department of Mechanical Engineering, Lulea University of Technology, 2000.

[73] A. D. Roberts and D. Tabor, "The extrusion of liquids between highly elastic solids," *Proceedings of the Royal Society A: Mathematical, Physical and Engineering Sciences*, vol. 325, no. 1562. pp. 323–345, 1971.

[74] G. Poll, A. Gabelli, P. G. Binnington, and J. Qu, "Dynamic mapping of rotary lip seal lubricant films by fluorescent image processing," in *Fluid Sealing. Fluid Mechanics and its Applications*, vol. 8, Nau B.S. (eds), Ed. Dordrecht: Springer, 1992, pp. 55–77.

[75] C. Myant, T. Reddyhoff, and H. A. Spikes, "Laser-induced fluorescence for film thickness mapping in pure sliding lubricated, compliant, contacts," *Tribol. Int.*, vol. 43, no. 11, pp. 1960–1969, 2010.

[76] C. H. Hidrovo and D. P. Hart, "Emission reabsorption laser induced fluorescence (ERLIF) film thickness measurement," *Meas. Sci. Technol.*, vol. 12, no. 4, pp. 467–477, 2001.

[77] D. Gasni, M. K. Wan Ibrahim, and R. S. Dwyer-Joyce, "Measurements of lubricant film thickness in the iso-viscous elastohydrodynamic regime," *Tribol. Int.*, vol. 44, no. 7–8, pp. 933–944, 2011.

[78] S. Okura and T. Oya, "Complete 3D dynamic analysis of blade reversal behavior in a windshield wiper system," *SAE Trans.*, vol. 1, no. 724, p. 12, 2003.

[79] R. Grenouillat and C. Leblanc, "Simulation of chatter vibrations for wiper systems," *SAE*, vol. 1, no. 798, p. 10, 2002.

[80] S. Goto, H. Takahashi, and T. Oya, "Clarification of the mechanism of wiper blade rubber squeal noise generation," *JSAE Rev.*, vol. 22, no. 1, pp. 57–62, 2001.

[81] S. Rosen and P. Howell, *Signals and systems for speech and hearing*, 2nd ed. London: Brill, 2011.

[82] A. K. Banerjee, "Influence of kinetic friction on the critical velocity of stick-slip motion," *Wear*, vol. 13, no. 3, pp. 107–116, 1968.

[83] F. Van De Velde and P. De Baets, "Mathematical approach of the influencing factors on stick-slip induced by decelerative motion," *Wear*, vol. 201, no. 1–2, pp. 80–93, 1996.

[84]   Le Rouzic, J., Le Bot, A., Perret-Liaudet, J., Guibert, M., Rusanov, A., Dou-minge, L., Bretagnol, F., and Mazuyer, D., "Friction-induced vibration by Stribeck's Law: Application to wiper blade squeal noise," *Tribol. Lett.*, vol. 49, no. 3, pp. 563–572, 2013.

[85]   F. P. Bowden and D. Tabor, *The Friction and Lubrication of Solids*. Oxford: Oxford Classic Texts in the Physical Sciences, 1960.

[86]   P. L. KO, "Quasi-harmonic friction induced vibration," Master thesis, Department of Mechanical Engineering, The University of British Columbia, Vancouver, 1971.

[87]   H. Blok, "Fundamental Mechanical Aspects of Boundary Lubrication," *SAE Int.*, vol. 35, no. 2, pp. 54–68, 1940.

[88]   L. Eaton, *Friction Instability*, 1st ed. London: The Macmillan Press, 1975.

[89]   A. M. Ozvald, "Reactive Ionomers : N-vinylimidazolium Bromide Derivatives of Poly (isobutylene- co -isoprene) and Poly (isobutylene- co - para - methylstyrene)," Master thesis, Chemical Engineering, Queen's University Kingston, Ontario, Canada, 2012.

[90]   K. L. Johnson, K. Kendall, and A. D. Roberts, "Surface Energy and the Contact of Elastic Solids," *Proc. R. Soc. A Math. Phys. Eng. Sci.*, vol. 324, no. 1558, pp. 301–313, 1971.

[91]   F. Hejda, P. Sola, and J. Kousal, "Surface Free Energy Determination by Contact Angle Measurements – A Comparison of Various Approaches," *WDS'10 Proc. Contrib. Pap.*, vol. 3, no. 3, pp. 25–30, 2010.

[92]   G. Binnig and C. F. Quate, "Atomic Force Microscope," *Phys. Rev. Lett.*, vol. 56, no. 9, pp. 930–933, 1986.

[93]   J. R. Bell and S. J. Rothberg, "Laser Vibrometers and Contacting Transducers, Target Rotation and Six Degree-of-Freedom Vibration: What Do We Really Measure?," *J. Sound Vib.*, vol. 237, no. 2, pp. 245–261, 2000.

[94]   Y. Fujii and T. Yamaguchi, "Dynamic Characteristics Measurements of a Car Wiper Blade," *JSME Int. J. Ser. C*, vol. 49, no. 3, pp. 799–803, 2006.

[95] J. Mackerle, "Rubber and rubber-like materials, finite-element analyses and simulations: a bibliography (1976-1997)," *Model. Simul. Mater. Sci. Eng.*, vol. 6, no. 2, pp. 171–198, 1999.

[96] R. P. Glovnea, A. K. Forrest, A. V. Olver, and H. A. Spikes, "Measurement of sub-nanometer lubricant films using ultra-thin film interferometry," vol. 15, no. 3, pp. 217–230, 2003.

[97] B. Valeur, *Molecular fluorescence: principles and applications*. Weinheim: Wiley-VCH Verlag GmbH, 2001.

[98] C. W. Myant, "Experimental techniques for investigating lubricated , compliant , contacts," Doctoral Degree thesis, Department of Mechanical Engineering, Imperial College London, 2010.

[99] R. Kirkpatrick and C. L. Muhlstein, "Performance and durability of octadecyltrichlorosilane coated borosilicate glass," *J. Non. Cryst. Solids*, vol. 353, no. 27, pp. 2624–2637, 2007.

[100] D. Janssen, R. De Palma, S. Verlaak, P. Heremans, and W. Dehaen, "Static solvent contact angle measurements, surface free energy and wettability determination of various self-assembled monolayers on silicon dioxide," *Thin Solid Films*, vol. 515, no. 4, pp. 1433–1438, 2006.

[101] A. H. Muhr and A. D. Roberts, "Rubber abrasion and wear," *Wear*, vol. 158, no. 1–2, pp. 213–228, 1992.

[102] J. Miles, "Parametrically Forced Surface Waves," *Annu. Rev. Fluid Mech.*, vol. 22, no. 1, pp. 143–165, 1990.

[103] S. Douady, "Experimental study of the Faraday instability," *J. Fluid Mech.*, vol. 221, no. 1, p. 383, 1990.

[104] J. Xu and D. Attinger, "Acoustic excitation of superharmonic capillary waves on a meniscus in a planar microgeometry," *Phys. Fluids*, vol. 19, no. 10, p. 108107, 2007.

[105] L. D. Landau and V. G. Levich, "Dragging of a Liquid by a moving plate," *Acta Physicochim. URSS*, vol. 17, no. 42, pp. 42–54, 2012.

Appendices

Appendix A

Effect of material on natural frequency of the wiper blade for F, H, X and Q_1step material for P37611 and P32311 wiper profiles.
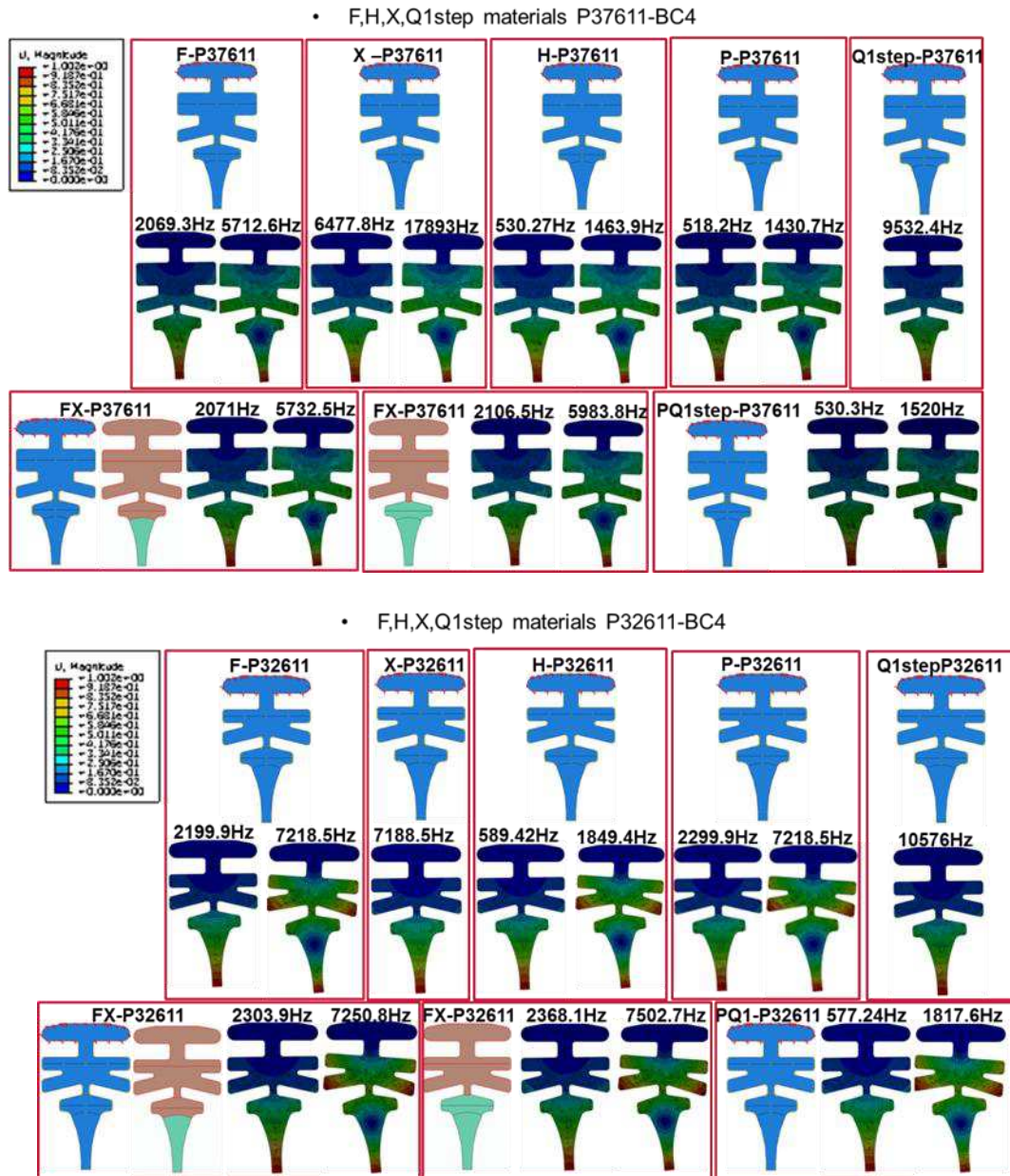

Figure 113. Effect of material on natural frequency of the wiper blade for F, H, X and Q_1step material for P37611 and P32311 wiper profiles.

The effect of geometry (profile) on the natural frequency of the wiper profile for PQ material is shown in Figure 114.
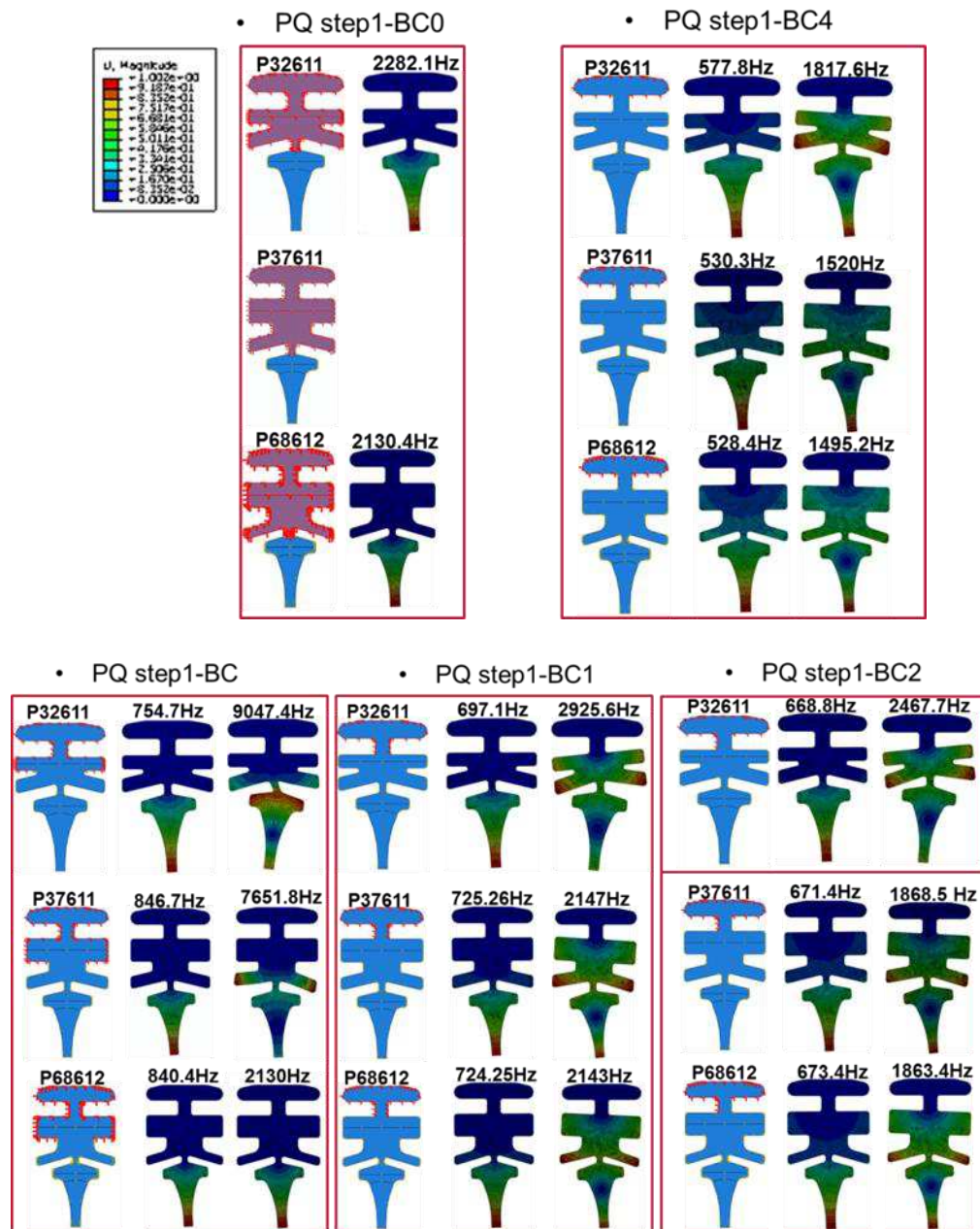

Figure 114. Effect of geometry on the natural frequency of the wiper profile for PQ material.

Appendix B

B 1   Film thickness measurements using an EHD rig

The EHD rig was used to qualitatively measure the water film thickness inside the contact and the residual film for a commercial wiper profile and a triangular specimen under different loads, speeds and attack angles. Wiper profiles of different shapes were used to evaluate qualitatively the influence of geometry on residual film thickness and the water film inside the contact under different loads, speeds and supply flow rates. The different geometries of the wipers used in the EHD set-up are shown in Figure 115. The lower parts of the commercial wiper as well as triangular specimen are made from the same material, but their geometries differ.
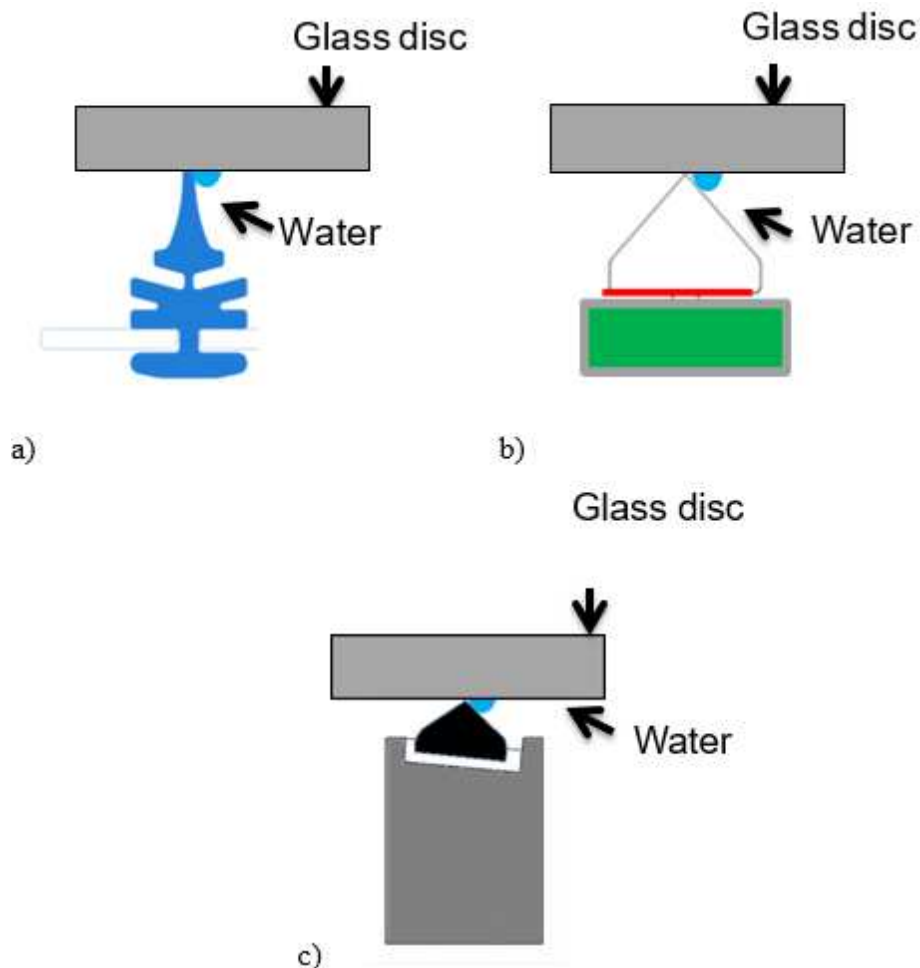

Figure 115. EHD set-up and different geometry of wiper: a) commercial wiper profile, b) triangular wiper and c) Holder tilting wiper by 5°.

A Masterflex peristaltic pump-L/S 6-600 rpm with accurate flow rates was used for supplying the water with dye at the rubber/glass contact, which was necessary due to the inverted nature of the contact. A 3D printed tilted holder was also used to simulate different angles of the wiper with respect to the windscreen (see Figure 115c) to simulate contact conditions found on actual automotive windscreens. In order to study the water film in contact, two objective lenses with different magnification (5X and 10X) were used, which helped us to determine if a water film is present in contact or not.

B 1.1 Effect of load and speed on water film thickness for commercial wiper and triangular specimen

The load was varied from 20 to 50 N/m and the speed from 26 to 395 mm/s, while the flow rate was kept constant. Figure 116 shows how fluorescent images, captured by camera, are converted into intensity maps or intensity profiles using Matlab.
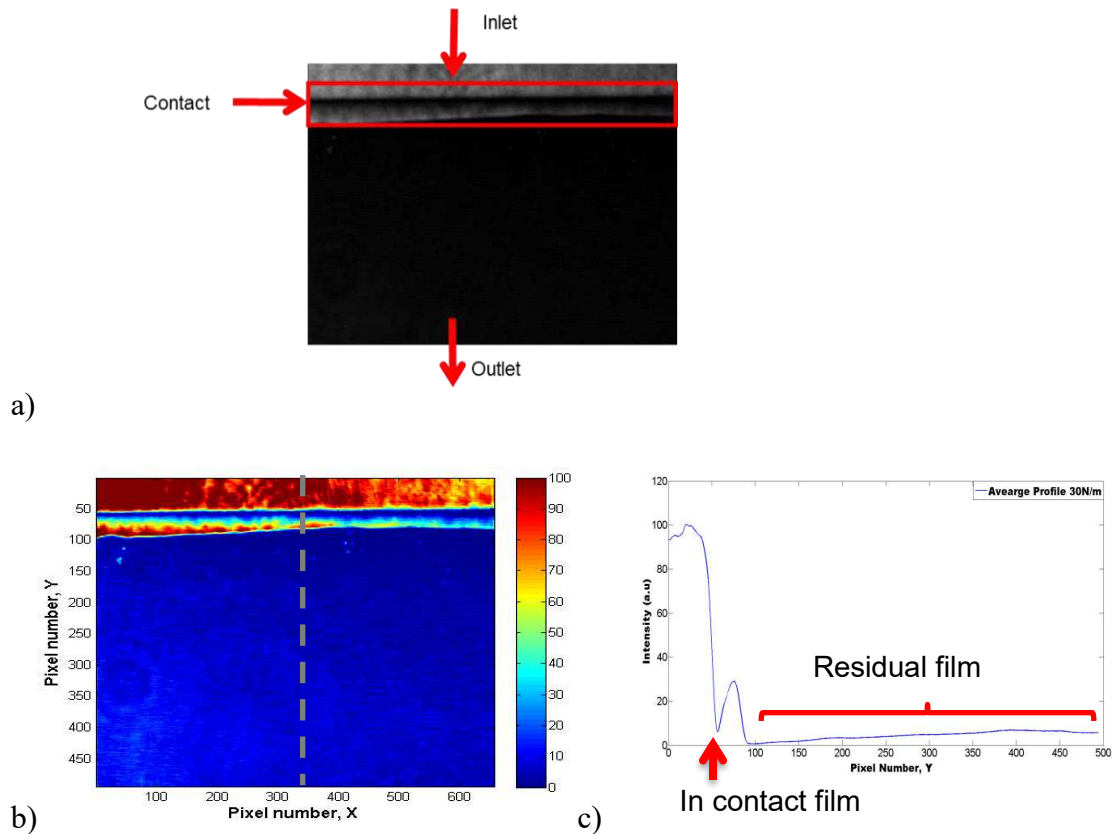

Figure 116. Wiper blade film thickness processing steps: a) Fluorescent image captured by camera, b) Intensity map and c) Intensity profile.

Figure 117 shows the variation of the intensity with load of the film in contact and that left on the glass, at a sliding speed of 184 mm/s for a) a commercial wiper profile and b)

a triangular specimen. Each point in these plots was obtained by acquiring a fluorescence image under the specific test conditions, applying the normalisation described in Chapter 3, and then averaging the relevant region (either within the contact in the wiping zone).

It can be seen from Figure 117 that the water film inside the contact and the residual film on the glass decreases and then increases with load for a commercial wiper blade. This unusual behaviour can be explained as follows. For relatively low loads, the pressure is proportional to normal force, and the increase in pressure leads to a decrease in film thickness.

However, for higher loads the pressure is reduced due to the bending of wiper blade and therefore in this regime, the film thickness increases with normal load. This emitted intensity from the triangular specimen's contact does not show this behaviour in such a pronounced fashion, since the contact pressure for this geometry increases monotonically with load.
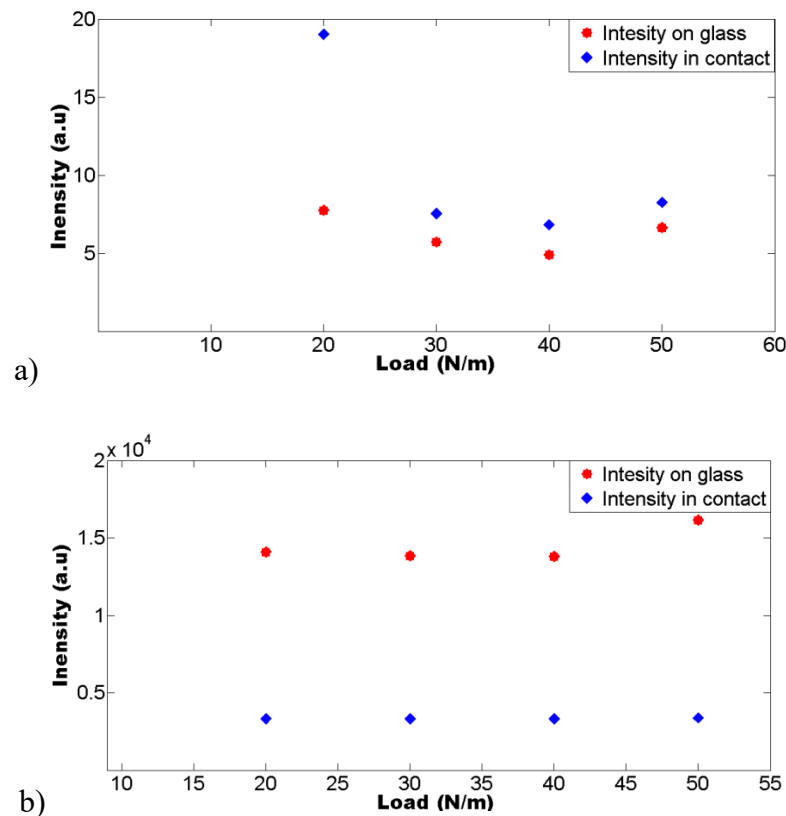

a)

b)

Figure 117. Intensity of fluorescence from in contact and residual water film for a) normal wiper blade and b) triangular specimen versus load at 184 mm/s.

172

Figure 118 shows the effect of speed on the in contact and residual film thickness for a) the commercial wiper profile and b) the triangular wiper at 30 N/m with a water supply flow rate of 25 ml/min. The film inside the contact and residual film for both the wiper and the triangular specimen all decrease as the speed increases.

This result is contrary to that predicted by hydrodynamic theory, which states that film thickness increases with entrainment speed. This discrepancy might be caused by starvation as the water falls away from the contact due to gravitational and centrifugal forces.
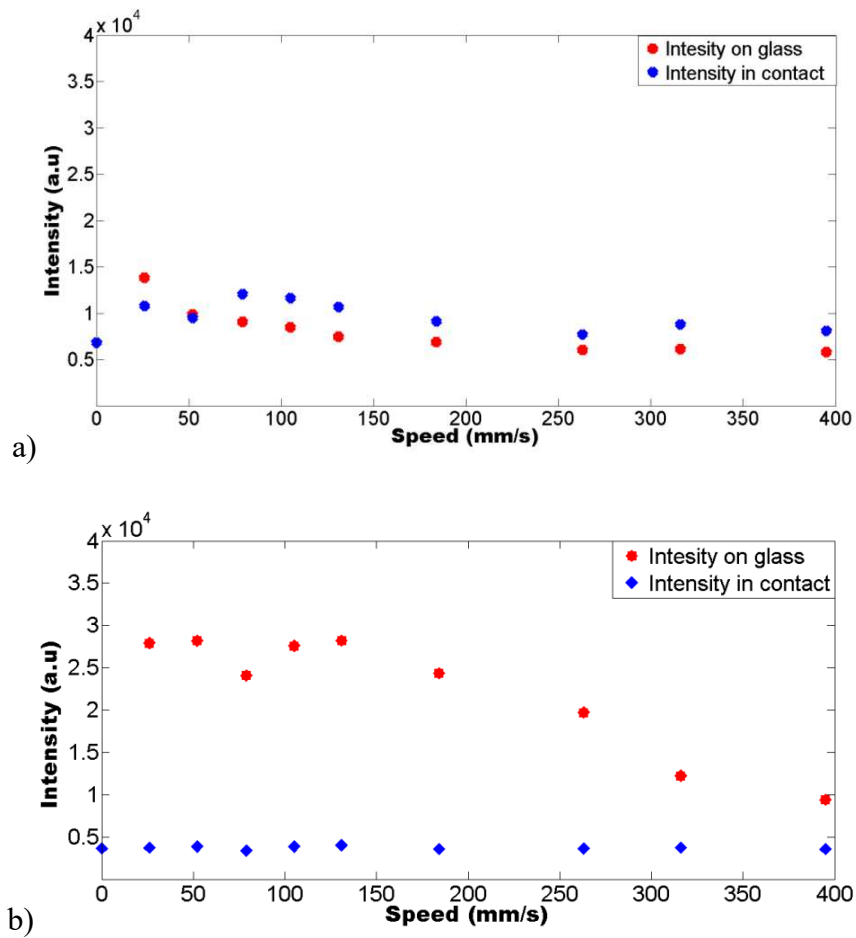

a)

b)

Figure 118. Intensity of fluorescence from in contact and residual water films vs. sliding speed, for a) commercial wiper and b) triangular specimen, at 30 N/m with 25 ml/min water supply flow rate.
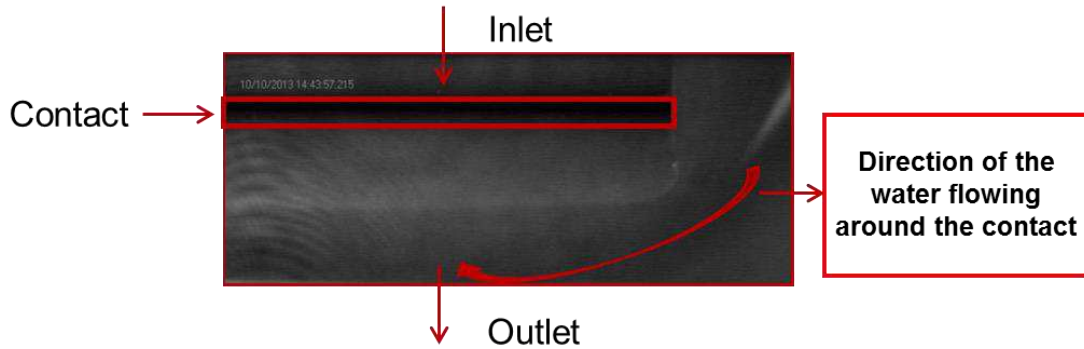
Figure 119. Fluorescent image of the water flowing around the EHD contact while the wiper blade is sliding on the glass disc.

Figure 117 shows that the water film inside the contact is thicker for the commercial wiper profile than for the triangular specimen. This is because the contact pressure for triangular specimens is higher than the commercial wiper for the same load applied, which allows less water to be dragged into contact. This figure also plots the variation in fluorescence intensity with sliding speed. However, there is no discernible trend in the contact film thickness while the residual film thickness varies considerably. This highlights a problem experienced with the EHD rig set-up: due to the contact being upside down, the water remaining on the glass is easily removed at high speed, due to centripetal forces.

The residual film for the triangular specimen is larger than that for the commercial wiper profile. It is believed that this is because the triangular wiper height is less than a normal wiper blade, which allows more water to flow around the contact. A fluorescent image of the water flowing around the EHD contact while the wiper blade is sliding on the glass disc is shown in Figure 119. These unexpected findings (caused by the flow of water around the edge of the wiper) are peculiar to the test setup used in which the wiper is only 10 mm long and is located beneath the glass. Since, in practice a longer length of wiper is used and the wiper is located above the glass, these effects are not believed to play a significant role under actual automotive wiping conditions. It is for this reason that later on in the chapter, film thickness measurements are made using the CETR rig, in which the water is on top of the glass and will not so easily flow around the contact.

The effect of the load and speed on wiper blade using the -5° tilted holder were investigated and compared with a non-tilted holder. Here, a 10X objective was used to verify whether there is any difference between the water film thicknesses inside the contact in the static condition and when sliding at a speed of 26 mm/s). The data is presented in terms of a profile of fluorescence intensity. The intensity value inside the contact at 26 mm/s is larger than that at 0 mm/s, suggesting that there is indeed a detectable water film inside the contact (see Figure 120).
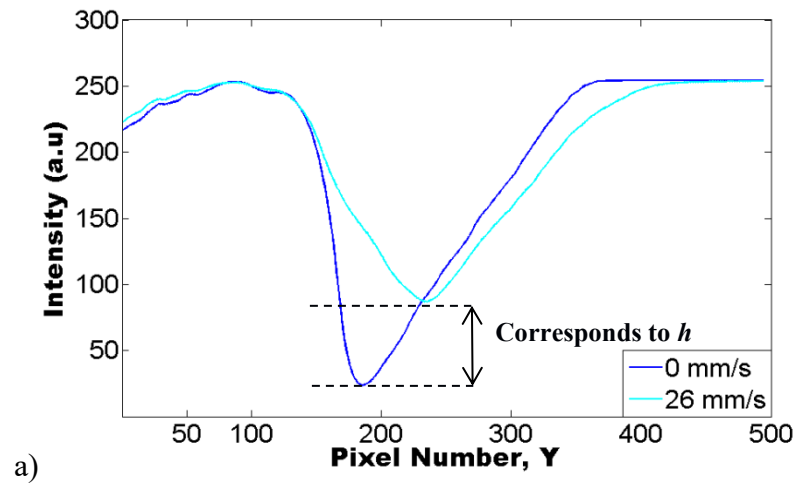

a)

Figure 120. Intensity profiles of commercial wiper profile, obtained using non-tilted holder at 0mm/s and 26 mm/s with load of 30N/m.

The intensity profile data presented in Figure 121, not only gives information on the film thickness within the contact and left on the windscreen, but can also be used to study the deflection of the wiper outside the contact. For instance, the deflection (*i.e.*, the angle between the blade and the glass, also known as "contact angle") of the wiper in contact with glass can be calculated from the intensity profiles of the wiper for different speeds (see Figure 121). This information may be used to validate finite element simulations of wiper deformation in future projects.

The intensity values of the residual film from Figure 121 are different from the residual film values in Figure 120 because when the videos were recorded the intensity values from Figure 120 were saved as compressed videos. Besides, a 10X magnification lens was used to visualise the film inside and outside the contact, which changed the recorded intensity values.
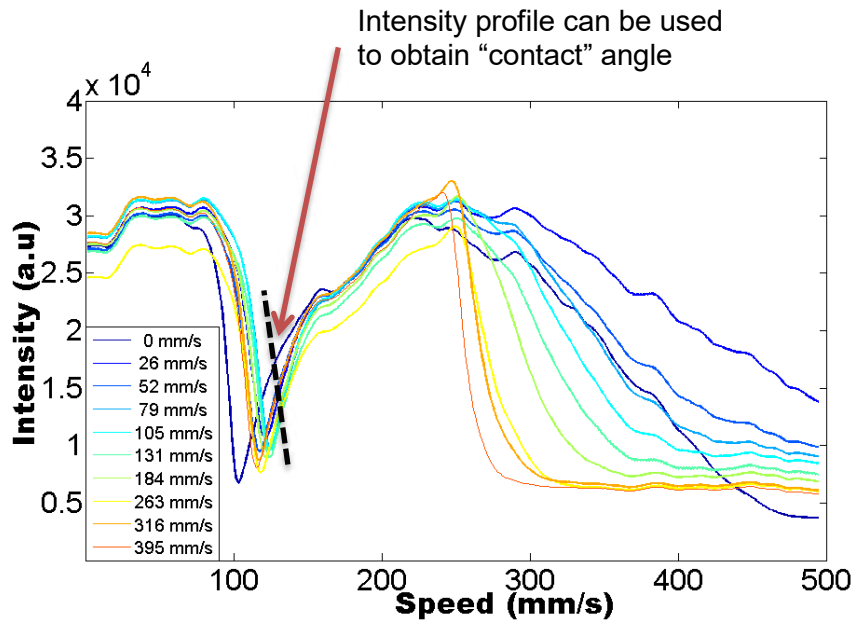
Figure 121. Intensity profiles of wiper at 30 N/m varying with speed.

In order to mimic the real loading condition in a windscreen wiper system, a tilted holder was used to hold the wiper when the water film was measured. When a tilted holder was used to measure the water film, the thickness of the residual film was observed to be higher than the residual film for non-tilted holder (Figure 122a and b). This is believed to be because a greater volume of water is entrained into the contact with the tilted contact geometry.

When an EHD rig was used to evaluate water film, several problems were observed as outlined below:

- The wiper/glass contact is upside down and water falls around due to gravity;
- Water flies off from the contact due to the centrifugal forces;
- The EHD load system is not stable, when low loads are applied on wiper;
- Friction and water film thickness could not be measured at the same time.

To avoid these problems, the CETR tribometer and inverted fluorescent microscope were developed, and used to measure the residual film for wiper blades with and without defects.
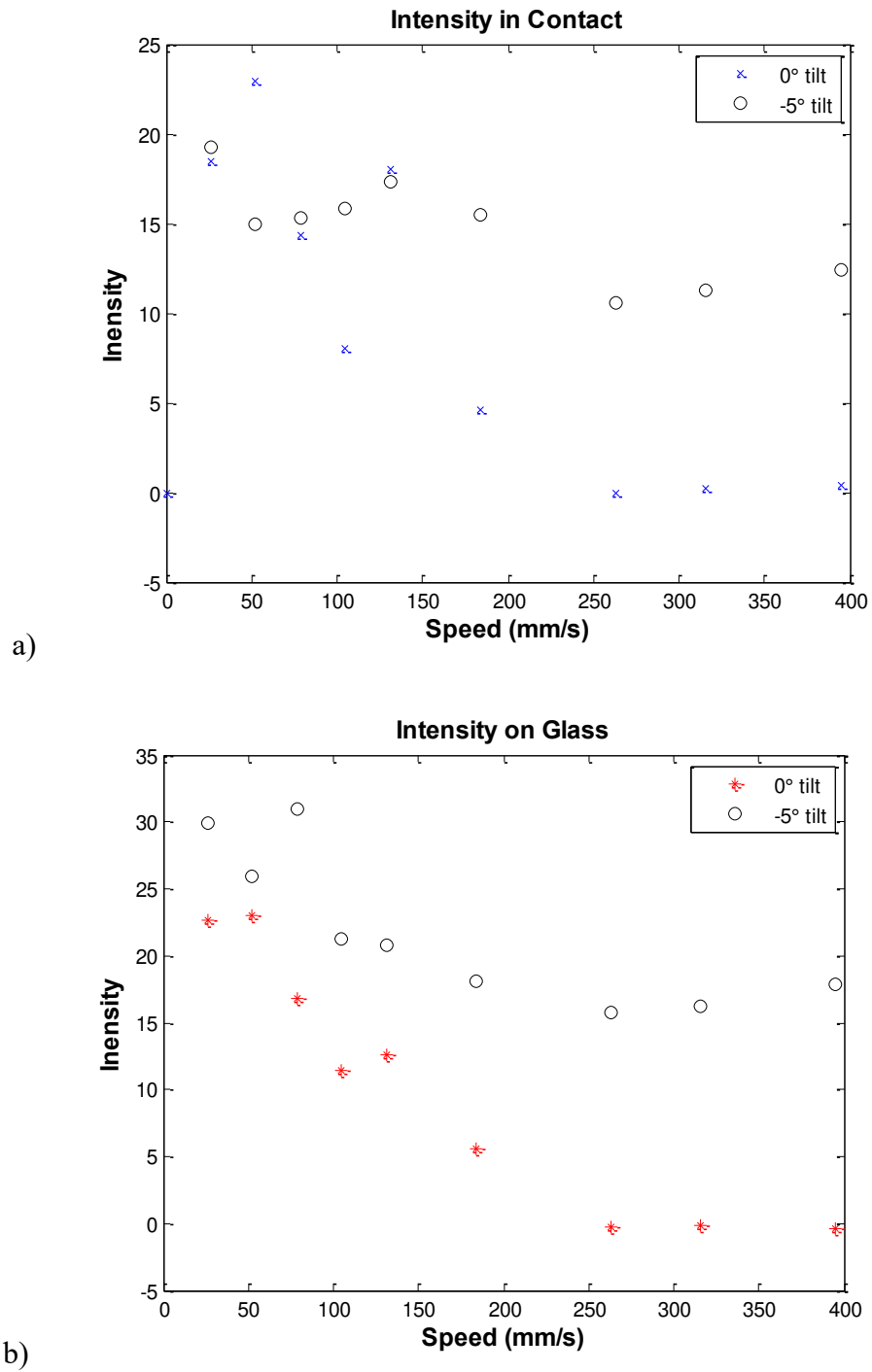
a)

b)

Figure 122. Comparison between a) the film in contact and residual film for commercial wipers and b) triangular specimens, when tilted and non-tilted holders were used.

Summary

When the LIF was used in combination with EHD rig, it was seen that the residual film is thicker for triangular specimens than for commercial wiper, while the film in contact is thicker for commercial wiper than that for triangular specimens. These results were explained on the basis that more water flows around the triangular specimen than commercial wiper. A thicker in-contact film for commercial wiper was due to lower contact pressure while thinner in-contact film was attributed to the higher contact pressure on the triangular specimens when subjected to the same load.

Film thickness inside and outside the wiper contact was studied by varying speed and load. The residual film and in contact film decreased and then increased as load was increased for the commercial wiper, whilst for triangular specimens the residual film and in contact film thickness decreased monotonically with load. Due to the wiper contacts being upside down, several issues with the flow of water were encountered, which led me to adapt the LIF technique to be used on the CETR tribometer.